200 Years Since Davy

DOI: 10.1002/anie.200900373

A Molecular Perspective on Lithium–Ammonia Solutions

*Eva Zurek, Peter P. Edwards, and Roald Hoffmann**

Keywords:
ammonia · lithium · metal–nonmetal transitions · molecular orbitals · solvated electrons

Dedicated to Professor Ron Catterall on the occasion of his 72nd birthday, and in memory of Mike (Michell) J. Sienko

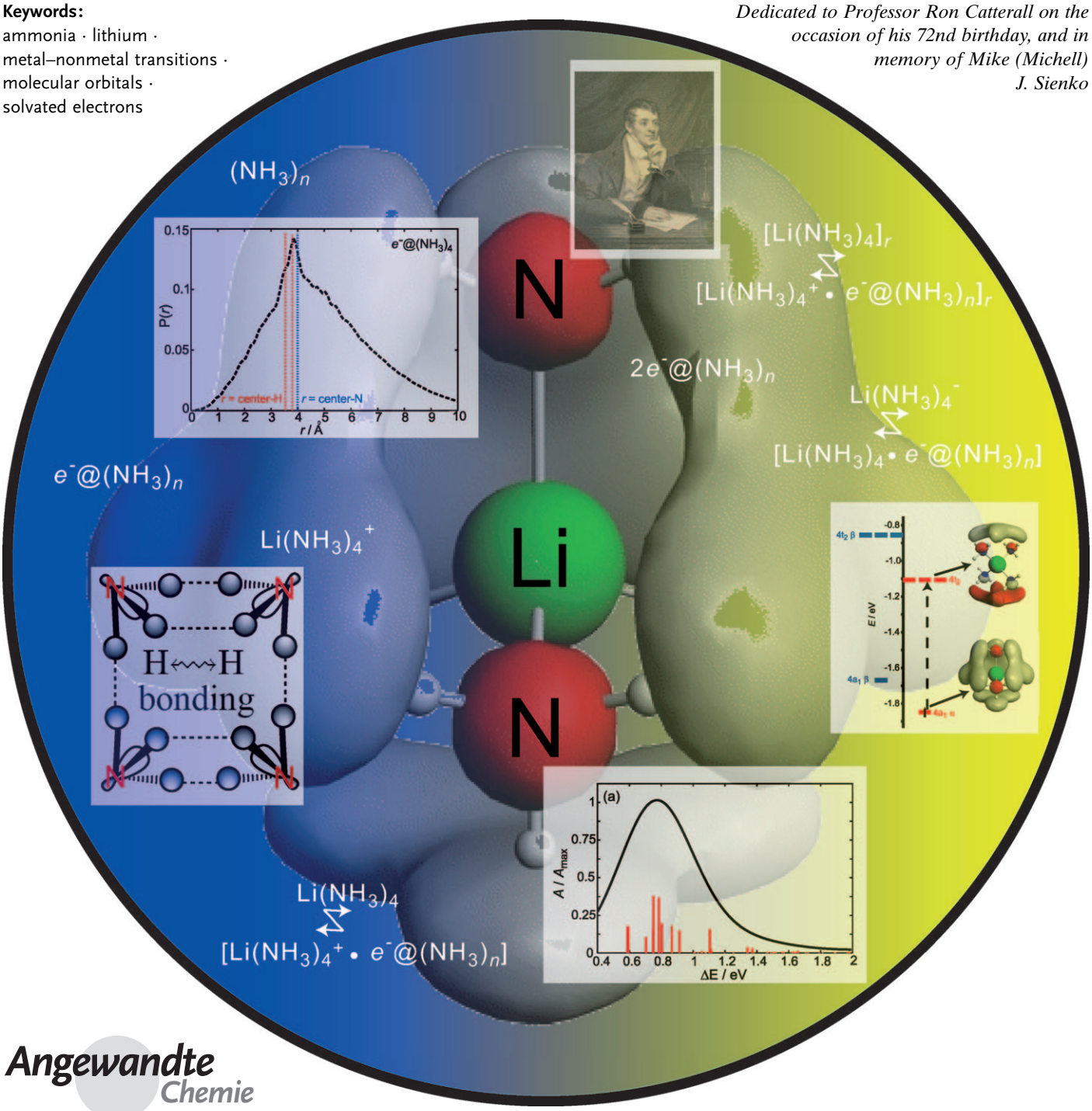

A detailed molecular orbital (MO) analysis of the structure and electronic properties of the great variety of species in lithium–ammonia solutions is provided. In the odd-electron, doublet states we have considered: $e^-@(NH_3)_n$ (the solvated electron, likely to be a dynamic ensemble of molecules), the $Li(NH_3)_4$ monomer, and the $[Li(NH_3)_4^+ \cdot e^-@(NH_3)_n]$ ion-pairs, the Li 2s electron enters a diffuse orbital built up largely from the lowest unoccupied MOs of the ammonia molecules. The singly occupied MOs are bonding between the hydrogen atoms; we call this stabilizing interaction H⇜⇝H bonding. In $e^-@(NH_3)_n$ the odd electron is not located in the center of the cavities formed by the ammonia molecules. Possible species with two or more weakly interacting electrons also exhibit H⇜⇝H bonding. For these, we find that the singlet (S = 0) states are slightly lower in energy than those with unpaired (S = 1, 2…) spins. TD–DFT calculations on various ion-pairs show that the three most intense electronic excitations arise from the transition between the SOMO (of s pseudosymmetry) into the lowest lying p–like levels. The optical absorption spectra are relatively metal–independent, and account for the absorption tail which extends into the visible. This is the source of Sir Humphry Davy's "fine blue colour" first observed just over 200 years ago.

From the Contents

1. Introduction

1.1. A Brief History

Surely the earliest observations of the spectacular blue and bronze colors of alkali metal–ammonia solutions can be traced to the work of Sir Humphry Davy. Ammonia has been known for centuries, thanks to its biological origin. Davy, in 1807, first isolated potassium and then sodium. Thus, in 1807 and 1808 he had ammonia, potassium, and sodium available for his use. In his experiments to prove that potassium was indeed an element, and not a hydride of potash, he reacted grains of potassium with dry, gaseous ammonia to produce the beautiful colors of the concentrated, and then dilute films of potassium–ammonia. Ammonia was not liquefied until 1823 by Michael Faraday (at Davy's suggestion), and hence Davy was seeing the dissolution of metallic potassium by dry gaseous ammonia. These observations were not published by Davy, but were uncovered by one of us in 1981 from a search of his laboratory notebooks.[1–3] The notebook entries are reproduced in Figure 1. They illustrate that 200 years ago Davy observed the characteristic visual signature of these solutions; their "*fine blue colour*".

Hannay and Hogarth in 1879 and 1880 also reported that gaseous ammonia dissolves metallic sodium (in essence, reproducing Davy's observations on potassium and gaseous ammonia) and that these "*gaseous solutions*"—perhaps today they would be called cold plasmas[4]—had lifetimes of at least a few seconds.[5,6]

More than 50 years after Davy, W. Weyl independently made similar observations on the solubility of alkali metals in liquid ammonia.[7] This was the first description in the literature of what we now recognize as the preparation of a solution of a metal in liquid ammonia (actually made by the action of dry ammonia gas under pressure on potassium using a Faraday tube). Weyl, mistakenly, thought of these solutions as "*metal ammoniums*"; that is compounds in which one or more of the hydrogen atoms in NH_4 is replaced by a metal

[*] Dr. E. Zurek, Prof. R. Hoffmann
Department of Chemistry and Chemical Biology, Cornell University, Baker Laboratory
Ithaca, NY 14853 (USA)
E-mail: rh34@cornell.edu
Prof. P. P. Edwards
Department of Chemistry, Inorganic Chemistry Laboratory, University of Oxford
South Parks Road, Oxford, OX1 3QR (UK)

Supporting information for this article is available on the WWW under http://dx.doi.org/10.1002/anie.200900373.

atom. Metal–ammonia solutions were usually referred to as metal ammoniums well into the twentieth century.

The study of metal–ammonia solutions was materially advanced by W. Seely in 1871 who gave the first clear and forthright recognition of the "*nonchemical*" solvent action of ammonia, based on his own experiments, and corrected what he termed as Weyl's "*imperfect comprehension of the fundamental facts*", pointing out that "*the blue liquid is a simple solution of Na in ammonia*".[8] Seely further noted: "*I mean that these metals dissolve in the ammonia as salt dissolves in water*".

During the first part of the twentieth century, E. C. Franklin and C. A. Kraus probably did more to elucidate the chemistry of liquid ammonia solutions than everybody else combined[9] (see Section 1.2). It is perhaps little known that their work was prompted by the research and insight of H. P. Cady, carried out while he was an undergraduate!

Whilst working on cobalt ammine complexes, Cady proposed that ammonia in these (and other "double salts") must function in a manner akin to water in salts with water of crystallization. He suggested further that liquid ammonia would probably be found to resemble water in its physical and chemical properties—thus adding a second to our list of ionizing solvents. Cady's undergraduate work, carried out without supervision, published in 1897, was perhaps the first physical chemistry study of liquid ammonia solutions.[10]

It was Kraus and co-workers, in truly classic studies over a period of almost half a century, who obtained the quantitative data on the electrical conductance and other physical properties which has formed much of the experimental basis for the development and testing of various models for these solutions.[11]

Kraus recognized that solutions of the alkali metals (as well as the alkaline earth metals) are truly unique; they constitute a direct link between electrolytes, on the one hand, and metals on the other.[12]

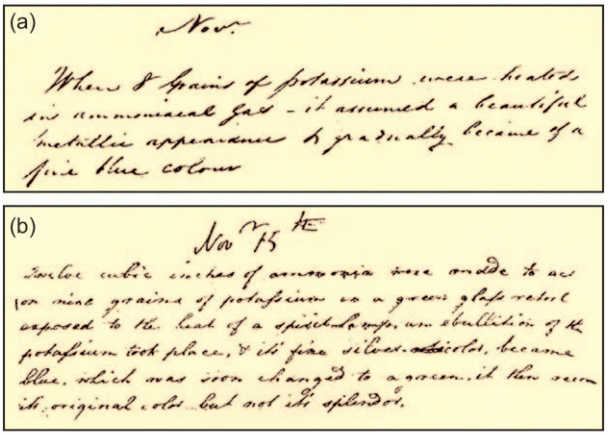

Figure 1. Top: Two entries[1–3] from the laboratory notebook of Sir Humphry Davy for the period October 1805–October 1812. a) 14 November 1808: "When 8 grains of potassium were heated in ammoniacal gas—it assumed a beautiful metallic appearance and gradually became a fine blue colour." b) 15 November 1808: "Twelve cubic inches of ammonia were made to act on nine grains of potassium in a green glass retort exposed to the heat of a spirit-lamp, an ebullition of the potassium took place, and its fine silver-color became blue, which was soon changed to a green. it then resumed its original color but not its splendor." Below: The colors of lithium–ammonia solutions, illustrating how they change with concentration—from pure solvent, to saturation. Figure taken from http://www.phys.ucl.ac.uk/department/AnnRev2003/cmmp.html.

Eva Zurek (center) was born in Kraków, Poland, in 1976. After a brief stay in Austria her family immigrated to Canada when she was 5. She obtained an MSc in theoretical chemistry from the University of Calgary in 2002 (Ziegler; methylaluminoxane), and completed her PhD in 2006 at the Max Planck Institute for Solid State Research in Stuttgart, Germany (Andersen; Wannier functions, metal–fullerene clusters, and carbon nanotubes). She was a postdoctoral fellow at Cornell University with Roald Hoffmann when the metal–ammonia work was done, and is currently an assistant professor at SUNY Buffalo. She never dreamed that she would learn so much about these spectacular solutions!
Peter Edwards' (left) interest in these fascinating solutions dates back over thirty years to his PhD with Ron Catterall at Salford University, their joint project with Sir Nevill Mott of Cambridge, and to his period as Fulbright Scholar with Mike Sienko at Cornell. The solutions—their bright blue and metallic bronze colors, ability to transform from nonmetallic to metallic, and their remarkable separation into coexisting metal and nonmetal layers—present us with a venerable chemical system exhibiting all the electronic properties of the metallic, nonmetallic, and superconducting states of matter.
Roald Hoffmann (right) has been fortunate enough to be allowed to do calculations on, and think about, nearly every molecule and extended structure under the sun. And some hidden from the sun. But, even though Mike Sienko, a colleague and friend, talked to him about the incredible properties of metal–ammonia solutions, frankly Roald never imagined he would wind up thinking about them. Mike would have loved the story that emerges.

1.2. Chemical and Physical Properties of Metal–Ammonia Solutions

Alkali metals and other metals dissolve readily in anhydrous liquid ammonia yielding intensely colored solutions, characterized by a fine blue color for dilute solutions and a copper/bronze color for concentrated solutions (see Figure 1). The dissolution process in these solutions results in the alkali metal valence s electron being spontaneously ionized into the solvent. At low metal concentrations, this leads to the formation of solvated metal cations as well as solvated electrons. Kraus was the first to identify the negative carrier of electricity in metal–ammonia solutions as being the electron liberated from the metal via the dissolution process $M \rightarrow M^+ + e^-$, resulting in electrons which were "free" or associated with ammonia.[13] In 1921, Kraus noted in a study of the conductance versus concentration behavior of metal–ammonia solutions[14] "… *it appears that the blue color of the solution, as well as the other properties which are characteristic of the solution, are due primarily to the negative carrier* …". Kraus' 1907 proposal came only 10 years after the discovery of the electron.

In 1916 G. E. Gibson and W. L. Argo[15] concluded that the characteristic, intense blue color of the solutions was due to one (or more) of the following species: a) un-ionized molecules or atoms of the metal, b) unsolvated, or free, metallic electrons, or c) solvated electrons. This is the first time the term "solvated electrons" was invoked. They first favored (b), but subsequently[16] came to the firm conclusion that the blue color is due to solvated electrons.

As the metal concentration is increased in dilute solutions, the equivalent conductance decreases, much as it does for ordinary salts in ammonia, signifying the onset of interactions between solvated electrons and solvated cations to yield ion-pairs ($M_s^+e_s^-$). A still further increase in the concentration, up to 1 mol% metal[17] (1 MPM), the solvated electrons interact with one another and their spins become paired. There is an extensive literature on magnetic measurements of metal–ammonia solutions giving evidence for spin-pairing, but it is fascinating to note that the first such reported measurements were by N. W. Taylor and G. N. Lewis[18] in 1925, who noted that "*the molecules of ammonia to which electrons are attached do not all remain free, but pair with each other.*"

E. Huster,[19] in 1938, was the first to measure the magnetic susceptibility of metal–ammonia solutions as a function of concentration, highlighting, as Kraus, that these solutions allow one to probe the genesis of metallic properties as a function of electron concentration. Huster noted,[19] in surprise, that sodium–ammonia solutions are strongly diamagnetic at intermediate concentrations, and low temperatures. He suggested an equilibrium between electrons as well as sodium cations on the one hand, and diatomic molecules, Na_2, on the other.

S. Freed and N. Sugarmann,[20] some 5 years later, found the measured magnetic susceptibilities of metal ammonia solutions generally lower than those computed for a system of free electrons. An even more drastic departure from the free electron gas model was realized in the temperature dependence of the susceptibilities, which decrease rather than increase with decreasing temperature. They proposed that electrons in ammonia readily interact to form diamagnetic pairs, to account for the decrease in electronic paramagnetism of the solutions below that expected for a system of non-interacting electrons.

Remarkably, by a concentration of some 0.5 MPM, electron spin-pairing throughout the solution is essentially complete, with over 90% of the electrons in solution being in the spin-paired, diamagnetic state. The precise nature of this spin-paired state and the mechanism leading to the spin-pairing interaction are still not completely understood; a variety of models have been advanced for this diamagnetic species. Electrochemical studies by Schindewolf and Werner[21] have characterized the spin-paired species as an ion trimer, or an ion-triple—a cluster of two single-electron solvated-electron species in association with a cation, also solvated ($e_s^-M_s^+e_s^-$), having a stoichiometry of M^-. A very similar unit can be constructed from two solvated electrons and two solvated cations ($M_s^+e_s^-M_s^+e_s^-$), with a stoichiometry of M_2. These spin-paired diamagnetic species in metal ammonia solutions have also been termed bipolarons.[22]

Within this dilute concentration range one therefore has to consider several equilibria involving electrons and metal ions as well as the solvent. We also have an equilibrium between paired (diamagnetic) and unpaired (paramagnetic) electrons, as well as paired electrons interacting with metal ions, and all of this occurring within a host interacting solvent, liquid ammonia.

A further increase in the alkali metal concentration (from 1 to 8 MPM) brings about a "transition to the metallic state" (TMS, see box below), yielding a bronze/gold-colored liquid within which the solvated electrons are now genuinely delocalized, and the solutions truly metallic. Cooling solutions with a concentration of about 4 MPM leads to a startling liquid–liquid phase separation where the more concentrated gold metallic phase floats on top of the more dilute—but denser—blue one.[23] Near to saturation (ca. 21 MPM) the bronze solutions have an atomic conductance which is higher than that of liquid mercury.[11] Remarkably, in going from the dilute to the concentrated regime, the overall density of the solutions is found to *decrease* by about 30%. The phase diagram of lithium–ammonia solutions[23] is given in Figure 2, together with the associated composition dependence of the (dc) electrical conductivity.[24] We also highlight the probable locus of the TMS in the composition/temperature plane.

Transition to the Metallic State (TMS)

Between 1 and 8 MPM, the electrical conductivity of lithium–ammonia solutions increases by a factor of 10^4. As early as 1897, Cady had observed[10] that the conductivity of sodium–ammonia solutions increases with concentration, contrary to that of electrolytes and noted "*the solution seems to conduct like a metal and not an electrolyte*". This spectacular variation in conductivity has been ascribed to a metal to nonmetal transition (MNMT) of the type envisaged by Sir Nevill

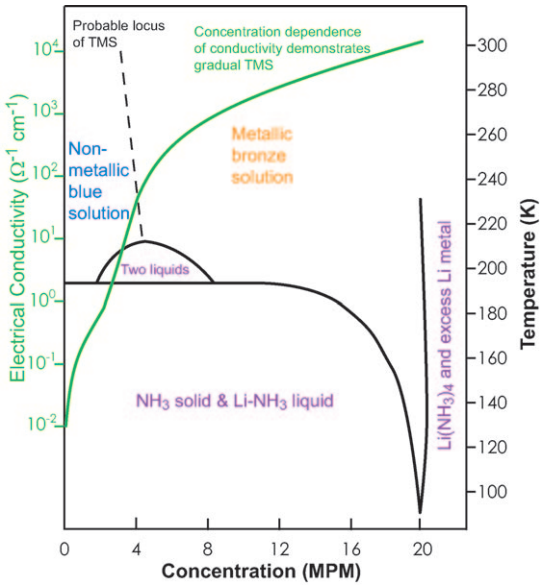

Figure 2. The phase diagram for lithium–ammonia solutions. Data have been adapted from Figure 3 of Ref. [23]. We also show the electrical conductivity data across the entire composition range at −60 °C; these data have been taken from Ref. [24].

Mott.[25] We will refer to this electronic and thermodynamic phase transition as the transition to the metallic state (TMS).

Does the world need another acronym for the time-honored MNMT?[26–28] Well, here's the problem: Though Davy did see a bronze to blue color change (Figure 1a), the usual experimental protocol (and also the way a significant number of theories approach the problem) is to increase the mass of metal dissolved, so that one observes a nonmetal to metal transition. And NMMT simply does not trip off the tongue as easily as MNMT, as an acronym or sounded. C. N. R. Rao has termed the MNMT as "turning copper into wood", which (nothing against wood, which we love dearly) somehow seems not as much fun as turning wood into copper. We therefore introduce TMS in honor of Nevill Mott's classic paper on the subject, entitled "*The Transition to the Metallic State*".[25]

Three general models have been proposed for the TMS in metal–ammonia solutions. One has its origins in percolation theory in which the existence of microscopic inhomogeneities is assumed in these disordered materials. Cohen and Jortner[29] proposed that concentration fluctuations dominate the electronic (and thermodynamic) processes by which the TMS ultimately takes place. The second centers on the interplay of the Mott–Hubbard and Anderson models of the MNMT transition; specifically the TMS is often recognized at a characteristic "Mott density" for metallization.[23,30] The third, and oldest, model dates to the work of K. F. Herzfeld[31]—remarkably published in 1927—in which a dielectric, or polarization catastrophe marks the occurrence of the TMS.

Despite the fact that the TMS in metal–ammonia solutions is one of the best-studied among systems of comparable complexity, a detailed, accepted interpretation of the transition is still lacking.

The unusual behavior of these systems has fascinated scientists—and also engineers[4]—for years,[9] and stimulated a tremendous amount of experimental and theoretical work (see for example, Refs. [32–37] and the "Colloque Weyl" Series[38–44]). Magnetic resonance has usefully been employed to characterize and interrogate the electronic structure, concentration, and nature of the various species within these solutions, and a number of paramagnetic and diamagnetic candidates have been proposed.[1,2,45–49] The paramagnetic ones include:[45] solvated electrons (e_s^-), electron–cation ion-pairs ($M_s^+e_s^-$), monomers, and solvated metal atoms (M_s^0). Some of the diamagnetic entities which have been proposed are ammonia molecules associated into clusters of various sizes, ion-triples ($e_s^-M_s^+e_s^-$), ion-quadruples ($M_s^+e_s^-M_s^+e_s^-$), and genuine (gas-like) alkali metal anions (M^-). Below we will introduce a new microscopic notation for these, a notation that explicitly considers the degree of solvation. And we will suggest other possible entities that may exist fleetingly in solution.

Neutron diffraction has also been utilized to study the microscopic structure of these systems. Recent work on lithium–ammonia solutions has indicated that $Li(NH_3)_4^+$ is the dominant ionic species present.[50,51] The hydrogen bonding present in liquid ammonia is progressively disrupted with increasing metal concentration. For compositions below saturation, the decrease in hydrogen bonding was greater than that expected if ionic solvation effects alone were taken into account.[50,51]

It has been widely accepted that the solvated, or "excess" electron resides inside voids or cavities with a radius of 2.5–3.0 Å within the solvent.[33,38–44] The solvation sheath has been estimated to be made up of seven or eight ammonia molecules with their nitrogen atoms pointing roughly radially "out".[52] Molecular dynamics simulations have shown that the solvated or "excess" electrons tend to form peanut-shaped bipolarons.[53,54] Recent computational work on saturated lithium–ammonia solutions by Chandra and Marx has led to the suggestion that the electrons do not reside *within* the voids, but rather near to the hydrogen atoms at the void/solvent interface.[55] Our findings will concur with this study. A large amount of theoretical work has also focused on the nature of the composition-induced TMS.[29,30,33,34,47,56–58]

A schematic summary of some of these various entities, and of the characteristic properties of the solutions as a function of metal concentration, is given in Figure 3. As noted, we will modify this nomenclature to take into account microscopic solvation. But the use of existing labels at this juncture is a useful construct for our further discussion. We do not include in the list molecular entities such as $LiNH_2$, solvated or not. Metal–ammonia solutions are actually metastable to the reaction $2M + 2NH_3 \rightarrow 2MNH_2 + H_2$.[9,38–44,59] For lithium we calculate this reaction as being exothermic by 54.3 kcal mol^{-1} in solution, but it has a large activation barrier (it can be catalyzed).

Despite tremendous experimental and theoretical efforts, we think that a detailed microscopic understanding of metal–ammonia solutions across the entire composition range—from electrolyte to metallic—is still lacking. In this Review we aim to provide the static, chemical part of the story. Through a

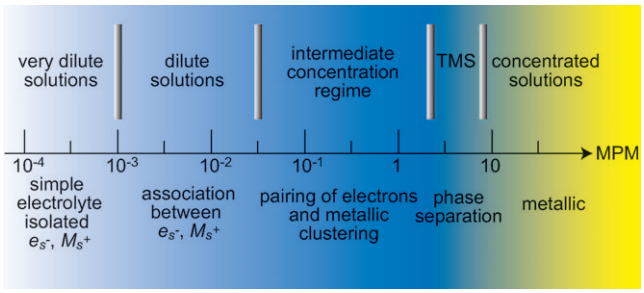

Figure 3. A rough summary of different key properties (derived from experiment), as they vary with lithium concentration in lithium–ammonia solutions. In the intermediate concentration range, extensive pairing of electrons takes place, metallic clusters begin to form, and the magnetic properties foretell a change in electronic structure in the approach to the TMS. Most e_s^- are spin-paired between 5×10^{-2}–1 MPM. The "Mott density"[23] for the TMS is 4 MPM. At saturation $\sigma\sim1.5\times10^4\ \Omega^{-1}\,cm^{-1}$. In terms of atomic conductance, this is higher than mercury at room temperature. Genuine free electron behavior is observed for concentrations greater than 10 MPM. Boundaries between these regions are not precisely defined and are somewhat arbitrary.

spin \ charge	$q = 0$	$q = +1$	$q = -1$	$q = -2$
$S = 0$	$(NH_3)_n$	$Li(NH_3)_4^+$		
$S = 1/2$	$Li(NH_3)_4$ ⇄ $[Li(NH_3)_4^+ \cdot e^-@(NH_3)_n]$		$e^-@(NH_3)_n$	
$S = 0,1,2...$ (CR)	$[Li(NH_3)_4]_n$ ⇄ $[Li(NH_3)_4^+ \cdot e^-@(NH_3)_n]_n$		$Li(NH_3)_4^-$ ⇄ $[Li(NH_3)_4 \cdot e^-@(NH_3)_n]$	$2e^-@(NH_3)_n$

Figure 4. Just some of the species which may be present in lithium–ammonia solutions, classified according to their charge (q) and electronic spin (S) states. The color coding refers to the concentration regime in which they are likely to be found. At 0 MPM only $(NH_3)_n$, labeled in black, will be present. The electrolytic and metallic solutions may contain the species labeled in blue and gold, respectively. The zigzag arrow denotes a continuum of structures, tuned by the degree of microscopic solvation.

sequence of theoretical calculations we examine in microscopic, chemical, and orbital detail the various entities or species likely to be present in these solutions. We also study the interactions between them, and their electronic excitations. What we are not able to do is real-time dynamics of the interacting species. Nor do we have much to say about the precise details of the electronic transition to the metallic state, except in following the embryonic stages of the build-up of the underlying electronic band in these solutions.

1.3. Dramatis Personae

There is nothing simple about the microscopic chemistry of metal–ammonia solutions. The species likely to be present, varying with both metal concentration and temperature, include solvated cations (e.g. $Li(NH_3)_4^+$), neutral species (e.g. $Li(NH_3)_4$; previously denoted as a "monomer", Li_s), and anions (e.g. $(NH_3)_n^-$). These may be relatively free, but more likely solvated by yet more ammonia molecules in the liquid. Or indeed associated with each other. They may have closed electronic shells, or they may carry one or more unpaired electrons ($S = 0$, $^1/_2$,1, or greater). We are fully aware of the ambiguity inherent in even talking about a "molecule" or the "species" in such a dynamic and complex liquid, in which the association of a solvent molecule with a given species may be fleeting. Nevertheless, we hope to show the merit of attempting to describe such solutions in this way.

Figure 4 summarizes the various molecular species we have found to be important, grouped according to their charge (q) and electronic spin (S). Several pieces of notation should be spelled out at this point. The asperand, @, is used to denote an electron whose electronic wavefunction is delocalized over a group of associated ammonia molecules, namely the realization of the entity that we call the solvated electron (or a pair of electrons, so solvated). A dot, ·, denotes association of individual species in space, proximity to be specified. The "zigzag" arrow, ⇄, denotes a continuum of structures, one species continuously evolving into another upon increasing the degree of explicit microscopic solvation. For example, $Li(NH_3)_4 \rightleftarrows [Li(NH_3)_4^+ \cdot e^-@(NH_3)_n]$ denotes the continuous transformation of $Li(NH_3)_4$ to an ion-pair, as it is progressively solvated by ammonia molecules.

The interaction of two species containing a single unpaired electron leads to the formation of systems which can be characterized by several spin states ($S = 0,1,2,\ldots$) whose energies (we shall find) are within a few kcal mol^{-1} of each other. We will refer to these as coupled radicals, CRs. Our notation obviously had its origins in organic chemistry (see Scheme 1), where diradicals such as carbenes (**A**),

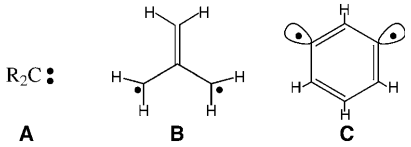

Scheme 1. Some organic diradicals.

trimethylenemethane (**B**), *meta*-benzyne (**C**), have long been discussed, calculated, and observed. There are inorganic systems as well, often discussed in terms of a transition metal complex high-spin–low-spin balance, or questions of electron transfer. Another possible terminology could be "weakly coupled spin isomers", but for brevity we will employ the CR notation.

It is evident that solvation is critical in defining the geometrical and electronic structure of the species present in metal–ammonia solutions, and their resulting intrinsic physical and chemical properties. The setting, a "host" solvent—not vacuum, but a bulk macroscopic liquid of ammonia molecules interacting with each other and with molecules in solution—influences, or even dictates, the behavior of our characters. Indeed, even the concentration-induced TMS is "matrix-bound" in that it takes place entirely within the (host) solvent, liquid ammonia.[32] We approach the treatment of solvation in two ways, microscopic and macroscopic. In the microscopic approach, we have included a number of explicit

ammonia molecules (the following detailed discussion will give specifics), while in the macroscopic approach we use a continuum model, described in Section 2.

Let us make a brief introduction of the cast of molecular characters here; their electronic and geometrical structure (and peculiarities) will be described in detail in the sections that follow.

For $S=0$ we have (going from left to right in Figure 4): $(NH_3)_n$, a single ammonia molecule ($n=1$), or more likely a cluster of ammonia molecules hydrogen-bonded to each other ($n\geq 2$), and $Li(NH_3)_4^+$. We will show later that $Li(NH_3)_4^+$ may also be solvated via hydrogen bonding to a number of ammonia molecules. The $S=^1/_2$ species include $Li(NH_3)_4$ ($q=0$), which we will refer to as "the monomer", and $e^-@(NH_3)_n$ ($q=-1$), the solvated electron. The association of solvent molecules with $Li(NH_3)_4$ can lead to the formation of the $[Li(NH_3)_4^+ \cdot e^-@(NH_3)_n]$ ($q=0$) ion-pairs.

The interaction of any two (or more) $S=^1/_2$ radical species yields the class of coupled radicals, CRs ($S=0,1,2\ldots$). For example, the aggregation of $Li(NH_3)_4$ units results in $[Li(NH_3)_4]_r$ ($q=0$) clusters. These may come in close contact with solvent molecules forming the $[Li(NH_3)_4^+ \cdot e^-@(NH_3)_n]_r$ ($q=0$) cluster ion-pairs. An anionic type of CR, $[Li(NH_3)_4 \cdot e^-@(NH_3)_n]$ ($q=-1$), can come about from the association of $Li(NH_3)_4^-$ and NH_3. It too may represent a continuum of structures. Two electrons held within a cluster of ammonia molecules, $2e^-@(NH_3)_n$ ($q=-2$), are also a CR system. To make the situation even more complicated (and interesting), two or more CRs can interact in order to form larger cluster systems, i.e., $[2e^-@(NH_3)_n]_r$.

After analyzing the electronic structure of each of these more or less likely denizens of the lithium–ammonia sea, we discuss our results in light of experimental data and comment on the species likely to be present at different metal concentrations. Finally, we illustrate that the excitation energies of a number of the species considered are in good agreement with experimental optical absorption spectra of metal–ammonia solutions.

Different Ways of Labeling the Same (or Different) Things

When you have anything of interest to human beings (scientists or not), Babel comes, with its multiplicity of names. Couple this to another human tendency, which is to rename unknown quantities at the drop of a hat (easier than finding out what they really are!), and you get the situation we are in. There are many and varied names for the real or imagined species in metal–ammonia solutions.

We try here to relate some of the existing nomenclatures to our molecular scheme, pointing out both the strengths and weaknesses of the various terminologies (including the one we use).

Our own approach is a molecular one. So we refer to a Li^+ ion in ammonia as $Li(NH_3)_4^+$ or $[Li(NH_3)_4^+ \cdot (NH_3)_n]$, differentiating between a complexed, but unsolvated $Li(NH_3)_4^+$, and a solvated one. The number of ammonia molecules, n, has of course to be specified. Also, as described in the text, we use a macroscopic solvation model in addition to such a specified microscopic chemical stoichiometry. Solvation or not, when we write $Li(NH_3)_4^+$, we mean four ammonia molecules in the first coordination sphere (and a favored tetrahedral geometry), and not three and not five. Those—$Li(NH_3)_3^+$ and $Li(NH_3)_5^+$—may exist, metastable, but are unlikely in solution. There is not only theoretical but experimental evidence for this.

The prevalent literature nomenclature for this species is Li_s^+. The strength of this nomenclature (Li_s^+) is also its weakness—there is no geometric or stoichiometric information about any particular coordination sphere.

The neutral $Li(NH_3)_4$ species (or one associated with yet more ammonia molecules) is a central actor in our paper. In the metal–ammonia literature this is called "the monomer", sometimes given the symbol Li_s.[38–44]

The solvated electron has been descriptively labeled in the literature as e_s^-. This represents an excess electron introduced into the solvent, an electron which interacts with ammonia molecules in a first, second solvation shell and indeed beyond.[48] Our notation for this species is $e^-@(NH_3)_n$. One needs more geometric detail in both notations (again, their strength may be in their *lack* of such detail)—we provide it in the text, and for e_s^- it is given by the various realizations of a model proposed by Catterall and Mott, to be discussed.

The richness of nomenclature comes to the fore around the ion-pairs. We have here in the literature a confluence of nomenclature which come from fields external to metal–ammonia solutions (such as electrochemistry and physical organic chemistry—we have in mind terms such as loose, contact, and solvent-separated, ion-pairs). Some of these are illustrated in Figure 5. The names for the various entities are generally intimately tied to the experimental techniques available to the practitioners who studied them—mainly ESR and NMR, and not structure determinations of the crystallographic or electron diffraction kind.

For example, Catterall and Edwards[60] write an equation which superficially appears very simple: $M_s^+ + e_s^- = M_s$. In our molecular nomenclature we label the reactants in this

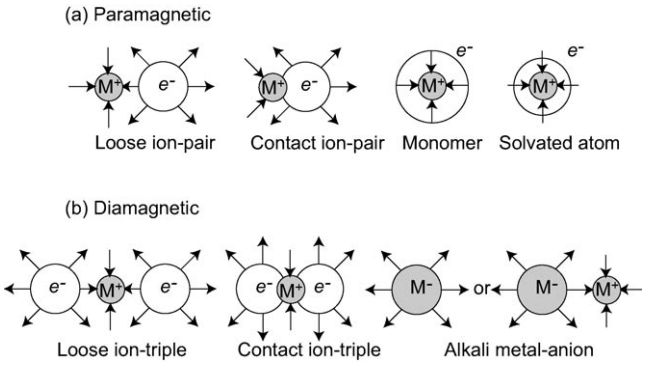

Figure 5. a) Paramagnetic, and b) diamagnetic metal-based species that may be found in metal–ammonia solutions, as outlined in Ref. [2]. The arrows stand for ammonia molecules and indicate the presumed orientation of their dipole moments.[45]

equation as $Li(NH_3)_4^+$ and $e^-@(NH_3)_n$. We also examine the degree of association of the species. One can think of $[Li(NH_3)_4^+ \cdot e^-@(NH_3)_n]$ as a collision complex in the above reaction, or as an approach to the product. We call this an ion-pair. For different n (or varying the distance between ion partners) we can specify the distribution of the unpaired electron—is the excess electron wavefunction primarily on the lithium or in the ammonia cluster? And we could (and do) examine the equivalent of M_s here, a $Li(NH_3)_4$ solvated by some ammonia molecules. The existing literature often uses the terms "loose" and "contact" ion-pairs. The graphic descriptions in Figure 5 give hints to what these species could be.

One can rewrite many of the formulae we use in a variety of ways. For example, $[Li(NH_3)_4 \cdot e^-@(NH_3)_n]$ may be thought of as $[e^-@(NH_3)_{n-m} \cdot Li(NH_3)_4^+ \cdot e^-@(NH_3)_m]$, provided the ion-pair has the correct geometry and charge distribution. The latter notation immediately links this species to the ion-triples often discussed in the literature, $e_s^- M_s^+ e_s^-$ (see Section 1.2).

Our molecular nomenclature does have the advantage of stoichiometric and structural specificity—four ammonia molecules around a lithium, in a tetrahedral geometry, an ammonia cluster near a $Li(NH_3)_4^+$, in a definite geometry, with specific ammonia orientations. That specificity is also a potential disadvantage in the real world of a dynamic ensemble of multiple species in liquid lithium–ammonia solutions.

Do not despair. We will *try* to keep the notation clear. And new experimental techniques will eventually make good sense of what happens in these fascinating solutions.

2. Methods of Computation

The computations were performed using the Amsterdam Density Functional (ADF) package.[61,62] We have applied the revised Perdew–Burke–Ernzerhof (revPBE) non-hybrid gradient density functional[63–66] along with the Vosko–Wilk–Nusair (VWN)[67] local spin-density approximation (LSDA).

In all cases we have employed a valence triple-ζ Slater-type basis set with polarization functions (TZP) and a 1 s frozen core for N from the ADF basis-set library. A primary source of concern in calculations on anions is the basis set: we employed an all-electron even-tempered valence quadruple-ζ basis set with three polarization functions and one set of diffuse s, p, d, and f STOs (ET-QZ3P(1)) for Li, Na, and K. A ZORA relativistic valence quadruple-ζ Slater-type basis set with polarization functions (QZ4P) and the zeroth-order regular approximation (ZORA) Hamiltonian[68–70] was used for Cs.

For a subset of the species studied we have tested how the bonding energies and absorption spectra depend on the basis set used for H. The TZP, Vdiff (non-relativistic basis with extra diffuse functions) and ET-QZ3P(1) basis sets were considered. If the systems contained a metal atom, the bonding energies obtained with the different H basis sets varied by less than 2 kcal mol^{-1} and the excitation energies by (typically much) less than 0.1 eV. The bonding energies of the $e^-@(NH_3)_n$ and $2e^-@(NH_3)_n$ systems displayed a greater basis set dependence; however, for all of the basis sets tested the same trends were found. Unless otherwise noted, the results given were obtained with the higher-quality ET-QZ3P(1) basis.

For species with an even number of electrons, when a given symmetry constraint arose in a half-filled HOMO, a symmetry-breaking distortion was applied, resulting in a geometry with a lower energy and a closed-shell electronic configuration. When an odd number of electrons was present, the structures shown here afford a single unpaired valence electron (doublet) for which spin-unrestricted DFT was employed. In a number of cases we have specifically considered $S=1$ and $S=2$ spin states. No quartets were studied.

All of the orbital isosurface diagrams and contour plots given herein have been calculated in the gas phase. The orbital numbering excludes the N 1s frozen cores. When taking the contour diagrams, we defined a minimum contour value (typically 10^{-3}–10^{-2}), the number of contours plotted, and used a logarithmic scale.

The effects of solvation were approximated macroscopically by the COSMO method[71–73] as implemented in ADF.[74] This model assumes that the solute is embedded in a molecular-shaped cavity within a dielectric continuum characterized by a static dielectric constant ε. The charge distribution of the solute induces charges on the surface of the cavity, the sum of which is opposite to the charge of the solute molecule. The electrostatic solvation energy is calculated as the interaction between the surface charge and 1) the nuclear charge, 2) the electron density, and 3) the surface charges (self-interaction). Other non-electrostatic contributions to solvation arising from cavitation, dispersion, and repulsion are modeled as functions of the surface area of the cavity. Since the COSMO equations are only valid for conductors, for real solvents the charges are scaled by $f(\varepsilon) = \varepsilon - 1/\varepsilon + x$ where x is an empirical scaling factor (here we use the default $x=0$). Full geometry optimizations were carried out using the solvent excluding surface, a dielectric constant of 16.9 for ammonia, and atomic radii of 1.16 (H)/1.4 (N)/1.5 (Li)/1.9 (Na)/2.3 (K)/2.8 Å (Cs). It should be pointed out that dispersion, which is not included in COSMO, is likely to be important for species with very diffuse orbitals.

The ΔE values given in the text are energy differences (products minus reactants) for specified reactions. They do not include zero-point or vibrational finite-temperature corrections. We provide both gas- (ΔE_{gas}) and solution-phase results (ΔE_{solv}). The latter were calculated with energies obtained from optimizations carried out with the COSMO model.

Vertical excitation energies have been calculated using TD-DFT[75,76] as implemented in ADF[77,78] and are compared to those obtained by the Δ-SCF method.[79] Herein, we only give the excitations with non-zero oscillator strengths. The TD-DFT results indicate that the most intense excitations can be described by a single electron transition between well-defined configurations, i.e., the main component contributes $\geq 90\,\%$ to the transition.

3. Ammonia

3.1. The Orbitals and Excited States of NH_3

The ammonia molecule is a willing, non-innocent, partner in all that happens in ammonia solutions. Of course, by its very presence, ammonia effects the ionization of the *n*s valence electron from the alkali atom, a process that requires 5.39 eV for Li, 5.14 eV for Na, and 4.34 eV for K, in the gas phase. So we need a firm notion of ammonia's electronic structure and also its properties.

Aside from its N 1s electron pair, NH_3 has eight electrons in four occupied orbitals, $1a_1$, 1e, $2a_1$. These are illustrated in Figure 6. Above these filled MOs are three empty orbitals

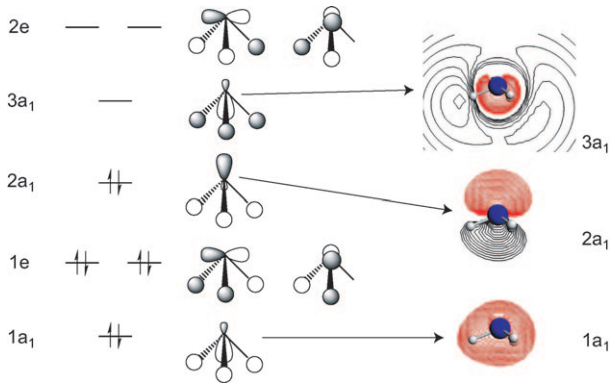

Figure 6. The middle column depicts the traditional, iconic representations of the ammonia orbitals. To the right are shown the calculated contour diagrams of the orbitals of a_1 symmetry. The plane in which the contour diagram is plotted contains one N–H bond. The energy scale is schematic.

($3a_1 + 2e$) which can be thought of as the delocalized equivalent of localized N–H σ* orbitals, just as the $1a_1 + 1e$ are derived from the three N–H σ bonds. The $2a_1$ is the ammonia lone pair, so important in the Lewis basicity of the molecule.

This is a valence-electron basis picture of NH_3. Omitted from it, yet a) essential to a description of anionic states, and b) emerging in extended basis set calculation of the kind we do (have to do, to make sense of metals in liquid ammonia), are higher principal quantum number functions—3s,3p, even 3d on N, 2p on H. Rydberg states are critically important for Li and NH_3 in Li/NH_3 solutions.

The drawings in the middle column of Figure 6 are traditional iconic representations. What do these orbitals look like, especially the critical a_1 orbitals which will interact well with the lithium atom? In the right side of Figure 6 we show contour diagrams obtained from our extended basis set calculations. Note the overall "united atom" appearance of these—$1a_1$ is like a 2s orbital on a nitrogen atom (that is the main contribution to it), $2a_1$ like a $2p_z$, and $3a_1$ like a 3s of the united atom. This characteristic of the ammonia orbitals was noted and used by K. S. Pitzer in his thinking about metal–ammonia solutions.[80] The most striking deviation from the iconic orbital drawings is the very diffuse, Rydberg-like $3a_1$ orbital whose outer, nearly spherical node comes very close to the hydrogen atoms. This is enhanced by substantial contributions of higher lying orbitals to $3a_1$: 3s on N but also 2p on H. The position of this node and the potential involvement of the p orbitals on H have been previously pointed out by Pitzer[80] and O'Reilly.[81]

In its ground state ammonia is pyramidal with C_{3v} symmetry. All of the observed excited electronic states of ammonia below the first ionization energy are due to excitations from the $2a_1$ lone pair to higher lying Rydberg orbitals. Computations have shown that the eight lowest-lying excited states are Rydberg-like.[82] These are all accompanied by a change in the geometry of the molecule to a planar, D_{3h} configuration. Thus, each electronic excitation is also coupled to the out-of-plane umbrella inversion mode, and the spectrum of the molecule is rich in vibronic structure.[83] A multitude of excited electronic states lie below the first ionization potential of ammonia (10.85 eV).[84] The two lowest-lying transitions ($2a_1 \rightarrow 3a_1$, $2a_1 \rightarrow 2e$) are found at around 6.5[85] and 8.0 eV.[83]

In contrast to the behavior of metal–ammonia solutions—and of critical importance—in the gas phase a single NH_3 molecule does not bind an extra or excess electron, that is, does not possess a positive electron affinity. It has been estimated that in the gas phase, a cluster must contain at least 30[86] or 35[87] ammonia molecules in order to bind an excess electron. Cluster vertical ionization potentials have indicated that the excess electron is localized within a cavity inside the cluster.[87] However, recent experiments on the solvation dynamics of electrons in finite-sized clusters of ammonia have been able to make systems as small as $(NH_3)_{13}^-$.[88] An excellent discussion of the evolution of various physical properties as a function of the cluster size is given in Ref. [89]. There, cluster size equations, describing the transition from a large finite cluster to the bulk system, are presented.

3.2. Hydrogen Bonding

Ammonia has a substantial dipole moment of 1.47 *D*,[90] reasonably approximated by computations at the CCSD(T) level of theory.[91] Of course, NH_3 forms moderately strong hydrogen bonds which are important in determining the phase diagram of this molecule. The disruption of that hydrogen bonding in the liquid through the formation of $Li(NH_3)_4^{0,+,-}$ and the solvated electron, $e^-@(NH_3)_n$, is an essential feature of metal–ammonia solutions. So let us get a good picture of the hydrogen bonding in clusters made up from the molecule.

After several years of controversy, sophisticated experiments and high-level calculations (see Refs. [92, 93] and references therein) have reached an agreement on the structure of the simplest neutral ammonia aggregate, the dimer. Instead of an essentially linear hydrogen bond in the equilibrium structure (as is found in water), the corresponding ammonia bond is somewhat bent, as shown in Figure 7a. In fact, the dimer is fluxional and it has been proposed that the "symmetrical, twin hydrogen bond", C_{2h} structure depicted in Figure 7b is a transition state for interconverting two C_s geometries.[94] The best calculations we have seen

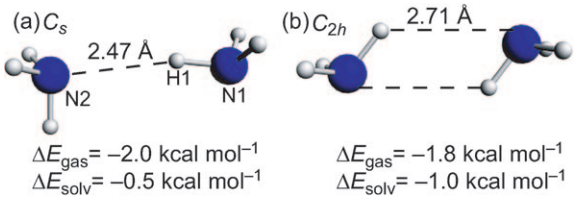

Figure 7. Optimized geometries of two ammonia molecules hydrogen-bonded to each other. The ΔE values are for the reaction: $n\,NH_3 \rightarrow (NH_3)_n$, in gas and solution phase, and the H–H distances in vacuo are given.

(obtained at the W2 level of theory which is an extrapolation towards the full CCSD(T) basis set limit) indicate that the eclipsed C_s configuration is the minimum, with a hydrogen-bond energy of 3.13 kcal mol^{-1} and an H1–N1···N2 angle of 20.7°.[92] These same computations show that the potential energy surface is very flat and the C_{2h} structure is only 0.01 kcal mol^{-1} less stable.

The functional we used gave a reasonable account of the hydrogen bonding in NH_3. A recent study has analyzed how well different functionals describe hydrogen-bonding interactions.[95] We find the C_s structure to be the minimum (though, as the numbers in Figure 7 show, the hydrogen bond is found to be about 1 kcal mol^{-1} weaker than the best computed values), with an H1–N1···N2 angle of 8.7°. The difference in energy between the equilibrium and transition state structure is 0.2 kcal mol^{-1}. The gas-phase association energy of the C_{2h} TS is in reasonable agreement with other DFT values (–2.7 kcal mol^{-1}).[96] For both structures, solvation effects decrease the strength of the hydrogen bond.

4. $Li(NH_3)_4^+$: The Complexed and Solvated Lithium Cation

Neutron diffraction experiments have indicated that tetrahedral $Li(NH_3)_4^+$ is the dominant ionic species present in lithium–ammonia solutions.[50,51] Moreover, inelastic X-ray scattering measurements,[97] supported by theoretical calculations,[98] have identified excitations that are associated with $Li(NH_3)_4^+$. This is a simple ammonia-solvated Li^+ ion. Or (a far stretch) it can be viewed as being isoelectronic with neopentane, 2,2-dimethylpropane.

Does Li^+ in fact prefer to have four ammonia molecules in its first coordination sphere? We have optimized the geometries of the $Li(NH_3)_n^+$ (n = 1–5) complexes shown in Figure 8. The Li–N bonds stretch slightly as the coordination of the metal increases. The magnitude of the binding energy per n also decreases with increasing n (see Table 1). There appear to be no barriers to the exothermic addition of each successive ammonia, up to four.

But adding the fifth ammonia is different. First the reaction (with solvation) is nearly thermoneutral, endothermic by only 0.7 kcal mol^{-1}. The starting geometry for $Li(NH_3)_5^+$ was a trigonal bipyramidal-like structure with C_{3v} symmetry (the hydrogen atoms prevent this system from having D_{3h} symmetry). During the optimization one of the Li–N bonds broke, yielding a slightly distorted $Li(NH_3)_4^+$,

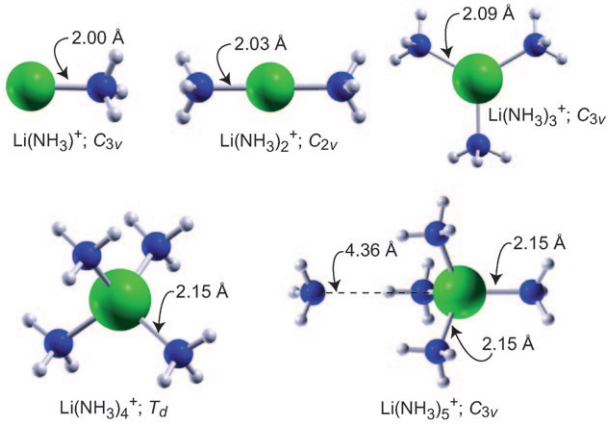

Figure 8. Optimized geometries of $Li(NH_3)_n^+$ (n = 1–5) complexes. The gas-phase Li–N distances are also provided.

Table 1: The $\Delta E/n$ (kcal mol^{-1}) for the reaction: $Li^+ + n\,(NH_3) \rightarrow Li(NH_3)_n^+$ (n = 1–5), in both gas ($\Delta E_{gas}/n$) and solution ($\Delta E_{solv}/n$) phase.

n	$\Delta E_{gas}/n$	$\Delta E_{solv}/n$
1	–39.0	–13.1
2	–35.7	–12.6
3	–31.0	–11.4
4	–26.6	–9.3
5	–22.5	–7.3

with an ammonia molecule nearby. Clearly, Li^+ can be coordinated by up to four ammonia molecules, the fifth NH_3 is only weakly associated.

In Figure 9 we provide an MO interaction diagram for $Li(NH_3)_4^+$. Actually, the diagram is one computed for neutral $Li(NH_3)_4$, a species we will have much to say about shortly. The orbital occupation shown however is for the cation under discussion here, $Li(NH_3)_4^+$. The HOMO of the cation consists of the triply degenerate t_2 orbitals, one of which is illustrated in Figure 10. These are primarily composed of the $2a_1$ ammonia lone pairs (this is also the case for the HOMOs of the $Li(NH_3)_n^+$ (n = 1–3) complexes). However, the t_2 orbitals

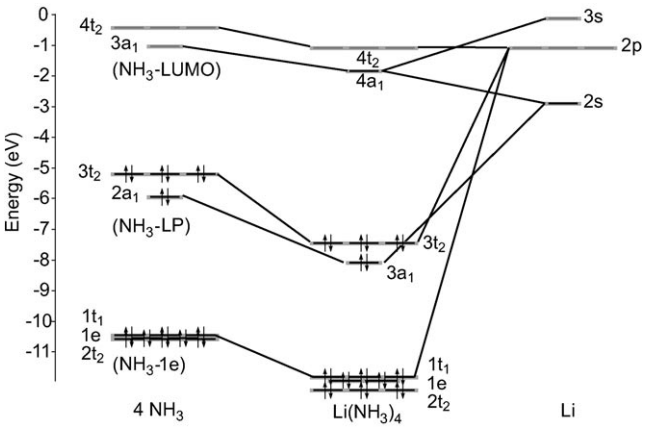

Figure 9. An (approximate) interaction diagram for the formation of $Li(NH_3)_4$ from lithium and four ammonium molecules. Note that the electron occupation shown is for the cation. LP = lone pair.

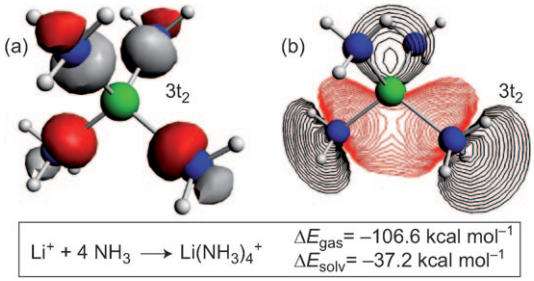

Figure 10. a) An isosurface (±0.065 au), and b) contour diagram of one of the triply degenerate $3t_2$ HOMOs of the tetrahedral $Li(NH_3)_4^+$ ion. The plane of the contour passes through two Li–N and two N–H bonds.

also contain some symmetry-allowed Li 2p character. The molecule has a large gap (6.3 eV, gas phase) between filled and unfilled levels. Our calculated gas-phase binding energy for $Li(NH_3)_4^+$ (106.6 kcal mol^{-1}) is in good agreement with the results of MP2 (105.2 kcal mol^{-1}) and B3LYP (110.1 kcal mol^{-1})[99] studies. The continuum solvation model significantly decreases the binding energy to 37.2 kcal mol^{-1}, since it naturally has a larger stabilizing effect on Li^+ than it does on $Li(NH_3)_4^+$.

Comparison of the gas-phase Mulliken charges on the hydrogen atoms in $Li(NH_3)_4^+$ (+0.20) with those of ammonia (+0.09) indicate substantial polarization of the bound ammonia. This in turn suggests that the hydrogen bonding between the $Li(NH_3)_4^+$ and ammonia may be stronger than between two NH_3 molecules. Therefore, we have considered systems where one and two ammonia molecules are hydrogen-bonded to $Li(NH_3)_4^+$, as illustrated in Figure 11. Our

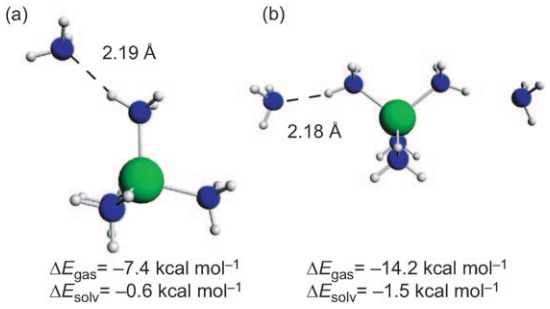

Figure 11. a) A single ammonia, and b) two ammonia molecules hydrogen-bonded to $Li(NH_3)_4^+$. The ΔE values are for the reaction $n(NH_3) + Li(NH_3)_4^+ \rightarrow [Li(NH_3)_4^+ \cdot n(NH_3)]$, in both gas ($\Delta E_{gas}$) and solution ($\Delta E_{solv}$) phase, and the H–H distances in vacuo are given.

results indicate that the hydrogen bonds in these species are about 5 kcal mol^{-1} greater in strength than in ammonia itself (Figure 7), with correspondingly shorter N–H distances. Moreover, the binding energy per H-bond is approximately the same for $[Li(NH_3)_4^+ \cdot NH_3]$ as for $[Li(NH_3)_4^+ \cdot 2NH_3]$, suggesting this trend may continue as long as steric repulsion between solvent molecules does not come into play. Once again, macroscopic solvation decreases the hydrogen-bond strength; the effect is particularly dramatic for $Li(NH_3)_4^+$. This is due to the fact that solvation has a greater stabilizing effect on systems with dipoles, and on charged systems that are smaller. Hence, it stabilizes ammonia and $Li(NH_3)_4^+$ more than it does $[Li(NH_3)_4^+ \cdot NH_3]$.

5. $Li(NH_3)_4$: The First Solvation Shell

Neutron diffraction experiments have shown that lithium in ammonia has four NH_3 molecules in the first solvation shell.[50,51] This points to the simplest $S = {}^1/_2$ system in lithium–ammonia solutions as being the $Li(NH_3)_4$ monomer. Nonetheless, just as for the cation, we have examined the coordination of one to five ammonia molecules to a neutral lithium atom (as in Figure 8).

Table 2 shows that the magnitude of the bonding energy per n does not differ greatly for the different species. Once again, lithium was found to coordinate up to four ammonia molecules—the fifth Li–N bond broke, leading to the formation of a $[Li(NH_3)_4^+ \cdot e^-@(NH_3)]$ ion-pair, to be discussed further in Section 7. Thus the complex with four ammonia molecules will be the most likely one in solution, but it is not impossible that the species with fewer ammonia molecules have a fleeting, temporal existence.

Table 2: $\Delta E/n$ (kcal mol^{-1}) for the reaction: $Li + n\,(NH_3) \rightarrow Li(NH_3)_n$ (n = 1–4), in gas ($\Delta E_{gas}/n$) and solution ($\Delta E_{solv}/n$) phase.

n	$\Delta E_{gas}/n$	$\Delta E_{solv}/n$
1	−14.1	−8.0
2	−13.6	−7.7
3	−13.7	−8.3
4	−12.8	−7.4

Not surprisingly, ammonia molecules bind to Li^0 more weakly than to Li^+ (see Table 1). However, the net gas-phase binding energy for the dominant species in solution, the $Li(NH_3)_4$ monomer, 51.2 kcal mol^{-1} in the gas phase, is still quite large. This value is in good agreement with B3LYP (54.1 kcal mol^{-1}) and MP2 (46.9 kcal mol^{-1}) results,[99] as well as those obtained using pseudopotentials (49.1 kcal mol^{-1}).[100] It is also comparable to the MP2 binding energy of $Na(NH_3)_4$, which was calculated as being 41.0 kcal mol^{-1}.[101] Solvation is found to somewhat decrease the binding energy. This is understandable since NH_3 has a dipole moment (and will therefore be stabilized by solvent effects), whereas Li and $Li(NH_3)_4$ do not.

5.1. The Singly Occupied Molecular Orbital (SOMO)

Metallization (Figures 2, 3) could involve aggregation and band formation of $Li(NH_3)_4$ units. So it's essential to understand the electronic structure of this monomer, the potential building block for the metallic state. In Figure 9, we presented an approximate interaction diagram for the formation of $Li(NH_3)_4$ from Li and four ammonia molecules arranged in the same tetrahedral fashion as in $Li(NH_3)_4$. At these distances, the isolated ammonia molecules interact with

each other just a little, as can be seen by the small splitting of the 1e, and somewhat larger splitting of the $2a_1$ (lone pair) orbitals in the left hand side of the figure. The lowest energy combination of the individual ammonia $2a_1$ orbitals arises when all of the lone pairs have the same phase at the center of the tetrahedron. The corresponding triply degenerate combinations have the correct symmetry to interact with the Li 2p orbitals, as was mentioned previously in Section 4.

The LUMO of the aggregate of four ammonia molecules by themselves is composed of the NH_3 $1a_1$ and $3a_1$ orbitals and interacts with Li s orbitals to form the $4a_1$ SOMO of $Li(NH_3)_4$. The LUMO of the $Li(NH_3)_4$ system, of t_2 symmetry, is less than 1 eV higher in energy. Later on we will examine the excited states of $Li(NH_3)_4$ in some detail, for they are possible contributors to the distinctive color of metal–ammonia solutions.

The $4a_1$ SOMO of $Li(NH_3)_4$ is very important in the chemistry of metal–ammonia solutions, so it merits a closer look. The SOMO (Figure 12) is of a_1 symmetry and the

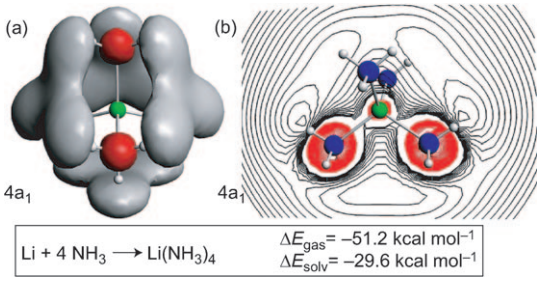

Figure 12. a) An isosurface (±0.02 au), and b) contour diagram of the $4a_1$ SOMO of the tetrahedral $Li(NH_3)_4$. The plane of the contour diagram contains two N–H bonds.

coefficients in the wavefunction indicate that it is composed of occupied (2s) and unoccupied Li (3s, 4s) functions, as well as $1a_1$ and $3a_1$ NH_3 orbitals (Figure 6). Examination of the contour diagram in Figure 12b clearly shows a nearly spherical region around the nitrogen atom (from the $1a_1$ contribution) and a node near a hydrogen atom (from $3a_1$). The small (and negative) NMR Knight shift for the protons[102,103] in metal–ammonia solutions has been explained by the presence of such a node in the electronic wavefunction near a hydrogen atom, which may occur if the orbitals are 3s-like around nitrogen, and 2p-like near hydrogen.[80,81] The pseudopotential calculations of Ref. [100] concluded that the valence electron is in a Rydberg-like state and its density is predominantly associated with the hydrogen atoms of the ammonia molecules. This is in agreement with our findings, which show that for the highest isosurfaces taken (at still higher ones the orbital disappears), the $4a_1$ SOMO is localized primarily around the nitrogen and hydrogen atoms. Knight shift experiments have shown that there is unquestionably very large unpaired electron spin density on the nitrogen atoms.[103,104]

Comparison of the SOMO of $Li(NH_3)_4$ with the HOMO of $Li(NH_3)_4^-$ (see the Supporting Information) suggests that the latter also contains significant contributions from the ammonia $1a_1$ and $3a_1$ orbitals. However, it appears that $3a_1$ mixing is somewhat smaller for $Li(NH_3)_4^-$, since for the same isosurface the cloverleaf region connecting the hydrogen atoms on adjacent ammonia molecules has disappeared (it is present for lower isosurfaces). In a one-electron picture (e.g. that given by the extended Hückel method) the LUMO of the cation, the SOMO of the radical and the HOMO of the anion would be identical. In reality, which is approximated by the DFT calculations, these orbitals differ in small but significant ways.

In Table 3 we provide the bond distances and angles in ammonia as well as for the cationic, neutral, and anionic monomeric $Li(NH_3)_4$ species. It is surprising that the Li–N bond (and with it the nearest-neighbor distances between two hydrogen or nitrogen atoms on adjacent ammonia molecules)

Table 3: A comparison of the calculated gas-phase bond lengths [Å] and angles [°] in NH_3, and the tetrahedral $Li(NH_3)_4^+$, $Li(NH_3)_4$, and $Li(NH_3)_4^-$ species.

Species	Li–N	N–H	H–H[a]	N–N[a]	H-N-Li	H-N-H
NH_3		1.02				105.8
$Li(NH_3)_4^+$	2.15	1.02	3.65	3.51	114.0	104.6
$Li(NH_3)_4$	2.11	1.03	3.57	3.45	113.3	105.4
$Li(NH_3)_4^-$	2.14	1.03	3.62	3.50	113.3	105.4

[a] H–H and N–N distances are given for the nearest neighbors on *adjacent* ammonia molecules.

is shortest in the neutral, and not in the cationic species. Not much happens to the NH_3 molecules upon coordination. Based on the σ* (N-H) origins of $3a_1$, one might have expected the N–H bonds to stretch, but they don't.

5.2. Intramolecular H⇜⇝H Bonding

We do find something very interesting in the secondary interactions between ammonia molecules in $Li(NH_3)_4$. Note that the SOMO of the neutral (and we believe important) $Li(NH_3)_4$ contains the largest amount of ammonia $3a_1$ character, and is itself of a_1 symmetry. The consequence of occupation of this orbital is therefore a bonding interaction between the hydrogen atoms on nearest-neighbor ammonia molecules (see the cloverleaf lobes in Figure 12). This *electronic/orbital-mediated bonding between two hydrogen atoms* is to be distinguished from normal hydrogen bonding, and also from the more ionic $H^{\delta+}\cdots H^{\delta-}$ bonding recently studied in a number of inorganic systems.[105,106] We introduce a new symbol, H⇜⇝H, to label the bonding between hydrogen atoms due to orbital overlap in a crucial occupied bonding orbital (here the SOMO of $Li(NH_3)_4$). The H⇜⇝H bonding interaction is small for any individual H–H pair in $Li(NH_3)_4$, *but* there are many such contacts. In $Li(NH_3)_4^+$ the $3a_1$ orbital is not occupied, hence there is no H⇜⇝H bonding.

We note the obvious—the $Li(NH_3)_4$ SOMO is like a big hydrogen atom (or alkali metal) SOMO. $Li(NH_3)_4$ is a pseudo-hydrogen, or, given its nodal structure along the Li-N–H bonds, a pseudo-potassium. In the Supporting Information we show that the $Li(NH_3)_n$ ($n=2,3$) complexes, whose

cations were previously discussed in Section 4, also exhibit intramolecular H⇜⇝H bonding.

5.3. Where is the Electron in $Li(NH_3)_4$?

The cloverleaf lobes in the wavefunction of the SOMO are very pictorial, but we wish to get still more information on the unpaired electron in $Li(NH_3)_4$. We have calculated the probability, $P(r)$, that the unpaired electron is a distance r from the lithium atom in $Li(NH_3)_4$ (Figure 13). Similar plots for neutral Li 2s and 3s orbitals provide a natural calibration.

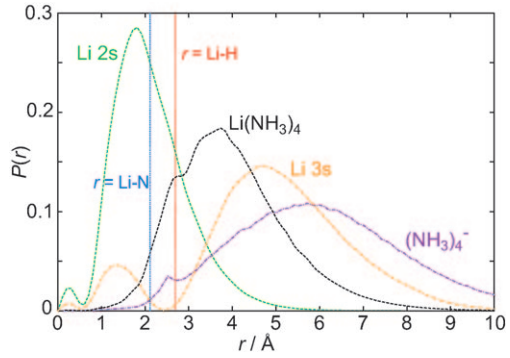

Figure 13. The (gas-phase) probability that the valence electron is a distance r from the lithium nucleus in the lithium atom (2s and 3s orbitals) and in $Li(NH_3)_4$. Also given is the probability to find an electron a distance r from the center of $(NH_3)_4^-$, which has the same geometry as $Li(NH_3)_4$ but without the lithium atom in the middle. The probability has been normalized so that $\int P(r)dr = 1$. The Li–N and Li–H distances in $Li(NH_3)_4$ are denoted by the blue and red lines, respectively.

For $Li(NH_3)_4$, $P(r) = 0$ near the lithium atom and it rises steeply as we approach the nitrogen atoms. The increase in $P(r)$ is due to the red lobes around the nitrogen atoms (Figure 12). Another sharp increase occurs between the nitrogen and hydrogen atoms. However, the maximum $P(r)$ is about 1.2 Å even farther out than the hydrogen atoms. This is due to the gray cloverleaf lobes which are a result of the intramolecular H⇜⇝H bonding (Figure 12). For $r \geq 4$ Å, the probability to find the electron decreases slowly, and does not effectively disappear until about 9 Å away from the lithium atom. Our results are qualitatively similar to those obtained using pseudopotentials[100,107] and Hartree–Fock calculations.[108]

The likeliest place to find the electron in $Li(NH_3)_4$ lies almost midway between the maximum $P(r)$ for an electron in the Li (gas-phase) atomic 2s and 3s orbitals. In order to determine how the presence of the lithium atom affects the probability distribution, we have also calculated $P(r)$ for $(NH_3)_4^-$ having the same geometry as $Li(NH_3)_4$. We can see that the two probability densities are quite different (Figure 13). For the anion, the maximum $P(r)$ is at about 6 Å and the probability does not completely go to zero even 10 Å away from the center of the cavity. In fact, the $P(r)$ for $(NH_3)_4^-$ does not differ substantially from that of a single $(NH_3)^-$ oriented so that the nitrogen and hydrogen atoms have the same distance to the origin as in $(NH_3)_4^-$. This indicates that there is virtually no interaction between the ammonia molecules in $(NH_3)_4^-$ oriented in this way (we will show later this is not always the case for different orientations of ammonia molecules) and therefore no H⇜⇝H bonding.

Thus, in $Li(NH_3)_4$ the lithium atom is instrumental in facilitating the H⇜⇝H bonding. This can be explained in one of two ways. In the completely ionic picture, the lithium valence 2s electron is transferred into the LUMO of $(NH_3)_4$. However, Coulombic attraction keeps the electron closer to Li^+ than it is to the center of the tetrahedron in $(NH_3)_4^-$. Another way to look at what happens is to place the electron in an orbital which contains Li 2s, 3s character, as well as contributions from the ammonia orbitals. The latter explanation is in agreement with the results obtained from the fragment analysis, and also with the Knight shifts deduced from Li NMR.[47,103]

We have also studied $Li(NH_3)_4^-$, a species that has occasionally been suggested in the literature. Details of this CR entity are given in the Supporting Information.

6. The Solvated Electron: $e^-@(NH_3)_n$

A central character in metal–ammonia solutions is a cavity composed of n ammonia molecules, with a net charge of −1. This is the microscopic model of the solvated electron, consistent with the volume expansion so prominent in these solutions.[38,39] We shall use the notation $e^-@(NH_3)_n$ when referring to these negatively charged cavities. Only a few static ab-initio studies on small $e^-@(NH_3)_n$ clusters have been performed.[109–112] Such clusters have been seen in a few molecular dynamics simulations, for example Refs. [53,54].

Catterall and Mott proposed a sequence of steps occurring upon solvation of the electron, leading to cavity formation.[113] These are depicted very schematically in Figure 14: a) at first, one has a normal liquid ammonia structure in which the molecules are hydrogen-bonded to each other; b) the normal structure of molecules surround a defect in the liquid; c) when the electron enters the cavity, the dipoles of the ammonia molecules reorient, so as to destroy the hydrogen bonding (the hydrogen atoms of the ammonia molecules then point towards each other); d) thermal agitation, hydrogen–hydro-

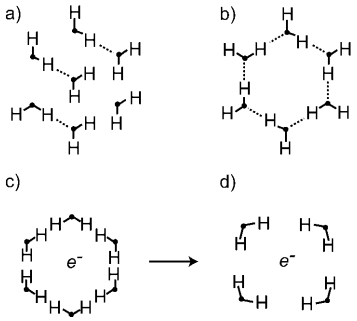

Figure 14. Schematic steps in the solvation of an electron in liquid ammonia, as proposed by Catterall and Mott[113,33] (see text for explanation). The third hydrogen on the ammonia molecules is pointing into the page.

gen and dipole–dipole repulsion (so-called Bjerrum defects[113]) causes the cavity to expand in order to minimize these defects.

Actually, some ten years prior to this explicit representation, Jortner postulated a similar picture, and transformed it into a physical model.[114] The highly successful Jortner model has its origins, in part, in the work of R. A. Ogg.[115–117] Jortner assumed that the electron is trapped within a cavity of ammonia molecules and regarded the solvent as a continuous, homogeneous medium, having a low-frequency and a high-frequency dielectric constant. The interaction of the electron with the medium gave rise to a constant potential within, and a varying potential outside the cavity (Figure 15). Jortner

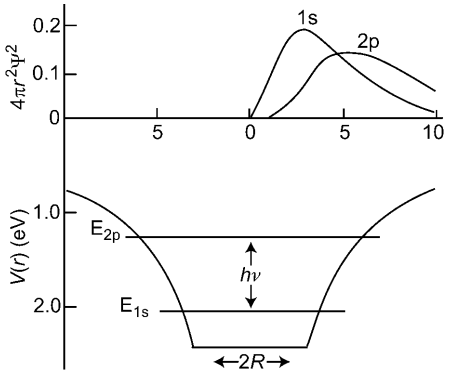

Figure 15. The potential $V(r)$ used by Jortner, and the corresponding probability to find an electron a distance r away from the center of the cavity in the 1s and 2p levels. A transition between these two energy levels gives rise to the absorption maximum. Data adapted from Ref. [114].

provided a variational solution for the ground 1s and first excited 2p states of such a potential, and the absorption maximum was attributed to a transition between the two. Assuming a cavity radius of 3–3.2 Å gave a 1s→2p transition of about 0.8 eV, in excellent agreement with experiment. From its conception in 1959 until this day, the transparency—and ease of application—of the Jortner model has shaped our thinking on the solvated electron. Thus, we will look for real correspondences with that model further on in our study.

6.1. Intermolecular H⇜⇝H Bonding

What we aim to provide here is a delocalized, molecular orbital description of electron solvation, specifically identifying the orbital the excess electron enters. Isolated NH_3^- itself is not bound, as was noted previously. Nevertheless, it is useful to consider what happens when an electron, or part of it, is transferred to NH_3. The consequence is a (complete or partial) filling of the $3a_1$ orbital illustrated in Figure 6.

If several negatively charged ammonia molecules orient so that the hydrogen atoms point towards each other ("H-in": not the optimum bonding arrangement for neutral ammonia molecules), a bonding orbital forms from the diffuse lobes of the individual NH_3 $3a_1$ LUMOs. An electron can enter the lowest energy MO (of "s" pseudosymmetry) built from these MOs. We will show explicit representations of this orbital soon, for different cavity sizes. Importantly, this MO is bonding between the hydrogen atoms in a way similar to the situation we have already encountered (see Figure 12) in $Li(NH_3)_4$—it is H⇜⇝H bonding. We schematically illustrate such an orbital for an (almost) square planar $e^-@(NH_3)_n$ in Figure 16a. If the ammonia molecules were oriented so that their hydrogen atoms pointed *out* of the cluster center, as shown in Figure 16b, there would be less *inter*-molecular H⇜⇝H bonding. Similar bonding has been predicted for negatively charged fluorocarbon cages.[118]

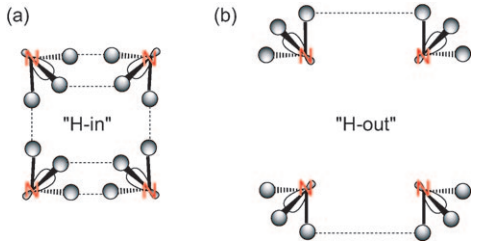

Figure 16. The hydrogen atoms in a (nearly) square planar arrangement of $e^-@(NH_3)_4$ can point: a) towards, or b) away from the center of the cavity. The dotted lines show the H-H contacts which exhibit some H⇜⇝H bonding. The $3a_1$ LUMO on each NH_3 is also schematically depicted.

In order to gauge the strength of these intermolecular H⇜⇝H bonds we have compared the overlap populations (OP) of the nearest-neighbor hydrogen atoms in the (nearly) square planar $e^-@(NH_3)_4$ (OP = −0.002), with those of the neutral cluster of the same geometry (OP = −0.009). We see that addition of the extra electron yields a less negative OP, that is, it strengthens the H⇜⇝H bond. These are very small numbers for sure, but there are many such H⇜⇝H interactions. The intramolecular H⇜⇝H bond in $Li(NH_3)_4$ (OP = 0.01) is also stronger than in the cationic $Li(NH_3)_4^+$ (OP = 0.001).

We have performed calculations on a number of $e^-@(NH_3)_n$ $(1 \le n \le 14)$ species, in which the hydrogen atoms were oriented so that they faced towards each other. Figure 17 provides the optimized geometries of the cavities with $n \ge 5$. A word of caution here—there may be many local minima for these clusters, all very close in energy. For example, the energy difference between the "square planar" (Figure 16a) and tetrahedral arrangements of $e^-@(NH_3)_4$ was found to be 0.7 and 2.0 kcal mol^{-1} in the gas and solution phase, respectively. In both of these geometries each hydrogen participates in a single H⇜⇝H bond. The H–H distances in the tetrahedral isomer are equivalent, whereas there are two different H–H bond lengths in the "square planar" one. Our main goal here is to examine the trends, and for this finding the global minimum (if one exists) is not crucial. Thus, we have considered only a few structural configurations. A fuller picture requires a molecular dynamics study of the kind carried out by Klein[53,54,119] and Marx.[55]

The SOMOs of the simplest $e^-@(NH_3)_n$ clusters are illustrated in Figure 18. Comparison of the contour diagram of the $3a_1$ SOMO of $(NH_3)^-$ in Figure 18a with the calculated

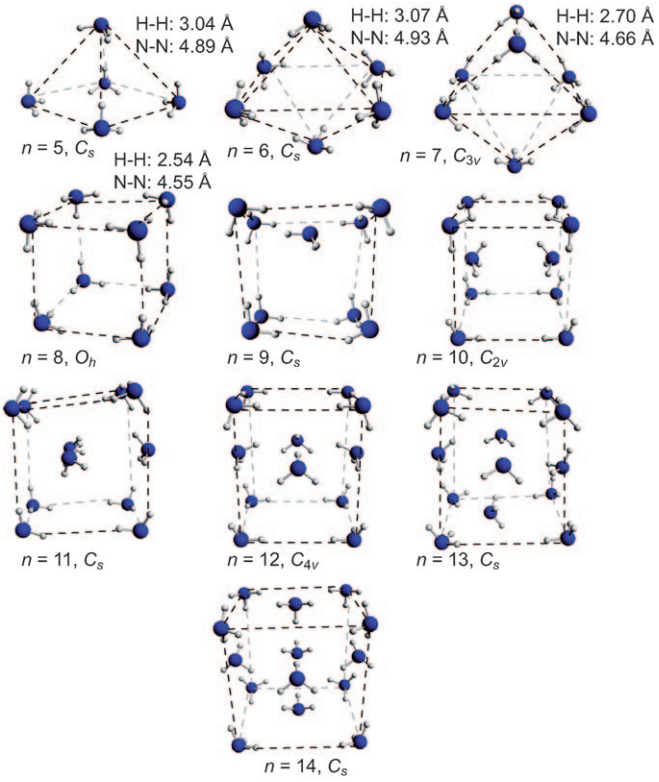

Figure 17. The geometries and symmetries of $e^-@(NH_3)_n$ ($5 \le n \le 14$) clusters. The dashed lines connect the ammonia molecules comprising the largest cavity and are given to guide the eye. For $n = 5$–8, the nearest-neighbor intermolecular H–H and N–N distances in vacuo are provided.

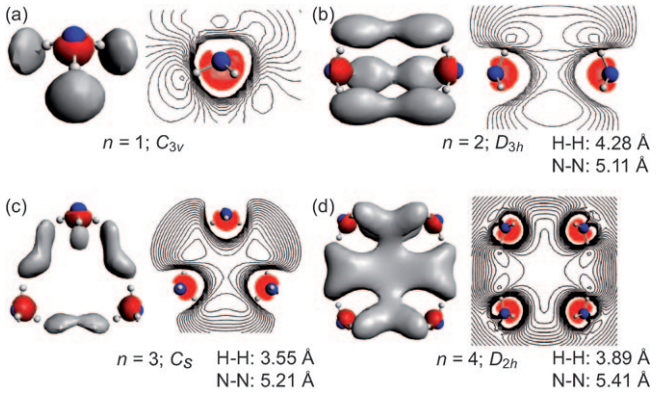

Figure 18. Isosurfaces (±0.016 au–±0.020 au, depending upon the species) and contour diagrams of the SOMOs of $e^-@(NH_3)_n$ species with $n = 1$–4. For $n = 1,2,4$ the plane of the contour bisects an N–H bond. For $n = 3$ the plane of the contour contains the three nitrogen atoms. The nearest-neighbor intermolecular H–H and N–N distances in vacuo are provided.

ammonia LUMO in Figure 6 reveals that upon filling by one electron the shape of the $3a_1$ orbital is slightly perturbed. However, the main features (i.e., the region around N and the node near H) remain. Figure 18b–d illustrate that when several ammonia molecules orient so that their hydrogen atoms point towards each other, the resulting SOMO is constructed from an in-phase combination of the gray lobes between the hydrogen atoms. This gives rise to the weak H⇜⇝H bonding interactions, to which we alluded to earlier. Figure 18d corresponds to the "H-in" configuration illustrated in Figure 16a. Clearly, the orientation of the ammonia molecules in these species does not allow for normal hydrogen bonding. Indeed, experimental results indicate that increasing the concentration of the solvated electron significantly disrupts hydrogen bonding.[50,51] *Thus, in ammonia solutions containing a solvated electron, conventional hydrogen bonding is replaced by H⇜⇝H bonding!*

6.2. *Is the Solvated Electron* Inside *the Ammonia Cavity?*

The solvated electron, $e^-@(NH_3)_n$, is such an unusual species for a molecular chemist that we would like to explore its electronic structure still further. The SOMOs of the various $e^-@(NH_3)_n$ species display a maximum around the nitrogen atoms and near the hydrogen atoms, consistent with the experimental N and H NMR Knight shifts[104] and a recent Wannier function analysis, which found that the excess electrons reside near the hydrogen atoms.[55] There is in the literature a history of calculations on hydrated and ammoniated electrons in which an approach somewhat different from ours is followed (see Ref. [111] and references within). In these studies, a basis function (effectively a pseudoatom) is placed at the center of the cavity. The electron is constrained to be in the center of the cavity, by the use of small basis sets.

Wishing to look at this electron distribution in another way, we have calculated the probability, $P(r)$, that the electron

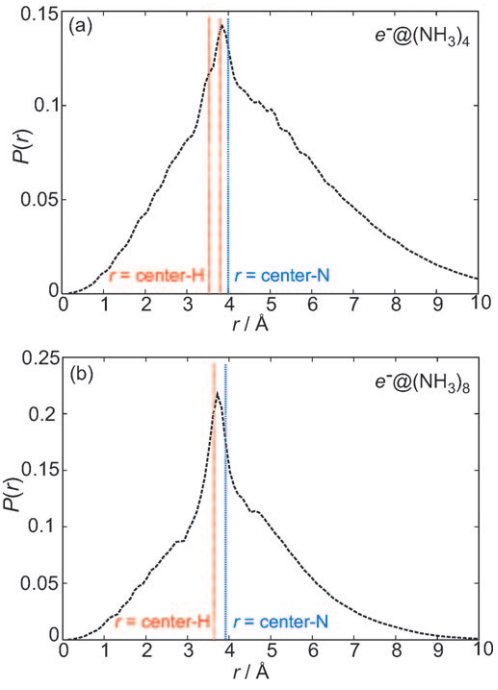

Figure 19. The (gas-phase) probability $P(r)$ that the electron is a distance r from the center of the a) $e^-@(NH_3)_4$ and b) $e^-@(NH_3)_8$ cavities illustrated in Figure 18d and Figure 17, respectively ($\int P(r)dr = 1$). The distance from the center of the cavities to the nitrogen and hydrogen atoms are indicated by the blue and red vertical lines.

is a distance r from the center of the cavity in $e^-@(NH_3)_4$ and $e^-@(NH_3)_8$ (Figure 19). For both species, the probability to find the electron at the center of the cavity is zero, and it increases rapidly, reaching a maximum in-between the hydrogen and nitrogen atoms. The increase in $P(r)$ comes about from the red lobes around the nitrogen atoms (see Figure 18) and even more so from the gray lobes near the hydrogen atoms which give rise to the H⇜⇝H bonding between the ammonia molecules. In these particular clusters the hydrogen atoms point towards each other, and therefore the maximum overlap between the gray lobes will occur when r is approximately equal to the distance between the hydrogen atoms and the center of the cavity. $P(r)$ decays very slowly, reaching zero for an r of about 10 Å.

It should be pointed out that the probability of finding the electron at the center of the cavity was also zero in Jortner's model[114] (Figure 15). $P(r)$ reached a maximum near the cavity radius, 3–3.2 Å, and decayed to zero about 10 Å away from the center of the cavity.[114] Thus, this work, Jortner's,[114] and the Wannier function study by Chandra and Marx,[55] all show that the electron is certainly *not* in the center of the cavity, but rather near the cavity surface, i.e., the region around the nitrogen and hydrogen atoms. The answer to the question posed in the title of this section is therefore "No".

6.3. Energetics of Ammonia Orientation

In order to gauge how much of a penalty one pays for having the ammonia molecules pointing *the wrong way* ("H-out"), we have performed a single-point calculation on the square $e^-@(NH_3)_4$, orienting the hydrogen atoms away from each other, but keeping the same N–N distance as in the fully optimized system, as illustrated in Figure 16b. The reorientation of the ammonia molecules destabilizes the system by 9.9 kcal mol^{-1}. Note that neither geometry is particularly attractive from the standpoint of normal hydrogen bonding. For the corresponding neutral molecules, the difference is much smaller ("H-out" is 1.6 kcal mol^{-1} below "H-in"). So the electron definitely stabilizes the "H-in" geometry.

We note that the $e^-@(NH_3)_4$ cavity in which the ammonia molecules have the same arrangement as in $Li(NH_3)_4$ ($P(r)$ for this system is given in Figure 13) are destabilized by 24.6 kcal mol^{-1} as compared to the "square planar H-in" species. Since this arrangement of ammonia molecules is even higher in energy than the "H-out" species, this suggests that even though the H⇜⇝H bonding in the "H-out" geometry is less than that of the "H-in", some is still possible. Indeed, examination of the "H-out" SOMO shows that there is residual H⇜⇝H bonding between the hydrogen atoms closest to each other, i.e., those connected by the dotted lines in Figure 16b.

Our results suggest that the strength of the H⇜⇝H bond in these "electron in a cavity" species is comparable to the hydrogen bond in a normal ammonia solution. For example, we calculated that a hydrogen-bonded tetramer (found to be the most stable isomer of $(NH_3)_4$ in Ref. [94]) is 11.4 kcal mol^{-1} more stable than four isolated ammonia molecules (gas phase). This is comparable with the 9.9 kcal mol^{-1} that comes from the reorientation of the ammonia dipoles in $e^-@(NH_3)_4$ ("H-in" vs. "H-out").

6.4. How Many Ammonia Molecules Make Up the Cavity?

In Table 4 we provide the gas- and solution-phase formation energies of $e^-@(NH_3)_n$ and $Li(NH_3)_4^+$ from $Li(NH_3)_4$ and ammonia. We note that the solvation energies should be taken with a grain of salt—they are dependent upon a number of parameters, for example the dielectric constant of the solvent and the atomic radii used to create the cavity

Table 4: The gas- and solution-phase energies (kcal mol^{-1}) for the formation of $e^-@(NH_3)_n$ ($1 \le n \le 14$) and $Li(NH_3)_4^+$ from $Li(NH_3)_4$ and NH_3.[a]

	$Li(NH_3)_4 + n(NH_3) \rightarrow Li(NH_3)_4^+ + e^-@(NH_3)_n$			$Li(NH_3)_4 + n(NH_3) \rightarrow Li(NH_3)_4^+ + e^-@(NH_3)_n$	
n	ΔE_{gas}	ΔE_{solv}	n	ΔE_{gas}	ΔE_{solv}
1	76.5	11.8	8	60.9	−1.5
2	72.6	3.1	9	55.0	−7.3
3	69.4	−0.3	10	53.2	−6.9
4	66.2	0.5	11	49.0	−7.2
5	64.0	−3.7	12	50.1	−7.0
6	61.3	−4.5	13	44.4	−6.5
7	60.6	−4.3	14	41.7	−5.8

[a] The $e^-@(NH_3)_n$ geometries considered are illustrated in Figures 17 and 18.

surface. Nonetheless, the trends obtained are illuminating. Solvation effects stabilize the charged species and lower ΔE (large and positive in the gas phase) by 50–70 kcal mol^{-1}. In comparison, solvation effects of about 40 kcal mol^{-1} have been calculated for the ion-pair separation energies of Group 4 transition metal catalysts in nonpolar solvents such as cyclohexane.[120] In general, the magnitude of the stabilization provided by the continuum solvation model decreases with increasing n, that is, with the number of explicit solvent molecules considered. When solvation is taken into account, our results predict that $e^-@(NH_3)_n$ with $n \ge 5$ may be stable.

Previous suggestions for the solvated electron have assumed simple cavities, the ammonia molecules roughly distributed on a sphere. On this point we got a surprise. Closer scrutiny of the systems containing more than eight ammonia molecules in Figure 17 reveals that in the optimized structure at least one of the ammonia molecules resides entirely or partially within the larger cavity. Thus, these clusters can be viewed as being composed of a single cavity with an explicit solvation shell, or two or more smaller cavities in close proximity to each other. Our findings suggest that the cavity may optimally contain 5–8 molecules, in reasonable agreement with other estimates of 7–8 ammonia molecules.[52,121] For all of the cavities considered, the N–N and H–H distances are quite large, owing to the diffuse nature of the $3a_1$ orbitals. The large N–N distances (see Figures 17 and 18) are also in accordance with experimental estimates of the cavity radius (2.5–3.0 Å).[50,51]

To summarize: the H⇜⇝H bonding which is achieved via the overlap of the partially occupied NH_3 LUMOs has led us to the conclusion that the optimum way for the ammonia molecules to orient in $e^-@(NH_3)_n$ is such that the hydrogen atoms point towards each other. The same conclusion may also be derived from considerations of the best way for an electron to interact with ammonia dipoles, implicit in the Catterall and Mott model.

Electrostatic and Quantum Mechanical Models

We need to address explicitly the seemingly very different perspective of the electrostatic models and quantum mechanical calculations in this field (and in other parts of chemistry as well). The quantum mechanical computations include electrostatic interactions in the Hamiltonian, of course. Electrostatic models, of immense explanatory power, are inherently non-quantum mechanical, and macroscopic. They provide an alternative, time-honored, way of explaining energetic relationships. To put it another way, the isolated ammonia molecule has a dipole and higher moments and so does any non-centrosymmetric arrangement of two interacting ammonia molecules. You can calculate the dipole–dipole interaction of two ammonia molecules (or a charge–dipole interaction of an electron with the dipoles), but the quantum mechanical computation on the dimer yields nothing like a dipole–dipole interaction of two ammonia molecules. The latter derives from a classical electrostatic and (on the scale of the individual ammonia molecules) macroscopic model for what happens when two ammonia molecules interact.

The usual philosophical perspective is that incommensurate models (the word is used in the sense of Thomas Kuhn[122]) are a sign of trouble, or a harbinger of conceptual change for a science. We don't agree—we think that such double interpretations are not only typical of real science (chemistry in particular), but good and healthy for chemistry. They allow us to explain and predict, and hence bridge macro and micro worlds in the design of experiment. In the case at hand, that of the solvated electron, the two models are a) an electrostatic model—whereby an electron is stabilized by dipole moments of ammonia molecules oriented in a specific way; and b) a molecular orbital model—the electron in a microscopic a_1 SOMO which features weak but ubiquitous H⇜⇝H bonding between ammonia molecules. We follow the insights offered by the second model, yet do not deny the understanding the first one presents.

7. Further Solvation of $Li(NH_3)_4$: The $[Li(NH_3)_4^+ \cdot e^-@(NH_3)_n]$ Ion-Pairs

7.1. Geometries and SOMOs

The solvated electron cavities cannot be isolated in solution from other species. Due to electrostatic attraction at least some of them will come in close proximity to a cationic monomer, $Li(NH_3)_4^+$, leading to the formation of $[Li(NH_3)_4^+ \cdot e^-@(NH_3)_n]$ ion-pairs.

Another way such ion-pairs can be conceptually constructed is by considering what happens when the number of explicit solvent molecules that interact with $Li(NH_3)_4$ is increased. This process of further solvating $Li(NH_3)_4$ is indicated in Figure 4, as $Li(NH_3)_4 \rightleftarrows [Li(NH_3)_4^+ \cdot e^-@(NH_3)_n]$. The notation implies an ensemble of species, differing in the degree of solvation and separation, in which an electron is effectively partially transferred from $Li(NH_3)_4$ to a nearby ammonia cavity, ultimately yielding the ion-pair.

In Figure 20 we show the geometry of one such neutral aggregate, $[Li(NH_3)_4^+ \cdot e^-@(NH_3)_4]$. There are many possible geometries this ion-pair may have, and we have only considered the one which is illustrated. It has C_{3v} symmetry and consists of an $e^-@(NH_3)_4$ pseudo-tetrahedron situated on

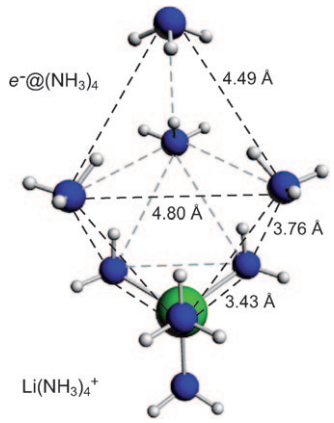

Figure 20. The geometry of an $[Li(NH_3)_4^+ \cdot e^-@(NH_3)_4]$ ion-pair with C_{3v} symmetry. The optimized N–N distances (gas phase) are also provided.

top of one of the triangular faces connecting the nitrogen atoms in the pseudo-tetrahedral $Li(NH_3)_4^+$ ion. The upper and lower tetrahedra are rotated about 60° with respect to each other. For this particular geometry, the nearest-neighbor N–N "intermolecular" distance (3.76 Å) is between a nitrogen in $Li(NH_3)_4^+$ and one in $e^-@(NH_3)_4$.

We have optimized the geometries of a number of these ion-pairs with $1 \le n \le 8$, and their SOMOs are illustrated in Figure 21. We note that given the SOMO delocalization, one could also view these species as $(Li^+ \cdot e^-)@(NH_3)_{4+n}$, that is a partially ionized lithium atom in an ammonia cavity/sea. Examination of the SOMOs reveals that the $3a_1$ orbital of *every* ammonia molecule, whether it is directly bound to lithium or not, is partially occupied. (The SOMO contains a red lobe around every nitrogen, and a gray lobe near every hydrogen. In some cases, it is necessary to lower the contour value slightly from that used in the Figure to see these contributions to the SOMO).

The process by which the LUMO of every ammonia molecule in this ion-pair becomes partially occupied can be thought to occur in one of two different ways. In the first, further solvation of $Li(NH_3)_4$ induces transfer of the electron to ammonia molecules in the second, third etc. solvation

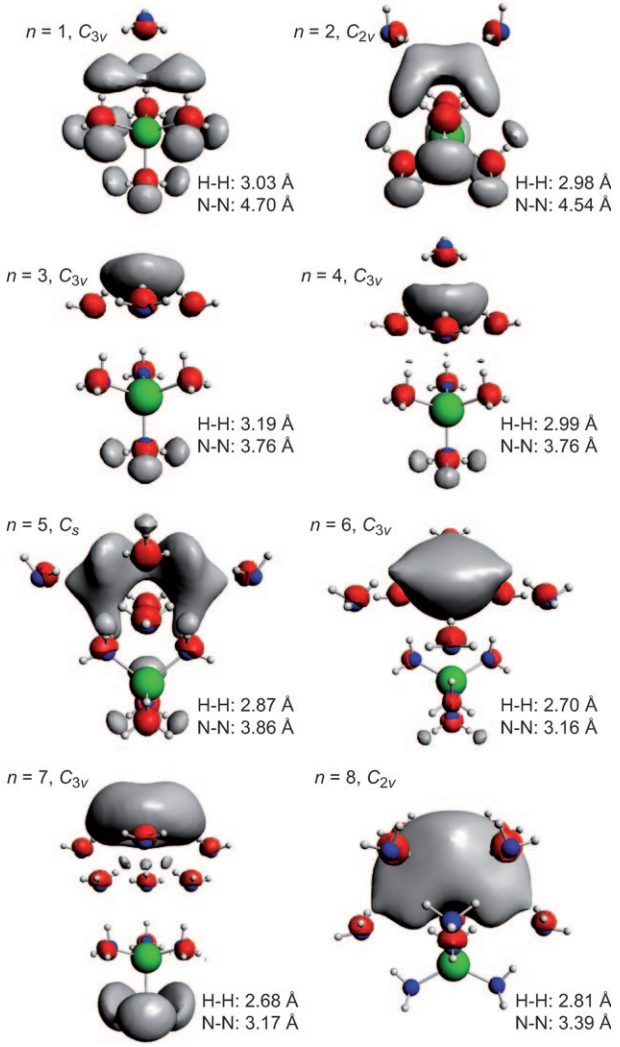

Figure 21. Isosurfaces (±0.015 au–±0.021 au, depending upon the species) of the SOMOs of the $[Li(NH_3)_4^+ \cdot e^-@(NH_3)_n]$ $(1 \le n \le 8)$ optimized ion-pairs. The nearest-neighbor intermolecular H–H and N–N distances in vacuo are also provided. Depending on the structure, these may be either between two ammonia molecules or between $Li(NH_3)_4^+$ and an ammonia molecule.

shells. In the second, the solvated electron species is attracted electrostatically to $Li(NH_3)_4^+$, and when these ions get close enough to each other some charge and spin reorganization occurs. In the next section we will probe the detailed location of the odd electron in the ion-pairs.

There may not be one well-defined geometry that characterizes $[Li(NH_3)_4^+ \cdot e^-@(NH_3)_n]$, but instead an ensemble of local minima, all close in energy to each other. This is due to the fact that there are myriad geometries which may lead to weak H⇜⇝H bonding between the many diffuse, partially occupied NH_3 LUMOs. Our geometry optimizations are limited by the starting geometries we employed, as well as the symmetry constraints used in the calculations. In order to determine the extent to which the geometry influences the energy, we have considered a number of different structural alternatives for the $n=1$ ion-pairs. These include, for example, systems where the hydrogen atoms of $e^-@(NH_3)$ point towards or away from $Li(NH_3)_4^+$.

To evaluate the relative stability of these structures, we calculate ΔE for two different modes of formation, given in Table 5. For $n=1$, the difference between the structures

Table 5: The gas- and solution-phase energies (kcal mol^{-1}) for the formation of the $[Li(NH_3)_4^+ \cdot e^-@(NH_3)_n]$ ion-pairs with $(1 \le n \le 8)$. Two different reaction pathways are considered.

	Reaction 1: $Li(NH_3)_4 + n(NH_3) \rightarrow [Li(NH_3)_4^+ \cdot e^-@(NH_3)_n]$		**Reaction 2:** $Li(NH_3)_4^+ + e^-@(NH_3)_n \rightarrow [Li(NH_3)_4^+ \cdot e^-@(NH_3)_n]$	
n	ΔE_{gas}	ΔE_{solv}	ΔE_{gas}	ΔE_{solv}
1[a]	−2.5–−0.3	−3.6–1.3	−79.0–−76.8	−15.4–−9.9
1[b]	−3.4	−0.2	−79.9	−12.0
2	−0.6	−4.8	−73.2	−7.8
2[b]	−6.2	−0.4	−78.8	−3.4
3	−6.1	−8.3	−75.6	−8.0
4	−6.6	−9.0	−72.8	−9.4
5	−8.5	−8.8	−72.6	−5.0
6	−14.3	−6.9	−75.6	−2.4
7	−17.4	−2.0	−78.0	2.3
8	−21.0	−11.1	−81.9	−9.6

[a] A number of possible geometries were considered. [b] These entries are for "normal hydrogen-bonded geometries" of $[Li(NH_3)_4^+ \cdot e^-@(NH_3)_n]$ similar to those illustrated in Figure 11.

lowest and highest in energy was less than 5 kcal mol^{-1}. The difference was somewhat larger for the calculations performed using the macroscopic solvation model. We also found that the configuration with the lowest gas-phase energy did not yield the most negative energy in solution. Thus, we should take care in drawing strong conclusions based upon these numbers. A molecular dynamics study would provide a fuller picture of the solution.

In order to determine whether or not these species could contain "normal" hydrogen bonds, we have also performed computations on $[Li(NH_3)_4^+ \cdot e^-@(NH_3)_n]$ $(n=1,2)$ whose geometries were similar to those illustrated in Figure 11. For these geometries, the lone pair of an ammonia molecule was oriented so that it pointed towards a hydrogen on $Li(NH_3)_4^+$. As Table 5 shows, the energies of these hydrogen-bonded ion-pairs are comparable to the structures whose SOMOs are illustrated in Figure 21. Thus, these are equally viable species. Examination of the SOMOs of the "normal" H-bonded species showed that also for these geometries the $3a_1$ orbital of every ammonia was partially filled.

As circumspect as we would like to be about the computations, there are some conclusions that we think we can draw. First, solvation has a smaller influence on the formation energies of the ion-pairs (from n ammonia molecules and $Li(NH_3)_4$, the first reaction pathway) then it does on the energetics of Reaction 2, the coming together of separated $e^-@(NH_3)_n$ and $Li(NH_3)_4^+$ species. This is, of course, due to the fact that the reactants and products are neutral in the first reaction. The unpaired electron density in the ion-pairs is nevertheless polarized (an important point to which we will return), so the effect of solvation is not completely negligible. Comparison of the energies of Reac-

tion 1 in Table 5 with those given in Table 4 reveals that whereas the formation energies of the ion-pairs are exothermic for all n, for the isolated cavities this is only the case when $n \geq 5$ and solvation is taken into account. In general for $n \geq 5$, ΔE_{solv} is slightly more negative for the ion-pairs, indicating that they are more stable than the infinitely separated $e^-@(NH_3)_n$ and $Li(NH_3)_4^+$. This is also clearly seen by examining ΔE for Reaction 2 in Table 5. However, if we take into account the fact that it is energetically favorable for $Li(NH_3)_4^+$ to hydrogen-bond with ammonia it appears that $Li(NH_3)_4 + (n+m)(NH_3) \rightarrow [Li(NH_3)_4^+ \cdot e^-@(NH_3)_{n+m}]$, and $Li(NH_3)_4 + (n+m)(NH_3) \rightarrow [Li(NH_3)_4^+ \cdot m(NH_3)] + e^-@(NH_3)_n$ may be competing reactions.

7.2. Where is the Electron in the Ion-Pair?

In order to determine where exactly the unpaired electron is located, we have also examined the net spin polarization of the $[Li(NH_3)_4^+ \cdot e^-@(NH_3)_n]$ $(1 \leq n \leq 8)$ ion-pairs depicted in Figure 21. The spin polarization is defined as the number of spin-α electrons minus the number of spin-β electrons in a given region of space. The calculated values, given in Table 6,

Table 6: The gas-phase net spin polarization (number of spin-α minus spin-β electrons) as determined by a Mulliken population analysis for the $[Li(NH_3)_4^+ \cdot e^-@(NH_3)_n]$ $(1 \leq n \leq 8)$ ion-pairs depicted in Figure 21.[a]

n	$Li(NH_3)_4^+$	$e^-@(NH_3)_n$
1	0.95	0.05
2	0.78	0.22
3	0.54	0.46
4	0.52	0.48
5	0.40	0.60
6	−0.03	1.03
7	0.19	0.81
8	0.17	0.83

[a] The spin polarization has been partitioned into a contribution associated with: $Li(NH_3)_4^+$, and the remaining ammonias $(e^-@(NH_3)_n)$.

have been partitioned into contributions on $Li(NH_3)_4^+$, and on the ammonia molecules making up the cavity. The numbers should be viewed with some caution, since they have been determined using a Mulliken analysis, and our basis contains diffuse functions on lithium which stretch out past the ammonia molecules bound to lithium (see Figure 13). Such unbalanced basis sets give trouble to the Mulliken population analysis. However, the ammonia molecules in the cavity are far away from the lithium atom and we should be able to determine the correct trends for how the spin polarization in $e^-@(NH_3)_n$ varies with n.

In general, as n increases the magnitude of the spin residing on the $Li(NH_3)_4^+$ part of the ion-pair decreases, and that on $e^-@(NH_3)_n$ increases. That is, the more explicit ammonia molecules that are placed in the vicinity of $Li(NH_3)_4$, the greater is the tendency for the electron to be transferred, and to be solvated by the surrounding ammonia molecules. This is also seen in the SOMOs illustrated in Figure 21. For $n = 1,2$, a large part of the wavefunction is located on the ammonia molecules which are coordinated to lithium. On the other hand, for $n = 6,8$ the gray lobe is primarily located between the ammonia molecules making up the cavity.

As we can see from our analysis, in general a smooth transition occurs from the excess electron being mostly on $Li(NH_3)_4$, to predominantly on the ammonia cluster. It is this continuity we mean to evoke by the $Li(NH_3)_4 \rightleftarrows [Li(NH_3)_4^+ \cdot e^-@(NH_3)_n]$ notation we introduced earlier in Figure 4.

7.3. A Different Way of Solvating $Li(NH_3)_4$

We have also considered a more symmetrical way in which $Li(NH_3)_4$ may be solvated, constructed by arranging 12 NH_3 molecules so that each one has an optimal hydrogen-bonding interaction with the central $Li(NH_3)_4$. Essentially, we have added an explicit second solvation shell. Such an aggregate has T_d symmetry. An isosurface of the SOMO is illustrated in Figure 22a. The excess electron is now primarily found within four cavities composed of three ammonia molecules each—perhaps it is more appropriate to write the formula of this species as $[Li(NH_3)_4^+ \cdot e^-@4(NH_3)_3]$.

Visual inspection of the SOMO suggests that the $3a_1$ LUMO of every ammonia is partially occupied. We see the

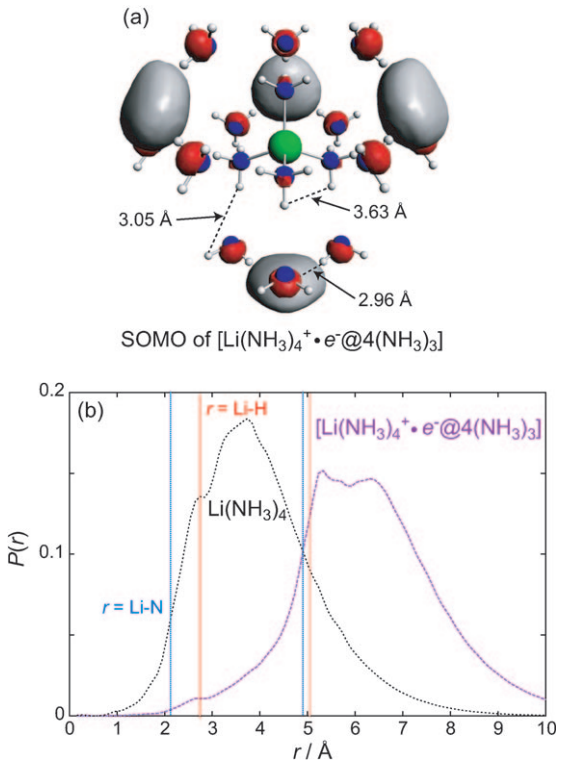

Figure 22. a) An isosurface (±0.015 au) of the SOMO of $[Li(NH_3)_4^+ \cdot e^-@4(NH_3)_3]$, which has T_d symmetry. b) The (gas-phase) probability ($\int P(r)dr = 1$) that the valence electron is a distance r from the lithium nucleus in $Li(NH_3)_4$ and in $[Li(NH_3)_4^+ \cdot e^-@4(NH_3)_3]$. The Li–N and Li–H distances in the first and second solvation shell in $[Li(NH_3)_4^+ \cdot e^-@4(NH_3)_3]$ are denoted by the blue and red lines, respectively.

main H⇜⇝H bonding interaction is between the ammonia molecules making up the four cavities which comprise the second solvation shell. This is because the shortest H–H distance, 2.96 Å, is between the hydrogen atoms in these cavities. For comparison, the shortest H–H distance in $Li(NH_3)_4^+$ is 3.63 Å, and between $Li(NH_3)_4^+$ and $e^-@(NH_3)_3$ is 3.05 Å. Moreover, the ammonia molecules in $e^-@(NH_3)_3$ are not arranged in such a way as to facilitate H⇜⇝H bonding with $Li(NH_3)_4^+$ since their lone pairs are oriented towards the hydrogen atoms in $Li(NH_3)_4^+$.

In Figure 22b we compare the probability to find the unpaired electron a distance r away from the lithium nucleus in $[Li(NH_3)_4^+ \cdot e^-@4(NH_3)_3]$ with that in $Li(NH_3)_4$. For the ion-pair, $P(r)$ starts to increase near the nitrogen atoms making up the first (coordinated) solvation shell, since the LUMOs of these ammonia molecules are partially occupied, albeit to a lesser extent than those of the second solvation shell. There is a sharp increase in $P(r)$ near the nitrogen atoms which comprise the second solvation shell. The most likely place to find the excess electron is slightly farther out than the hydrogen atoms in $e^-@(NH_3)_3$, as indicated by the gray lobes in the SOMO which arise from the H⇜⇝H bonding in the cavities. Clearly, the second solvation shell pulls the electron out even further than it is in $Li(NH_3)_4$.

Will the electron get pulled out even more if we add a third solvation shell? That depends on the geometry of the species, and will change during the dynamics. The system will want to maximize the H⇜⇝H bonding, so the electron will be found in the regions where the H–H distances give a maximal overlap between the diffuse ammonia LUMOs.

8. More than One Electron: Coupled Radicals

The aforementioned $S = {}^1/_2$ systems (each with a single unpaired electron) can interact with each other, giving rise to a plethora of species. We refer to these as *coupled radicals* (CRs) since they may in principle possess several spin states, all potentially close in energy to each other. Experiments indicate that already at very low concentrations, 10^{-3} MPM, the $S = {}^1/_2$ species start to spin-pair.[19,20,33,34,37] For the specific case of lithium–ammonia solutions, magnetic susceptibility studies reveal that between 10^{-3} and circa 0.5 MPM, a maximum spin-pairing takes place.[123] Within this section we will examine the CRs which may form, and also consider their various spin-states. It will be shown that the $S = 0$ spin states are more stable than the $S = 1,2,\ldots$ alternatives. However, the energy differences between the various spin-states are not large (see however, the discussion on energy scales given in the gray box over the page).

The interaction of the CRs could also be the first step in the formation of an electron band in the solution,—a matter of substantial interest in metal–ammonia solutions.

In Equations (1)–(3) we list the reactions between two or more $S = {}^1/_2$ species which lead to the formation of the simplest CRs. Here we only consider systems containing an *even* number of electrons, that is, possibilities such as $[Li(NH_3)_4]_3$ are not examined. Solvation of these will give other aggregates, which can also have a variety of different spin states as shown in Equations (1) and (3). Of course, $2e^-@(NH_3)_{n+m}$ may also be solvated, but we do not show this since it will simply lead to the formation of a larger cavity, or an explicit solvation shell around a smaller cavity. The products of a given reaction may also interact with those of another, giving rise to more complex, still larger systems.

$$n[Li(NH_3)_4] + m[Li(NH_3)_4] \rightarrow [Li(NH_3)_4]_{n+m=r} \xrightarrow{\text{solvation}} [Li(NH_3)_4^+ \cdot e^-@(NH_3)_n]_r \quad (1)$$

$$e^-@(NH_3)_n + e^-@(NH_3)_m \rightarrow 2\,e^-@(NH_3)_{n+m} \quad (2)$$

$$Li(NH_3)_4 + e^- \rightarrow Li(NH_3)_4^- \xrightarrow{\text{solvation}} [Li(NH_3)_4 \cdot e^-@(NH_3)_n] \quad (3)$$

Nothing is simple in the lovely and intricate microcosm of metal–ammonia solutions. So all of these possibilities, and perhaps others we have not yet thought of, need to be considered.

The exact concentration of the different CRs is likely to be critically dependent upon the MPM. For example, since neutron diffraction studies have indicated that at saturation all of the ammonia molecules are incorporated into the first solvation shell of lithium,[51,50] at this concentration one would expect only the unsolvated oligomers in Equation (1), $[Li(NH_3)_4]_r$, to form.

We have examined the CRs listed in Equations (1)–(3), and considered the effect of further solvation. We believe that the results of our calculations can be generalized to provide us with an understanding of the larger, more complex species that ultimately may form in lithium–ammonia solutions.

9. $[Li(NH_3)_4]_r$

As Equation (1) illustrates, two or more $Li(NH_3)_4$ units may interact to form $[Li(NH_3)_4]_r$ oligomers, with either paired or unpaired spins. Let us consider only the unsolvated oligomers here: their interaction with ammonia is discussed in the Supporting Information.

9.1. The Dimer, $[Li(NH_3)_4]_2$

For the dimer, $[Li(NH_3)_4]_2$, we have looked at a number of possible structural and spin ($S = 0,1$) isomers. The optimized geometries and HOMOs of the spin-paired alternatives are given in Figure 23. Their HOMOs are composed of the $4a_1$ SOMOs of $Li(NH_3)_4$; the maximum valence electron density is located around the nitrogen atoms and between the nearest-neighbor hydrogen atoms of the two $Li(NH_3)_4$ units. The gray lobes of these HOMOs are reminiscent of pillows shared by two $Li(NH_3)_4$ clusters. These inter-$Li(NH_3)_4$ bonding regions arise due to weak H⇜⇝H bonding between the SOMOs of the monomer (which, as we have shown earlier, contain character arising from the NH_3 LUMOs). The nearest-neighbor intermolecular H–H and N–N distances are actually quite large, due to the diffuse nature of the $Li(NH_3)_4$ SOMO. The $S = 1$ spin states have one electron in

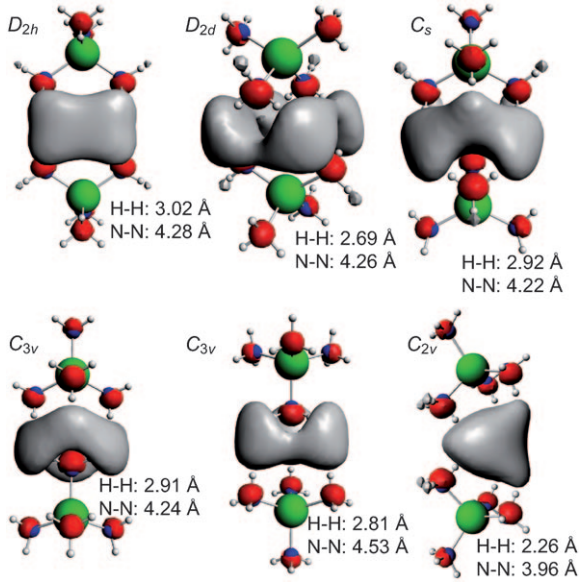

Figure 23. Isosurfaces (±0.02 au) of the HOMOs of the $[Li(NH_3)_4]_2$ coupled radicals with $S=0$, in a variety of geometries. The nearest-neighbor intermolecular H–H and N–N distances in vacuo are also provided.

the MO shown, and one in the corresponding antibonding orbital. The occupation of the latter leads to even longer H–H and N–N distances.

The gas- and solution-phase formation energies per $Li(NH_3)_4$ unit for both spin states are given in Table 7.

Table 7: The gas- and solution-phase energies (kcal mol^{-1}) per $Li(NH_3)_4$ unit for the formation of $[Li(NH_3)_4]_2$ and $[Li(NH_3)_4]_4$ from $Li(NH_3)_4$.[a]

	$2\,Li(NH_3)_4 \rightarrow [Li(NH_3)_4]_2$			
	$S=0$		$S=1$	
Symmetry	ΔE_{gas}	ΔE_{solv}	ΔE_{gas}	ΔE_{solv}
D_{2h}	−3.9	−4.6	0.4	0.0
D_{2d}	−3.7	−4.0	1.1	1.3
C_s	−4.1	−4.9	0.6	0.5
$C_{3v}(1)$	−3.6	−4.2	0.6	0.5
$C_{3v}(2)$	−3.7	−4.3	0.0	0.3
C_{2v}	−3.6	−6.6	0.5	−1.0
	$4\,Li(NH_3)_4 \rightarrow [Li(NH_3)_4]_4$			
	$S=0$		$S=1$	
Symmetry	ΔE_{gas}	ΔE_{solv}	ΔE_{gas}	ΔE_{solv}
C_{2v}	−3.6	−5.2	−0.5	−1.8

[a] The optimized geometries of the dimers and tetramer are illustrated in Figures 23 and 24, respectively.

Solvation has a negligible effect on the binding energy, due to the fact that both the products and reactants are uncharged. Comparison of the formation energies per r of the $S=0$ and $S=1$ systems shows that the former are about 4 kcal mol^{-1} larger in magnitude than the latter. In fact, the energies of the $S=1$ entities are approximately equivalent to that of two infinitely separated $Li(NH_3)_4$ clusters. This indicates that nothing is lost, and nothing is gained, in the formation of the unpaired spin isomers.

As we see, electron spin pairing is slightly favored, by about 4 kcal mol^{-1} per monomer unit. And yet these are classical biradical systems—we already mentioned other examples in chemistry that include carbenes, carbon chains, a multitude of π diradicals, and spin-balanced transition metal complexes. Each has its own peculiarity—that's what makes chemistry fun! Lets look at some general aspects of the CR metal–ammonia systems, focusing on this dimer.

Interestingly—and importantly—we see that the energies of the $[Li(NH_3)_4]_2$, $S=0$ CRs are all almost the same despite the very different geometries, and varying intermolecular distances. These oligomers display intermolecular H⇜⇝H bonding arising from an overlap of the SOMOs of the two individual monomer units. The diffuseness of the $Li(NH_3)_4$ $4a_1$ SOMO, and its approximate spherical character does not lead to a single optimal bonding interaction. To put it another way, the HOMOs of the $S=0$ species are malleable: no matter what the relative orientation of the two monomer units, there is a small bonding interaction, just as good as in any another reasonable geometrical alternative. After all, lithium–ammonia mixtures are liquids and dynamic systems with many local minima all close in energy to each other.

As noted previously, the nearly spherical symmetry of the $Li(NH_3)_4$ SOMO means it is similar to a big hydrogen (or alkali metal) SOMO. Taking the superatom analogy further, $[Li(NH_3)_4]_2$ can therefore be thought of as pseudo-H_2. Other superatom clusters include $AlPb_{10}^-$ and $AlPb_{12}^-$, whose stability has been attributed to their closed-packed structures and optimally filled electron shells.[124]

Thus, the relative orientation of one monomer unit with respect to the second one does not affect the energy of the dimer much (for H_2 it would not affect the energy at all). Moreover, the bonding and antibonding MOs of $[Li(NH_3)_4]_2$ possess the same nodal structure as those of H_2. For $S=0$, two electrons are found in the bonding HOMO, whereas for $S=1$ we have one electron in the bonding and one in the antibonding MO. The solvates of $[Li(NH_3)_4]_r$, $[Li(NH_3)_4^+ \cdot e^-@(NH_3)_n]_r$ are discussed in the Supporting Information.

Energy Scales: A Function of the Measurement, Where One Comes From, and Where the System Goes

In the course of our writing this paper, and the following few sections in particular, we came to an interesting mild disagreement among the co-authors. A typical CR problem is that one has singlet and triplet states separated by an energy an order of magnitude smaller than an N–H or an O–H or a C–H bond strength. For one of us the characteristic singlet–triplet splitting we calculate, 4.0 kcal mol^{-1} = 0.17 eV molecule^{-1}, seemed a small number, to the other a largish number.

Whence this difference in attitude? The person to whom 4 kcal mol^{-1} was small was thinking about kinetic persistence

of a molecule. So for a bimolecular reaction, with an initial concentration of 0.001M, pre-exponential factor of 10^5, a half-life of a day at room temperature requires an activation energy of 16.7 kcal mol^{-1}. The person to whom 4 kcal mol^{-1} was large was thinking of magnetism and magnetic resonance: typical Zeeman energies are about 10^{-4} eV, our spin-pairing energy is around 10^3 times that, or near $10\,kT$.

Admittedly, for dilute lithium–ammonia solutions, optical excitation (responsible for the fine blue color) and thermal excitation of electrons across a semiconducting energy gap (responsible for the conduction of electric current) are energy processes typically in the range of 0.5–5 eV. However, with increasing lithium concentration, our blue, electrolytic (semiconducting) solutions continuously transform into bronze, metallic liquids (Figure 1)—magnificent conductors of electricity. A basic issue will ultimately be: "How can one interrogate—and thence understand—the inevitable changes in the electronic wavefunction of our isolated or solvated electron as it transforms to the itinerant, delocalized electron in concentrated solutions?" In these fundamental considerations, it has been recognized for some time that magnetic, and magnetic resonance properties (in particular ESR) detect the progressive onset of such delocalization effects at much lower metal concentrations (carrier concentrations) than those seen from transport or optical property measurements.

In particular, magnetic resonance measurements are sensitive not only to the complete delocalization of carriers (obviously a signature of metallization), but also to the partial delocalization of the electronic wavefunction over, say, several sites in embryonic clusters in the approach to the metallic state.[47] Note that this latter process occurs without *the creation of free carriers and without the concomitant large scale changes in transport and optical properties.* Variations in the solvated electron inter-site exchange or effective hopping energy, arising from changes in the solvated electron wavefunction via the formation/break-up of microscopic cluster assemblies, need only to be of the order of the magnetic Zeeman or hyperfine energies (both typically in the range of 10^{-4} eV) for noticeable effects to be seen, for example, in electron spin relaxation rates.

In contrast, to detect the extensive delocalization of charge carriers by transport or optical properties requires the formation of thermally induced carriers, a process—certainly in dilute and intermediate concentration solutions—typically involving energy changes in the range of 0.1–5 eV. Obviously *at* the metallization point itself, such differences are not evident as the solvated electron wavefunction now transforms to that of an itinerant, delocalized state. Thus, in sodium–ammonia solutions, magnetic resonance, transport, optical, and thermodynamic properties suggest the rapid onset of complete delocalization (metallization) of the electronic wavefunction at concentrations greater than circa 5 MPM. However, remarkably, magnetic properties foretell a distinct change in the electronic structure of the solvated electron at concentrations between 0.5–1 MPM (where the electrical conductivity stands only at ca. 0.1 ohm^{-1} cm^{-1}).

Fundamental differences in energy scales as requirements for detecting changes *in electronic structure for metal solutions* (and indeed in all systems undergoing a TMS) must always be borne in mind. Indeed, the differences may, in part, account for disparities often found when comparing critical conditions for the TMS in materials and systems using different physical techniques.

The reader may be exasperated with our mixed use of units. The energies should be given in kJ mol^{-1} or eV molecule^{-1}. Most of the chemical community is used to kcal mol^{-1} for stability and thermochemical considerations, and to eV or wavenumbers/molecule for spectroscopic quantities—to be discussed shortly—while the physical community tends to favor eV molecule^{-1} for all. Here, the chemical convention will be followed. However, we note that 1 eV molecule^{-1} = 23.06 kcal mol^{-1} = 96.5 kJ mol^{-1} = 8066 cm^{-1}.

9.2. Larger Clusters of $Li(NH_3)_4$

For $r = 4$ two high-symmetry geometries that come to mind are square planar and tetrahedral. The level patterns for four s-type orbital interacting (D_{4h} and T_d pseudosymmetry) are $a_{1g} < e_u < b_{2g}$ for square planar, and $a_1 < t_2$ for tetrahedral. For a low-spin four-electron system, these systems are both Jahn–Teller active, expected to distort.

We have optimized the geometry of a rectangularly distorted square-planar tetramer with $S = 0$ and $S = 2$ spin states. Isosurfaces of the (HOMO-1) and HOMO of the spin-paired CR are shown in Figure 24. The former has a bonding

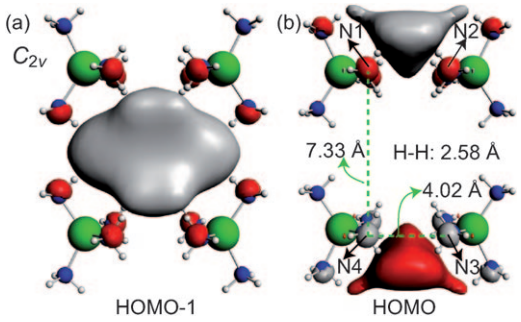

Figure 24. Isosurfaces (±0.016 au) of the a) (HOMO-1) and b) HOMO of a $[Li(NH_3)_4]_4$ coupled radical with $S = 0$. The nearest-neighbor intermolecular H–H and selected N–N distances in vacuo are also provided. Note: $N_1–N_2 = N_4–N_3$ and $N_1–N_4 = N_2–N_3$.

interaction in the center of the cluster between all of the $Li(NH_3)_4$ species and is of s pseudosymmetry, whereas the latter is of p pseudosymmetry. That is, it contains one node which bisects the long side of the rectangle. The LUMO (not shown) also has one node, perpendicular to the node of the HOMO. The (LUMO + 1) has two nodes, as expected. For the $S = 2$ systems, a single electron occupies each one of these four orbitals. They are just what one would expect for the MOs of a Jahn–Teller distorted H_4 or the π orbitals of cyclobutadiene. In Figure 25 we schematically illustrate these four orbitals for a rectangular H_4 cluster.

Clearly, the electron density obtained from the HOMO and (HOMO-1) displays a maximum between the hydrogen

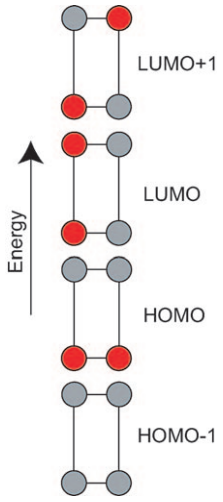

Figure 25. A schematic representation of the orbitals of an H_4 rectangle with $S=0$.

atoms belonging to monomers closest to each other. In fact, for clusters of any size, even solids, our results suggest that the maximum electron density arising from the valence electrons will be between the hydrogen atoms. This agrees with the results of plane-wave calculations on the molecular crystal of $Li(NH_3)_4$ which found that the electron density associated with the conduction states "wets" the hydrogen atoms and only partially fills the voids.[107] The nearest-neighbor intermolecular H–H and N–N distances in the tetramer are similar to those in the dimers.

Comparison of the formation energies of the $S=0$ spin isomers per $Li(NH_3)_4$ unit in the last row of Table 7 with those in the first six rows, reveals that they are all about 4 kcal mol^{-1}. Once again this illustrates that there is effectively no optimal configuration of $Li(NH_3)_4$ units. The gas- and solution-phase energies of the $S=2$ CR are only slightly lower than that of four isolated monomers, i.e., these systems display nearly negligible bonding between the $Li(NH_3)_4$ species. The N_1–N_2/N_4–N_3 and N_1–N_4/N_2–N_3 distances are 6.56 Å and 7.67 Å, respectively. That is, the fully spin-unpaired CR is more "square" than the more stable, spin-paired alternative. It is not possible for this system to attain full D_{4h} symmetry due to the underlying quasi-T_d symmetry of the constituent $Li(NH_3)_4$ units.

Is there a band building up from the interaction of $Li(NH_3)_4$ units? For the dimers we have considered, the splitting of the bonding and antibonding levels ranges from 0.37–0.53 eV; whereas in the tetramer the difference between the highest and lowest levels of the four level miniband is 0.036 eV, an order of magnitude smaller. This suggests that metallization and band formation could indeed be due to the aggregation of $Li(NH_3)_4$ units. In a future study, we will look at the build-up of this band.

10. Two Electrons in a Cavity: $2e^-@(NH_3)_n$

Another set of CRs can be formed from the interaction of two cavities, each "containing" a single electron ($e^-@(NH_3)_n$). There are two possible products of this reaction: a single large cavity with a net charge of −2 ($2e^-@(NH_3)_{n+m}$), or two singly charged cavities in close proximity to each other ($[e^-@(NH_3)_n \cdot e^-@(NH_3)_m]$). In the old nomenclature, these may be denoted as $(2e^-)_s$ and $e_s^- \cdot e_s^-$, respectively. Both have been invoked in the previous literature to explain the observed spin-pairing.[125–129] In both cases, the electrons may be either spin-paired ($S=0$) or unpaired ($S=1$). This set of CRs could also be formed via the transfer of two electrons from two $Li(NH_3)_4$ species to a cluster of ammonia molecules. We will consider both reaction pathways shortly.

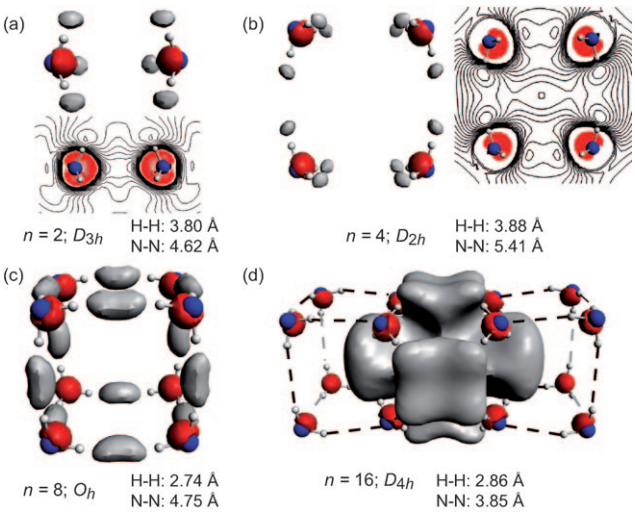

Figure 26. Isosurfaces (±0.0125 au–±0.015 au, depending upon the species) and contour diagrams ($n=2,4$) of the HOMOs of $2e^-@(NH_3)_n$ species with $n=2,4,8,16$ and $S=0$. The plane of the contours bisects one set of N–H bonds. The nearest-neighbor intermolecular H–H and N–N distances in vacuo are also provided.

In Figure 26 we illustrate the HOMOs and optimized geometries of $2e^-@(NH_3)_n$ ($n=2,4,8,16$) $S=0$ species. We note that for the clusters containing 4 and 16 ammonia molecules, the initial starting guesses for the geometry optimizations consisted of two $e^-@(NH_3)_2$ and two $e^-@(NH_3)_8$ cavities nearby each other. In both cases, the geometry optimization led to a single large cavity, suggesting that the formation of separated yet associated $[e^-@(NH_3)_n \cdot e^-@(NH_3)_m]$ entities is unlikely.

Comparison of the MOs in Figures 26 and 18 illustrates that the SOMOs of $e^-@(NH_3)_n$ differ slightly from the HOMOs of $2e^-@(NH_3)_n$. Nonetheless, the HOMOs of these CRs are also characterized by weak H⇜⇝H bonding interactions which occur due to the overlap of the partially filled NH_3 LUMOs, in complete analogy to what was found for the single electron in a cavity, $S=1/2$, systems. For the isomers with unpaired spins, one electron occupies the bonding orbitals illustrated in Figure 26, while the other electron resides within a p-like MO with a single node.

The nearest-neighbor intermolecular H–H and N–N distances provided in Figure 26 are once again large, due to the diffuseness of the ammonia $3a_1$ orbitals. It appears that for a given geometry, the equilibrium distances are bigger for $e^-@(NH_3)_n$ than for $2e^-@(NH_3)_n$ if n is small, whereas for large n the opposite occurs (compare the distances for $n=2,4,8$ provided in Figures 17 and 18, with those given in Figure 26). However, the limited amount of data prevents us from generalizing this to all possible geometries.

For all of the systems we have considered, the $S=1$ CRs are higher in energy than their $S=0$ counterparts in gas and solution phase, indicating that spin-pairing is likely to occur. The first reaction in Table 8 illustrates that the formation of a large cavity containing two spin-paired electrons from two singly charged, smaller cavities is energetically unfavorable in the gas phase. This is likely a result of electrostatic repulsion between the negative charges. Since macroscopic solvation

Table 8: The gas- and solution-phase energies (kcal mol^{-1}) for the formation of the $2e^-@(NH_3)_n$ with $n=2,4,8,16$. Two different reaction pathways are considered.[a]

	Reaction 1: $2[e^-@(NH_3)_{n/2}] \rightarrow 2e^-@(NH_3)_n$				**Reaction 2:** $2Li(NH_3)_4 + n(NH_3) \rightarrow 2Li(NH_3)_4^+ + 2e^-@(NH_3)_n$			
	$S=0$		$S=1$		$S=0$		$S=1$	
n	ΔE_{gas}	ΔE_{solv}	ΔE_{gas}	ΔE_{solv}	ΔE_{gas}	ΔE_{solv}	ΔE_{gas}	ΔE_{solv}
2	38.1	−9.2	28.2	5.0	191.1	14.4	190.7	29.7
4	32.7	−6.5	30.1	5.1	177.9	−0.4	184.8	12.3
8	34.4	−5.0	39.8	9.4	166.9	−4.1	181.8	11.4
16	11.1	−8.4	18.6	−5.2	133.0	−11.5	150.0	−7.2

[a] $2e^-@(NH_3)_n$ illustrated in Figure 26.

has a greater stabilizing effect on the doubly charged species than on the singly charged ones, ΔE_{solv} is exothermic. We should keep in mind, however, that only $e^-@(NH_3)_n$ with $n=$ 5–8 were predicted to be stable. Thus, even though the formation of $2e^-@(NH_3)_4$ from two $e^-@(NH_3)_2$ is exothermic, such a reaction will not occur since $e^-@(NH_3)_2$ is not stable.

Perhaps Reaction 2, the formation of $2e^-@(NH_3)_n$ and $2Li(NH_3)_4^+$ from $Li(NH_3)_4$ and ammonia, provides a better indicator of the likelihood of formation of the $2e^-@(NH_3)_n$ aggregates. Macroscopic solvation naturally stabilizes the doubly charged species and lowers ΔE by 73–90 kcal mol^{-1}, per e^-. The effect of solvation on the formation energies of $2e^-@(NH_3)_n$ is even greater than for the $e^-@(NH_3)_n$ species (see Table 4), since now we are dealing with doubly, as opposed to singly charged systems. When solvation is taken into account, our results predict that $2e^-@(NH_3)_n$ with $n \geq 4$ and $S=0$ may be stable.

11. Ammoniation of $Li(NH_3)_4^-$: The $[Li(NH_3)_4 \cdot e^-@(NH_3)_n]$ Coupled Radicals

$Li(NH_3)_4^-$, which may be formed via the addition of an unsolvated electron to $Li(NH_3)_4$, is in itself a CR, since it may conceivably have either an $S=0$ or $S=1$ spin state. The spin-paired isomer is 8.4 and 3.7 kcal mol^{-1} more stable, in gas and solution phase, respectively. As the right-hand side of Equation (3) shows, solvation of this cluster by ammonia molecules yields species with the formula $[Li(NH_3)_4 \cdot e^-@(NH_3)_n]$ that are CRs as well.

This set of CRs can also be produced via the addition of one more electron to the $S={}^1/_2$, $[Li(NH_3)_4^+ \cdot e^-@(NH_3)_n]$ ion-pairs illustrated in Figure 21 above. Another way of writing the formula for these entities, $[e^-@(NH_3)_{n/2} \cdot Li(NH_3)_4^+ \cdot e^-@(NH_3)_{n/2}]$, immediately shows that they can be viewed as the "ion-triples" ($e_s^- M_s^+ e_s^-$), which have been previously proposed in the literature.[45,46,48,130] The alternative notation: $Li(NH_3)_4^- \rightleftarrows [Li(NH_3)_4 \cdot e^-@(NH_3)_n]$, makes the point that once again this is a system with a range of internal electron transfer. These species are discussed further in the Supporting Information. Importantly, for all of the structures we considered, those with $S=0$ were lower in energy.

12. An Overview of the Systems Present at Different Concentrations

We want to turn what we have learned from our molecular calculations into a picture of lithium–ammonia solutions. Before we do so, it's important to explicitly write down the limitations we face.

1. While we have explored the most likely species, and tend to see their correspondence to the suggestions in the literature, theoretical and experimental, perhaps we missed some of import. Metal–ammonia solutions are a complex kinetic system. Not as complex as the atmosphere or a eukaryotic cell, but still very complicated.[131]
2. What sense does it make to talk of a discrete molecular species, even with explicit or implicit account of solvation, in a liquid? To the extent that there is directly observable short range order in lithium–ammonia solutions (such as has been observed using neutron diffraction studies[50,51]) we believe that there is ample reason to proceed.
3. Several of the structures we have considered lie on a potential energy surface with many energetic minima not well separated in energy. And the barriers between the

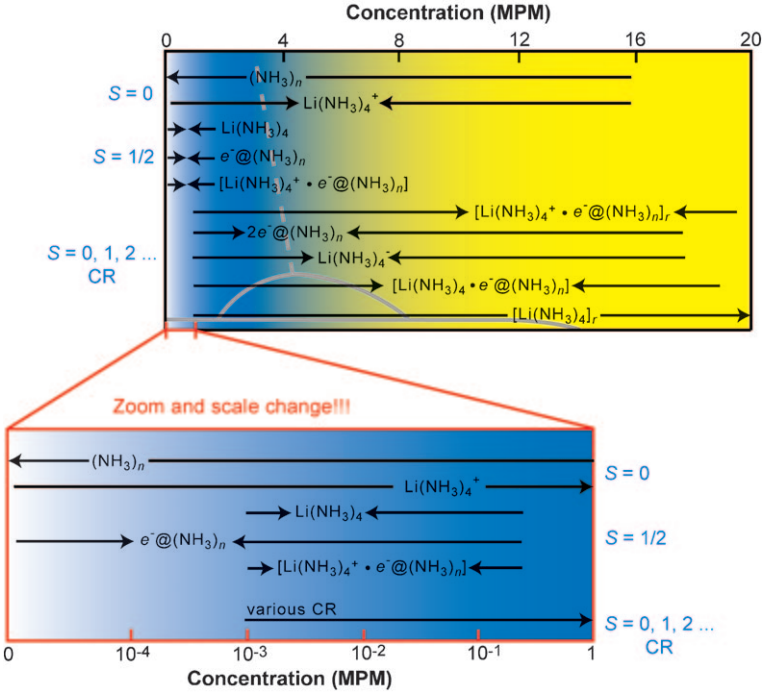

Figure 27. The species which are present in lithium–ammonia solutions, as derived from a combination of the theoretical work done here, and experimental information (see Figures 2 and 3). The black horizontal lines indicate the rough MPM region in which certain species are present. The arrows point to the MPM region where the species are at their highest concentration. The electronic spin (S) of groups of species is also shown. We provide a blow-up of the region between 0–1 MPM, in a logarithmic plot, since many things happen within this concentration regime. It should be emphasized that this is a very schematic picture: so far we only have a good idea of where the most simple species (i.e. $(NH_3)_n$, $[Li(NH_3)_4]_r$) lie on this plot.

local minima are not high (as they are, for instance, in organic chemistry). To put it one way, the entropy change in a free energy expression may be an important factor. We do not calculate it here. To put it another way, in order to supplement our present perspective, molecular dynamics, not done by us, is advisable.

With our limitations voiced, we think we do have a rough idea of what occurs in metal–ammonia solutions across a broad concentration range. In Figure 27 we provide a schematic picture of the species which may be present at various MPMs. There will also be a temperature dependence, but we do not address it here. These species will be discussed in more detail below, focusing on specific concentration regimes.

12.1. Dilute Solutions

For extremely low MPM ($<10^{-3}$), electron spin-pairing has not yet occurred, due to the fact that the concentration of the solvated electron is too low. That is, the probability that two electrons come in close enough proximity to form a CR is negligible. Therefore we need only to consider the $S=0$ and $S=^1/_2$ systems listed in Figure 4, i.e., the molecules which are not CRs. These are the five uppermost species indicated in Figure 27.

Clearly, one of the dominant entities in solution will be dynamic clusters of two or more ammonia molecules hydrogen-bonded to each other, $(NH_3)_n$. Upon addition of the metal, some of the ammonia molecules will react with lithium preferentially yielding $Li(NH_3)_4$—$LiNH_3$, $Li(NH_3)_2$, and $Li(NH_3)_3$ may be found, but will have a lower concentration. As we have shown in Section 5, this reaction is quite exothermic. The formation of (infinitely separated) $Li(NH_3)_4^+$ and $Li(NH_3)_4^-$ from $2\,Li(NH_3)_4$ units was found to be endothermic by 63.0/15.1 kcal mol^{-1} in gas/solution phase, indicating that the neutral monomer is more stable than the ions.

As illustrated in Section 6, the formation of infinitely separated $Li(NH_3)_4^+$ and $e^-@(NH_3)_n$ from $Li(NH_3)_4$ and $n$$NH_3$ may occur if the cavity contains between 5–8 ammonia molecules. In general, the ion-pairs $[Li(NH_3)_4^+\cdot e^-@(NH_3)_n]$ were more stable than the separated $Li(NH_3)_4^+$ and solvated electrons (Table 5). Yet, since $Li(NH_3)_4^+$ may hydrogen-bond with ammonia, $Li(NH_3)_4+(n+m)\,(NH_3)\rightarrow[Li(NH_3)_4^+\cdot e^-@(NH_3)_{n+m}]$, and $Li(NH_3)_4+(n+m)\,(NH_3)\rightarrow[Li(NH_3)_4^+\cdot m\,(NH_3)]+e^-@(NH_3)_n$ may be competing reactions.

In summary, even for low lithium concentrations many species may be found. These include ammonia molecules hydrogen-bonded to each other, $Li(NH_3)_4$, and the $[Li(NH_3)_4^+\cdot e^-@(NH_3)_n]$ ion-pairs. It is likely that most free $Li(NH_3)_4^+$ will form hydrogen bonds with ammonia molecules. Also, the isolated electron in a cavity species, $e^-@(NH_3)_n$, with $n=5$–8 are likely to be found. Our results suggest that the concentration of $Li(NH_3)_4$ will be greater than that of $Li(NH_3)_4^-$ and $Li(NH_3)_4^+$. The ion-pairs are also more likely to form than $Li(NH_3)_4^+$ and $e^-@(NH_3)_n$. And the location of the electron may be better indicated by the continuum $Li(NH_3)_4\rightleftarrows[Li(NH_3)_4^+\cdot e^-@(NH_3)_n]$.

12.2. Intermediate Concentration Range

This concentration range is perhaps the most difficult to describe, since within it spin-pairing starts to occur. It also marks the build-up towards the TMS. In principle *all* of the species illustrated in Figure 27 may be found in this range, but their concentrations will be dependent upon the MPM. They depend on temperature as well, but this is something we do not consider in our static calculations.

Let us start by outlining what may happen as we increase the concentration of the solvated electrons, so that that the probability of them coming in close enough proximity to interact with each other is high. Two or more of the $S=^1/_2$ species mentioned above can interact, yielding some of the CRs listed in Figure 4 and described above. Possible reactions were given previously in Equations (1)–(3). As indicated, solvation of the simplest CRs by ammonia leads to the formation of other species which are CRs as well. Our calculations showed that the spin-paired isomers were always lower in energy than those with $S=1,2$. As more lithium is added, the concentration of the $S=0$ CRs will increase, and that of the $S=^1/_2$ systems will decrease until at a certain point only the CRs (and other $S=0$ systems such as ammonia) will be found.

Some of the possible species which may be present in the solution in this concentration range include: $(NH_3)_n$, $Li(NH_3)_4^-$, $Li(NH_3)_4^+$, $[Li(NH_3)_4]_r$, $2\,e^-@(NH_3)_n$, $[Li(NH_3)_4^+\cdot n\,(NH_3)]$, as well as the $[Li(NH_3)_4^+\cdot e^-@(NH_3)_n]_r$ ion-pairs and $[Li(NH_3)_4\cdot e^-@(NH_3)_n]$. The number of potential species is greater than this, since each one of these CRs can interact with other ones to give still-larger CRs. The location of the electron may also vary with solvation, as implied by the $\rightleftarrows$ notation.

Two nearby cavities each containing a single electron, $[e^-@(NH_3)_n\cdot e^-@(NH_3)_m]$, are unlikely to be found, since these species optimized to give a single large cavity containing two electrons, $2\,e^-@(NH_3)_{n+m}$. The formation of $2\,e^-@(NH_3)_n$ and $2\,Li(NH_3)_4^+$ from $2\,Li(NH_3)_4$ and ammonia was found to be exothermic only for $n\geq 4$ (see Section 10). In general the $[2\,Li(NH_3)_4^+\cdot 2\,e^-@(NH_3)_n]$ solvates of $[Li(NH_3)_4]_2$ were lower in energy (see the Supporting Information), however since $Li(NH_3)_4^+$ may hydrogen-bond with ammonia $2\,Li(NH_3)_4+(n+m)\,(NH_3)\rightarrow[2\,Li(NH_3)_4\cdot 2e^-@(NH_3)_{n+m}]$ and $2\,Li(NH_3)_4+(n+m)\,(NH_3)\rightarrow[2\,Li(NH_3)_4^+\cdot m\,(NH_3)]+2\,e^-@(NH_3)_n$ may be competing reactions for large n. As we show in the Supporting Information, the formation of $[Li(NH_3)_4\cdot e^-@(NH_3)_n]$ and $Li(NH_3)_4^+$ from $Li(NH_3)_4$ and $[Li(NH_3)_4^+\cdot e^-@(NH_3)_n]$ is exothermic (in solution) even for small n.

Which CRs are present will depend crucially on the MPM. For example, for still relatively low metal concentrations there will not be enough $Li(NH_3)_4$ to give a substantial amount of $[Li(NH_3)_4]_r$ clusters, and other species such as $2\,e^-@(NH_3)_n$ may form. For high lithium concentrations, of course the opposite will be true. Also, since $2\,e^-@(NH_3)_n$ are only stable for large n, as we increase the MPM it is likely that their concentration decreases, whereas that of $[2\,Li(NH_3)_4^+\cdot 2\,e^-@(NH_3)_n]$ and $[Li(NH_3)_4\cdot e^-@(NH_3)_n]$ increases. We have schematically illustrated these trends in Figure 27.

Clearly, within this concentration range a large variety of species may be present. These include the CRs and the $S=0$ systems listed in Figure 4. Importantly, for all of the CRs we have considered, the spin-paired ones were lower in energy and are therefore more likely to be found. (Recall here the box on energy differences, and the different view that given techniques of experimental measurement engender). For example, the $S=0$ $[Li(NH_3)_4]_r$ are about 4 kcal mol^{-1} per r more stable than those with $S=1$. The higher-spin states are potentially occupied, as they are not that high in energy. What is clear from experiment is that the approach to the TMS (from the dilute, electrolytic side) is characterized by high concentrations of bipolaronic $S=0$ states.[32,3] The build-up of metallic bonding from this viewpoint remains to be studied.

The SOMOs of all of the CRs showed inter- and intramolecular H⇜⇝H bonding arising from the overlap of the partially filled ammonia $3a_1$ LUMOs. If we view a metal as being a system in which all of the electrons are completely delocalized, then one could perhaps say that the TMS occurs when *all* of the ammonia $3a_1$ orbitals are partially occupied.

12.3. Saturated Solutions

In saturated lithium–ammonia solutions (20–21 MPM), there are approximately four ammonia molecules for every lithium atom. Neutron diffraction experiments have shown that at this concentration all of the ammonia molecules are incorporated into the first (tetrahedral) solvation shell of the lithium atoms and that the hydrogen bonding in ammonia is completely destroyed.[51] These findings suggest that the dominant species present in saturated solutions are CRs which are built up from the $Li(NH_3)_4$ monomer. This is why in Figure 27 we indicate that $[Li(NH_3)_4]_r$ has its highest concentration at about 20 MPM.

As we have shown in Section 9 these monomer units can interact with each other to form a variety of $[Li(NH_3)_4]_r$ CRs. In all of the cases studied by us (dimers and tetramers so far) the $S=0$ species were more stable than higher spin states, indicating that spin-pairing is preferred. There was little preference for one geometry over another. The higher spin isomers lie not much higher in energy. For a given r, all of the geometrical isomers considered had roughly the same energies, suggesting there is no long-range order.

Our results so far indicate that saturated lithium–ammonia solutions are composed primarily of $[Li(NH_3)_4]_r$ where the electrons are spin-paired. Interestingly, ^{23}Na and ^{14}N Knight shifts in concentrated sodium–ammonia solutions as a function of temperature indicate thermal excitation of the electrons from a diamagnetic state into the conduction band—even near saturation.[132] This is a dynamic system with a rapid and facile interconversion between different dimers, tetramers, etc. It is noteworthy that in all of the species we have considered, the intermolecular N–N and H–H distances are quite large. The HOMOs show H⇜⇝H bonding between the nearest-neighbor hydrogen atoms, and contain a substantial contribution from the ammonia $3a_1$ LUMOs. A metallic band begins to build up.

13. The Absorption Spectrum of Metal–Ammonia Solutions

Perhaps part of the enduring fascination of metal–ammonia solutions lies in the strikingly beautiful blue color associated with the very dissolution process in dilute solutions. Indeed, Davy noted just over 200 years ago, the highly visual signature of these solutions—their "*fine blue colour*" (Figure 1).

Qualitatively, all dilute metal–ammonia solutions have absorption curves which are indistinguishable spectroscopically; each consists of a single absorption band, centered within the range of 0.8–0.88 eV.[130] The shape and location of the electronic transition do not change much in going from lithium to cesium in the alkali metals, nor from lithium to calcium to strontium. The metals europium and ytterbium also yield very similar absorption spectra.[33] Ammonia itself has combination bands in the same spectral region, but the absorption we speak of is a broad, well-characterized band, easily distinguished from the ammonia IR bands. The source of the remarkable blue color of metal–ammonia solutions is a long absorption tail of that band, trailing off to about 1.8 eV. Because of its metal independence—and the fact that similar bands are found in pulse radiolysis of *only* liquid ammonia,[133] the absorption band has been attributed to the ammoniated, or solvated electron.

The first reasonably complete and quantitative investigation of the absorption spectrum of sodium and potassium–ammonia solutions was carried out by Douthit and Dye.[134] Later work with other alkali, alkaline earth, and lanthanide metals, confirmed that the blue color was associated with an electron-containing species—the solvated electron.[135] A typical experimental example of the optical absorption spectrum is illustrated in Figure 28. Essentially the same spectrum has been obtained in recent femtosecond pump-probe experiments.[136]

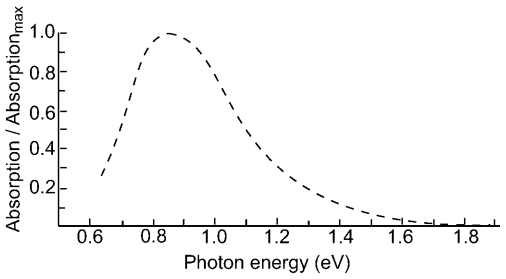

Figure 28. The experimentally obtained absorption spectrum due to the solvated electron.[137] Data taken from Ref. [33].

A particularly transparent, and at the same time quantitative model of the optical absorption of infinitely dilute metal–ammonia solutions was provided by Jortner in 1959.[114] He pictured the electron as being trapped within a cavity of ammonia molecules, as illustrated earlier in Figure 14d. The solvent was assumed to be a continuous and homogeneous medium with a low- and a high-frequency relative permittivity. The interaction of the electron with the medium gave rise

to a constant potential within, and a varying potential outside the cavity, shown above in Figure 15. Jortner provided a variational solution for the ground 1s and first excited 2p levels of such a potential, and the absorption maximum was attributed to a transition between the two electronic states. Assuming a cavity radius of 3–3.2 Å the energy of the 1s→2p transition was calculated to be 0.8 eV, in excellent agreement with experiment.

Jortner's model has been successful and influential, even as its limitations have been noted. For instance, in its simplest form, Jortner's model does not accurately describe the asymmetric long tail, the lineshape, nor the dependence of the absorption maximum on the temperature and concentration.[33] The slight red shift of the band with increasing concentration correlates well with a decrease in the paramagnetic molar susceptibility of the solutions, suggesting that it is a result of the formation of diamagnetic species.[130,138,139]

A later structural model for localized excess electron states in polar solvents, with particular reference to dilute metal ammonia solutions, was advanced by Copeland, Kestner, and Jortner.[140] This model took into account both the strong, short-range interactions of the electron and the first coordination layer of solvent molecules. It also considered the long-range interactions with the bulk ammonia medium. Even though the model provides predictions of the locations of higher electronic excited states for solvated electrons in ammonia, the lineshapes and other properties of the optical transition did not agree with experiment. Nevertheless, there is no question that Jortner's model captures the essential physics of the electronic transition.

With this background, we turn to the calculation of the vertical excitation energies of a number of species likely to be present in metal–ammonia solutions. The focus is again on very dilute solutions, those in which spin-pairing has not yet occurred. Solutions containing calcium, strontium, ytterbium, and europium have not yet been considered by us. We also do not attempt to model the temperature and concentration dependence. Such future studies could be carried out by averaging over the spectra obtained for snapshots taken during a molecular dynamics simulation.

13.1. Technicalities, and Initial Problems with Calculating the Spectra of the Solvated Electron

One way to calculate the excitation energies and oscillator strengths of large molecules from first principles is by time-dependent density functional theory (TD-DFT). Solvent effects can be incorporated using continuum solvation models. However, the computation of electronic transitions with DFT is not as straightforward as energetics or geometries, and errors of up to 0.5 eV are not untypical in TD-DFT calculations of excitation energies. In certain unfortunate situations TD-DFT can lead to dramatic errors, for example for charge-transfer excitations.[141] The Supporting Information contains a discussion of another way to calculate excitation energies, the Δ-SCF method,[142] which we used to check our results.

Our natural inclination was to first consider the $e^-@(NH_3)_n$, electron-in-a-cavity species from Section 6. Unfortunately, the excitation energies (both TD-DFT and Δ-SCF) for these entities were exceptionally sensitive to the basis set on hydrogen in gas and solution phase. Shkrob has performed TD-DFT calculations on a few $e^-@(NH_3)_n$ species.[110] Only one of these, an octamer, gave a bound excited state and the transition energy was 1.2 eV.

The asymptotically corrected SAOP functional, which has been shown to yield high-quality vertical excitation energies, in particular for Rydberg-like states[143] also did not alleviate our problems. We concluded that the excitations calculated for these isolated anionic aggregates, which involve transitions between very diffuse orbitals, are not reliable enough to make any meaningful conclusions.

13.2. Better Luck with Ion-Pairs

We did not give up after our technical problems with TD-DFT calculations on the solvated electron, and tried again with the ion-pairs $[Li(NH_3)_4^+ \cdot e^-@(NH_3)_n]$. As we will see, in the process we obtained an explanation of the lineshape of the absorption.

How to Read our Transition Diagrams

The transition diagrams we will show in this section have some features that may be unfamiliar, so a word of explanation is in order. The normal chemist's picture of an excitation is shown in the left of Figure 29. The TD-DFT calculations which we do are based on the doublet configuration, where $N_\alpha = N_\beta + 1$ (we have one more "spin-up" than "spin-down" electron). As a consequence of the unrestricted ground-state calculations employed, the α and β orbitals have

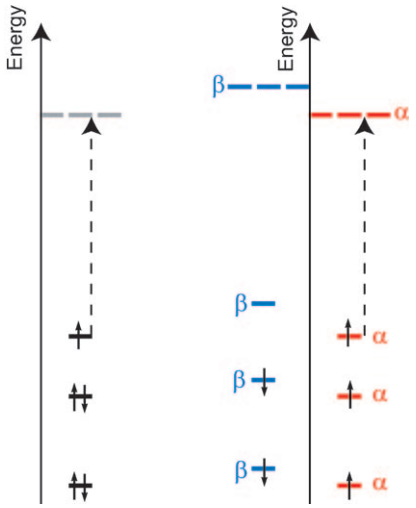

Figure 29. A schematic picture of the lowest-energy excitation in a molecule with a single unpaired electron.

different energies. The difference is small for doubly occupied levels; it can be substantial for a SOMO.

The level scheme (right of Figure 29) seems more complicated for it shows twice as many levels as the conventional diagram. But there is a close correlation between the two ways of looking at excitations. Since spin is conserved in these electronic transitions, we can never have an excitation from an "α" to a "β" level. Thus for clarity, we will place the blue β levels on one side, and the red α ones on the other, in the diagrams that follow.

As we have demonstrated previously in Section 7, the formation of $[Li(NH_3)_4^+ \cdot e^-@(NH_3)_n]$ ion-pairs, from either $Li(NH_3)_4^+$ and $e^-@(NH_3)_n$ or from $Li(NH_3)_4$ and n ammonia molecules, is exothermic. At very low metal concentrations, before spin-pairing has started to occur, it is probable that such ion-pairs are the dominant species in solution (other than ammonia molecules hydrogen-bonded to each other, of course). Hence, we have calculated the excitation spectra of $[Li(NH_3)_4^+ \cdot e^-@(NH_3)_n]$ ($n = 2$–4,8), in gas and solution phase. The data for $n = 3,4$ are given in the Supporting Information. We have tested how the excitation energies vary with the basis for hydrogen and also with the method employed (Δ-SCF vs. TD-DFT). The results of these tests (given in the Supporting Information) suggests that the computational methodology yields reliable results. In this way we were able to overcome our initial problems with the isolated solvated electron.

The simulated spectra of the $[Li(NH_3)_4^+ \cdot e^-@(NH_3)_n]$ ($n = 2,8$), are shown in Figure 30. For each of these ion-pairs the TD-DFT calculations gave three substantially intense transitions located between 0.6–1.1 eV in the gas phase, and at slightly higher energies in solution. The calculations revealed that all of these excitations can be described well by a single-configuration doublet–doublet transition.

In Figure 31 we illustrate the levels involved in the most intense transitions. The $e^-@(NH_3)_n$ cavities which lie near $Li(NH_3)_4^+$ have broken the tetrahedral symmetry of the aggregate. The SOMOs of these species are s-like, like the SOMO of $Li(NH_3)_4$. However the presence of the nearby ammonia molecules has caused them to deviate (more or less, depending on the geometry of the ion-pair) from being nearly spherical. The three lowest-lying excited states derive from excitations to p-like levels. These three levels (and thus excited states, since the excitation is from an a_1 level) are of A_1, B_1, and B_2 symmetry. All of the lowest lying levels to which electrons are excited are primarily composed of the $3a_1$ ammonia LUMOs.

For the $n = 2$ ion-pair, the first excitation is from the s-like SOMO into a p-like orbital whose "lobes" are primarily located on $e^-@(NH_3)_2$ and the two ammonia molecules coordinated to lithium furthest away from it (Figure 31 a). The orbitals of the two higher lying excited states are mainly localized on the ammonia molecules directly bonded to lithium.

Since the $n = 8$ and $n = 2$ ion-pairs are both of C_{2v} symmetry, the nodal planes of their lower unfilled levels have the same positions. However, whereas for the $n = 2$ species the orbitals involved in the two highest lying excitations are primarily localized on $Li(NH_3)_4^+$, for $n = 8$

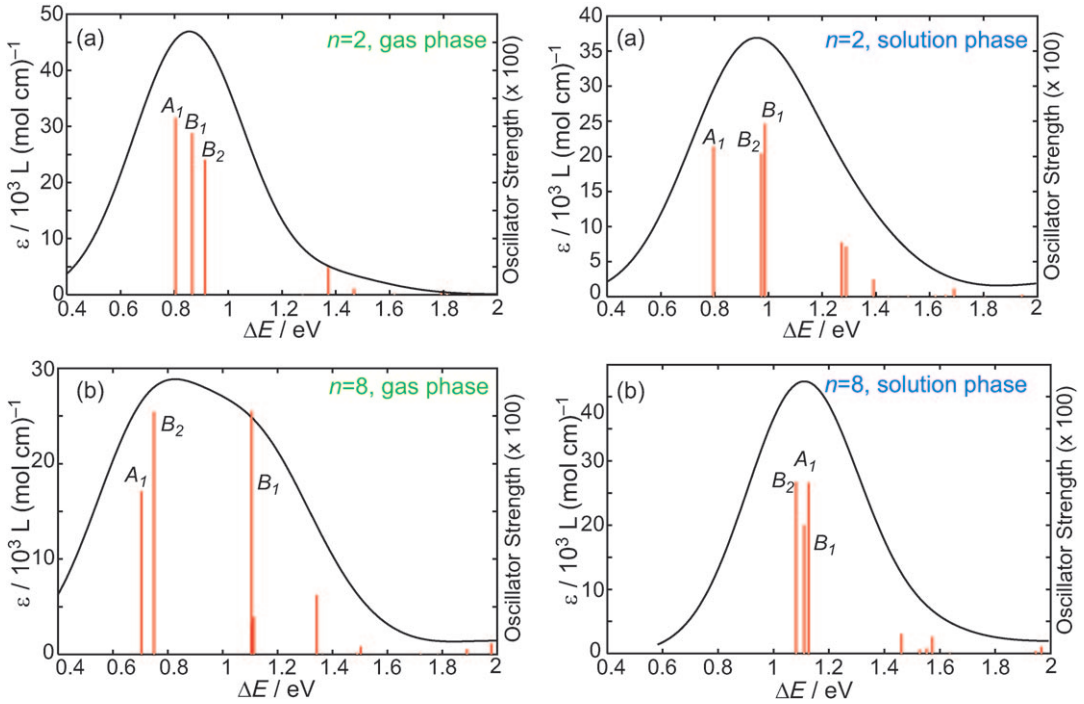

Figure 30. Calculated gas- (left) and solution-phase (right) absorption spectra of $[Li(NH_3)_4^+ \cdot e^-@(NH_3)_n]$ with a) $n = 2$, and b) $n = 8$, simulated by using a Gaussian function with a variance of $\sigma^2 = (0.2)^2$ eV, that is, a 0.2 eV broadening. This corresponds to a full width at half maximum of 0.47 eV. The vertical lines denote the excitations. The geometries of these ion-pairs are illustrated in Figure 31. $\varepsilon = A/[J]l$, where ε is the extinction coefficient, A is the absorbance, [J] is the concentration and l is the length of the sample.

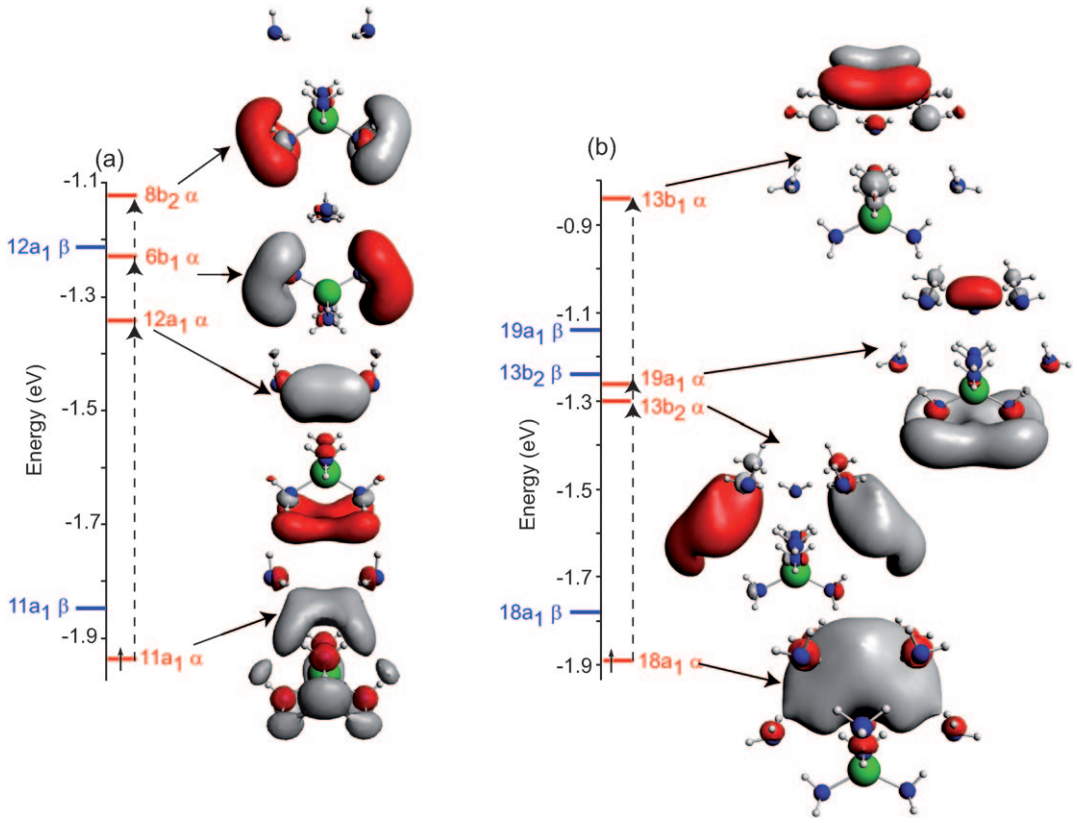

Figure 31. Gas-phase orbital energy diagrams for $[Li(NH_3)_4^+ \cdot e^-@(NH_3)_n]$ with a) $n=2$, and b) $n=8$ (C_{2v} symmetry). The levels involved in the doublet–doublet excitations are also shown.

they are mostly associated with the nearby ammonia molecules. Thus, as we add more and more explicit solvent molecules around $Li(NH_3)_4^+$, the SOMOs and orbitals to which excitations take place have progressively less contributions from the ammonia molecules covalently bound to $Li(NH_3)_4^+$. *That is, for large n, we are calculating the absorption spectrum due to the solvated electron.*

13.3. The Lineshape

A number of models have been put forward to describe the lineshape of the absorption spectra of metal–ammonia solutions. Jortner proposed that it was a result of excitations into levels higher than the 2p (3p, etc.).[114] Others have suggested that it is due to the presence of cavities with different radii,[144] or distortions of the cavity shape.[126]

The three most intense excitations are not the only contributions to the absorption spectra. As Figure 30 shows, in each spectrum there are numerous excitations with higher energies and relatively low oscillator strengths. These less intense excitations are the ones which give rise to the long tail which trails off somewhat past about 2 eV. Even though each individual excitation has a low intensity, there are many of them.

The high-energy excitations are due to transitions from the SOMOs of the ion-pairs into orbitals which are above the levels depicted in Figure 31. *Thus, the long high energy tail in the absorption spectra of lithium–ammonia solutions is primarily a result of excitations into orbitals higher in energy than the lowest unoccupied p-like states.*

Comparison of the experimental and calculated absorption spectra in Figures 28 and 30 shows that the gas-phase data agrees quite well with experiment. For all of the ion-pairs considered the absorption maximum is around 0.8 eV, and the lineshape looks quite similar to that obtained experimentally. The solution-phase calculations do not agree as well, since the absorption maxima are somewhat too high at about 1.0–1.2 eV. In fact, all of the excitations have slightly higher energies than those in the gas phase, and the long tail continues to past about 2.5 eV.

Lithium–ammonia solutions are dynamic systems which contain a large variety of different species at any given instant. Many of these entities may contribute to the overall absorption spectrum. We wanted to see what an "average" spectrum might look like. In the absence of a dynamics calculation, we have constructed an average spectrum assuming (a zeroth order approximation) that the metal–ammonia solution contains equal concentrations of the $n=2,3,4,8$ ion-pairs, and that these do not interact with each other or any other species. That is, we have taken the excitation energies and oscillator strengths of these ion-pairs and from them simulated a single spectrum using a Gaussian lineshape with a 0.2 eV broadening. The gas- and solution-phase averaged spectra obtained in this manner are given in Figure 32.

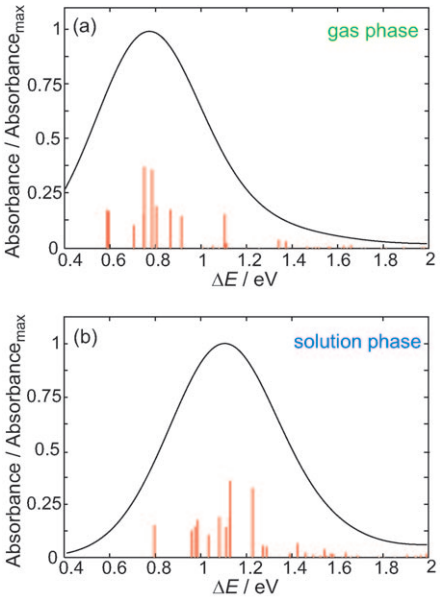

Figure 32. The average spectrum of a solution containing an equivalent amount of non-interacting $[Li(NH_3)_4^+ \cdot e^-@(NH_3)_n]$, $n = 2,3,4,8$, ion-pairs in the gas and solution phase. A Gaussian broadening of 0.2 eV was used.

Taking into account that there might be errors of up to 0.5 eV, both the gas- and solution-phase averaged spectra agree reasonably well with experiment (Figure 28). The gas-phase results look somewhat better: the absorption maximum is at circa 0.8 eV, and we reproduce the rough shape of the line. In the solution-phase spectrum, the maximum occurs at about 1.1 eV and in general the energies of the excitations are somewhat too high.

There may be reasons why we should not get good results from calculations that mimic solvation using a continuum approach. The SOMO and excited states are very diffuse, with substantial density past the radius used to construct the COSMO surface. COSMO has not been designed to describe the electronic structure of such systems, and therefore we consider the absorption spectra calculated for the gas phase to be more reliable.

In energy, the minima for these ion-pairs are very shallow. For example, the energy of the fully optimized $[Li(NH_3)_4^+ \cdot e^-@(NH_3)_2]$ species increases by 0.5/0.8 kcal mol^{-1} in gas/solution phase when the cation–anion distance increases by 2 Å. Moreover, the liquid is a dynamic system within which, at a given instant, some ion-pairs will be forming, whereas others will be breaking apart. Thus, the cation–anion distances will be constantly varying. Does this have an influence on the computed absorption spectra? As shown in the Supporting Information, at least for one ion-pair the answer to this question is "no". This leads us to conclude that the averaged spectra in Figure 32 do a reasonable job at approximating the results which could be obtained via averaging over different configurations obtained in a molecular dynamics simulation.

But as the next section shows, the absorption may hold further mysteries.

13.4. The $Li(NH_3)_4$ Monomer, an Alternative Chromophore

Before we found the ion-pair resolution to our problems of calculating the absorption spectrum of the solvated electron, we tried another tack. Among the other $S = {}^1/_2$ species listed in Figure 4 the monomer, $Li(NH_3)_4$, is the simplest. We wondered what its excited states might look like. Our calculations revealed that this system has only one excitation with a non near-zero oscillator strength. The energy of this excitation is quite robust and does not depend on the hydrogen basis sets, perhaps because in all cases a very flexible, diffuse basis on lithium has been used. The Supporting Information contains the computational evidence for different methods giving similar transition energies.

For $Li(NH_3)_4$ the excitation occurs between the s-like SOMO of a_1 symmetry into the triply degenerate $4t_2$ levels, as depicted in Figure 33a (see also the interaction diagram in Figure 9). The $4t_2$ orbitals are primarily composed of the $3a_1$ ammonia LUMOs, and they are like a big p-orbital wavefunction, each containing a single nodal plane. In comparison, the lowest excitation calculated by TD-DFT for $Li(NH_3)_4^+$ is at 6.3 eV, and has an oscillator strength that is an order of magnitude lower than that of $Li(NH_3)_4$. Clearly the cationic monomer does not contribute to the observed spectrum.

Very recently Ellis and co-workers have observed the electronic spectrum of gas-phase $Li(NH_3)_4$. The position and breadth of the absorption match well our prediction; the excited state is Jahn–Teller distorted, as expected.[145] So—and this is the surprise—both the gas- and solution-phase TD-DFT excitation energies of a $Li(NH_3)_4$ monomer are in very good agreement with the experimentally observed absorption maximum in dilute metal–ammonia solutions, which, as we noted, is found in the range of 0.8–0.88 eV. The Δ-SCF results are about 0.1 eV smaller than those obtained with TD-DFT, but still agree reasonably well with experiment. However, the simulated absorption spectrum (Figure 33b) is symmetric around the single excitation and does not reproduce the experimental lineshape, nor the long tail evident in Figure 28. We will return to this in a moment.

How could the $Li(NH_3)_4$ monomer possibly give a spectrum like that of the solvated electron, $e^-@(NH_3)_n$ (approximated by us as an ion-pair)? The chemical entities considered are quite different, but there are some remarkable similarities. In Jortner's model, the electron is bound within a spherical cavity of 3.0–3.2 Å, and the wavefunction extends beyond the cavity radius, approaching zero about 10 Å away from the cavity center. In $Li(NH_3)_4$ the electron is found within a quasi-spherical region of space centered on the lithium atom. The Li–H distance in $Li(NH_3)_4$ is 2.69 Å, and the wavefunction extends far out past the hydrogen atoms, reaching zero at about 9 Å. It is interesting that both approaches give virtually the same probability to find an electron a distance r away from the cavity center in the "s-like" orbital, $P(r)$ (see Figures 34 and 15). Also, the $P(r)$ for the electron in the $4t_2$ LUMOs of $Li(NH_3)_4$ is qualitatively

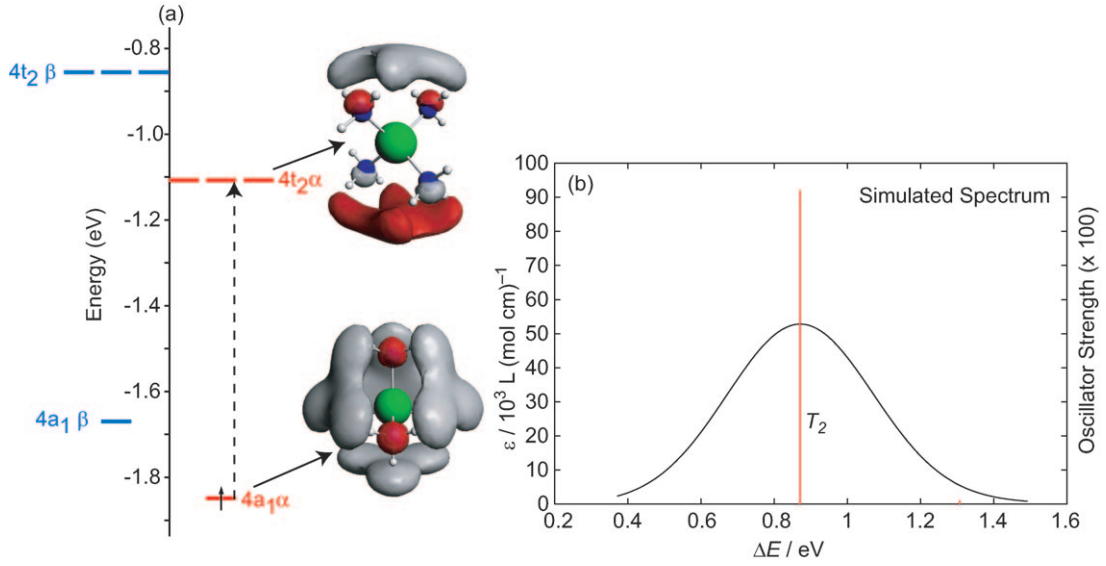

Figure 33. a) Gas-phase orbital energy diagram for $Li(NH_3)_4$. The levels involved in the doublet–doublet excitations are also shown. b) Gas-phase absorption spectrum, simulated by using a Gaussian broadening of 0.2 eV. The absorption maximum is at 0.86 eV. The theoretical solution-phase spectrum has the same shape, but the absorption maximum is at 0.75 eV.

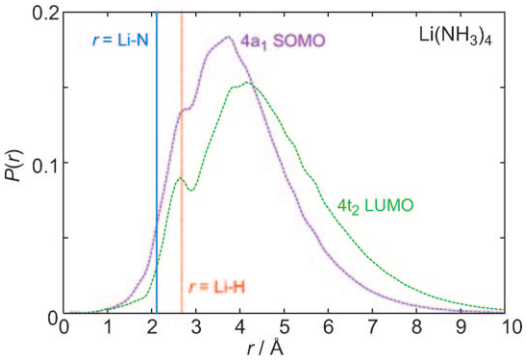

Figure 34. a) The (gas-phase) probability, $P(r)$, to find the excess electron a distance r away from the Li atom in the $4a_1$ SOMO and $4t_2$ LUMOs of the $Li(NH_3)_4$ monomer ($\int P(r)dr = 1$). The Li-N and Li-H distances are denoted by the blue and red lines.

similar to that of the 2p level in Jortner's cavity. They are not equivalent, of course, for example the probability distribution in the $Li(NH_3)_4$ monomer has more structure.

13.5. So What is Responsible for the Blue Color?

As the previous section describes, the $Li(NH_3)_4$ monomer also gives a near-infrared absorption. But does $Li(NH_3)_4$ really contribute to the absorption spectrum of lithium–ammonia solutions? It cannot be the only species giving rise to the spectrum, since it has a single excitation with a non-zero oscillator strength and therefore does not give the proper lineshape. And it is important to recall that whereas the blue color is characteristic of metal–ammonia solutions, it has also been observed in metal-free systems, *for example,* pulse radiolysis of neat ammonia.[133,146]

If we add the $Li(NH_3)_4$ monomer to the aforementioned average spectrum of the ion-pairs (Figure 32), with weight equal to that of one ion-pair, the gas-phase results are nearly identical. The solution-phase averaged spectrum becomes somewhat broader (since the excitation for $Li(NH_3)_4$ was calculated to be at 0.75 eV), however the maximum absorption is still at about 1.1 eV. Lithium–ammonia solutions are dynamic systems, with ammonia molecules solvating $Li(NH_3)_4$ to give the ion-pairs, which may break apart yielding $Li(NH_3)_4^+$ and $e^-@(NH_3)_n$, only to come back together again. *We suggest that both* $Li(NH_3)_4$ *and* $[Li(NH_3)_4^+ \cdot e^-@(NH_3)_n]$ *(a model for the solvated electron) contribute to the absorption spectrum of lithium–ammonia solutions.*

13.6. Metal Independence

Encouraged by the good agreement between theory and experiment, we wanted to see if the computed absorption spectra for $M(NH_3)_n$ and $[M(NH_3)_n^+ \cdot e^-@(NH_3)_m]$ systems with different metals were similar. After all, experiments have shown that the absorption spectrum is reasonably metal-independent.[130]

In this work we have focused only on species with M = Na, K, and Cs. We assumed that each of these metals are tetrahedrally coordinated by four ammonia molecules. We note that as the size of the metal increases, this assumption becomes progressively worse. For example, neutron diffraction experiments have suggested that sodium is solvated by about 5.5 ammonia molecules[147] and potassium is octahedrally coordinated.[148] On the other hand, cluster vertical ionization potential experiments have indicated that the first solvation shell is filled for sodium when $n = 4$.[149] Ellis and coworkers have shown that whereas lithium has four ammonia molecules in the first solvation shell,[150,151] a sodium atom can accommodate a maximum of six ammonia molecules.[152] It is

beyond the scope of this work to determine the most likely geometries and coordinations of these metals.

We have also not considered other metals, as interesting as they are, since many things remain unclear about their geometries and electronic structures. For example, in the *solid* $Ca(NH_3)_x$ ($x \approx 6$), it has been suggested that the ammonia molecules adopt an unusual, nearly planar structure.[153,154] Later experimental work concluded that the ammonia molecules retain their usual pyramidal geometry and that the solid contains a mixture of octahedrally and tetrahedrally coordinated calcium atoms.[155] On the other hand, neutron diffraction experiments of calcium–ammonia *solutions* have indicated that each calcium atom is solvated by 6–7 ammonia molecules.[156] The multiplicity (singlet or triplet) of these systems needs to be studied.

For the monomer model, $M(NH_3)_n$ (see the Supporting Information for details), as the size of the metal increases, the excitation energies decrease slightly. The gas-phase TD-DFT values are 0.86, 0.82, 0.74, and 0.69 eV for Li, Na, K, and Cs, respectively. For each of these metals, we have also calculated the absorption spectra of the same $[M(NH_3)_4^+ \cdot e^-@(NH_3)_n]$ ($n = 2,3,4,8$) ion-pairs which were considered for lithium in Section 13.3. The excitations and oscillator strengths were employed to calculate an average spectrum for the different metals shown in Figure 35. As was the case for lithium, the

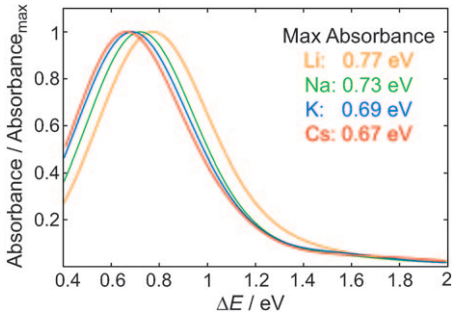

Figure 35. The average spectrum of a solution containing an equivalent amount of non-interacting $[M(NH_3)_4^+ \cdot e^-@(NH_3)_n]$, ($n = 2,3,4,8$; M = Li, Na, K, Cs) ion-pairs in the gas phase. A Gaussian broadening of 0.2 eV was used.

gas-phase absorption spectra are in reasonable agreement with experimental results. For these heavier metals, the absorption maxima is at about 0.7 eV, a little off. However, the lineshape is very similar for all of the metals considered. The absorption is more metal-independent than for the monomer model, but we also see the hint of a red shift as we move down Group 1. Once again, the absorption maximum in the solution-phase spectra is somewhat too high, at about 1.1 eV (see the Supporting Information). Including the excitations for $M(NH_3)_4$ in this average has little effect on the gas-phase spectra, and slightly broadens the solution-phase spectra.

The calculated TD-DFT absorption spectra of both $M(NH_3)_4$ and $[M(NH_3)_4^+ \cdot e^-@(NH_3)_4]$, where M = Li, Na, K, Cs, are relatively metal-independent. The hint of a red shift with larger M is interesting. Due to the fact that the orbitals which are involved in the excitations are primarily composed of contributions from the orbitals on ammonia, and in particular the $3a_1$ ammonia LUMO, we do not expect the excitations arising from $M(NH_3)_n$ with higher coordination numbers ($n > 4$), nor different ion-pairs to be substantially different than those we have calculated. Of course there may be some variations, but since the observed spectra are an average over many different species and geometries, slight changes will not perturb it much.

14. Summary and Outlook

200 years after their discovery, metal–ammonia solutions remain as fascinating as they were to Humphry Davy. One's sheer delight in their color is now augmented by knowledge of the microscopic entities (solvated electrons and ion-pairs) involved, as well as their properties (the transition to the metallic state, and liquid–liquid phase equilibria) which were not apparent in the early days.

The story we present here—essentially an orbital-based quantum chemical scrutiny of the major species in lithium–ammonia solutions, is incomplete. It lacks the essential dynamic side of a system of complex, competing equilibria. But we feel we have learned a lot. We also hope that our perspective stimulates further experimental and theoretical studies of these spectacular systems.

First, we introduced a new, moderately logical nomenclature for what are likely to be the most common species in metal–ammonia solutions; a nomenclature that explicitly addresses the degree of solvation. We distinguish, we believe productively, between the effects of charge and spin; on the way to metallization, many of the species in metal–ammonia solutions are weakly coupled diradicals with a multiplicity of spin states close to each other in energy.

In an important aside, we talk about the incommensurate yet productive languages of electrostatics and quantum mechanics for describing bonding in these and other systems. And we look for analogies between our perspective and the Catterall, Mott, and Jortner pictures of metal–ammonia solutions.

At very low MPM the solutions are likely to contain (along with hydrogen-bonded ammonia aggregates): $Li(NH_3)_4^+$—which may also hydrogen-bond with ammonia, $Li(NH_3)_4$, $e^-@(NH_3)_n$—the solvated electrons, and the $[Li(NH_3)_4^+ \cdot e^-@(NH_3)_n]$ ion-pairs. One may also view the monomer, $Li(NH_3)_4$, and ion-pairs, $[Li(NH_3)_4^+ \cdot e^-@(NH_3)_n]$, as a continuum of structures tuned by the degree of microscopic solvation, a situation symbolized by the $\rightleftarrows$ sign. In general, the ion-pairs are more stable than $e^-@(NH_3)_n$ and $Li(NH_3)_4^+$ at infinite separation. However, our results indicate that $e^-@(NH_3)_n$ cavities containing 5–8 ammonia molecules may be stable (in agreement with previous estimates). Larger cavities rearrange to place some ammonia molecules in the middle, effectively changing the cavity configuration.

Our analysis of the $Li(NH_3)_4$ monomer shows that the odd electron is in an a_1 orbital whose main density lies quite far out, outside the hydrogen atoms on ammonia. This MO is made up of a mixture of NH_3 $3a_1$*, and $1a_1$ orbitals, as well as

lithium Rydberg states. Similarly, in the solvated electron clusters, $e^-@(NH_3)_n$, which we studied for $n = 2$–14, an electron binds a group of ammonia molecules oriented far away from their optimal hydrogen-bonding orientation. The unpaired electron in the solvated electron cluster is hardly in the center of the distinct cavity, but near the hydrogen atoms of the ammonia molecules, in agreement with a recent computation by Chandra and Marx.[55]

In both cases—the monomer and the solvated electron—the odd electron is in a diffuse orbital that is bonding between the hydrogen atoms on different ammonia molecules. We describe the resulting weak bonding (weak, but many hydrogen atoms involved in it) as H⇜⇝H bonding. Optimal H⇜⇝H bonding is achieved when the hydrogen atoms point towards each other. This explains the experimental observation that for compositions below saturation, the decrease in hydrogen bonding is greater than that expected if ionic solvation effects are considered. It could be that H⇜⇝H bonding may also be present in the aquated electron,[157] organic electrides,[158,159] and electrons solvated in other amines.[46,160,161] Then there are other related systems where there cannot be any H⇜⇝H bonding, such as F centers and F′ centers (a single electron, or an electron-pair, in an anionic vacancy in ionic crystals), and inorganic electrides.[162]

A number of species which contain two, or more, solvated electrons are considered. We refer to these entities as coupled radicals (CRs), since they may have a multitude of different spin-states. However, for all of the species we have looked at, the spin-paired ($S = 0$) isomers were lower in energy than those with unpaired spins. The CRs which we have examined include: $2e^-@(NH_3)_n$ (two electrons in a cavity), $[Li(NH_3)_4^+ \cdot e^-@(NH_3)_n]_r$ ion-pairs, the $[Li(NH_3)_4 \cdot e^-@(NH_3)_n]$ ion-triples, and $[Li(NH_3)_4]_r$. And we show the beginning of band formation in the aggregation of $[Li(NH_3)_4]_r$ clusters, looking at up to four such monomers interacting.

Our calculations of the spectra of metal–ammonia solutions contain a surprise—the characteristic near-infrared band of these solutions, may be due both to the solvated electron (modeled in our calculations by the ion-pair $[Li(NH_3)_4^+ \cdot e^-@(NH_3)_n]$), and to the $Li(NH_3)_4$ monomer. However, the tail of this transition, responsible for the characteristic blue color, derives just from the ion-pair (solvated electron). The relationship to the Jortner model, an essential s→p transition, is traced. The long tail arises from transitions into levels higher in energy than the lowest unoccupied p levels.

There is much to be done. But we feel we have an essential orbital understanding of these venerable and remarkable solutions.

Abbreviations

COSMO	conductor-like screening model
CR	coupled radical
HOMO	highest occupied molecular orbital
LUMO	lowest unoccupied molecular orbital
MNMT	metal to nonmetal transition
MPM	mole percent metal
SOMO	singly occupied HOMO
TD-DFT	time-dependent density functional theory
TMS	transition to the metallic state

Initial calculations on this problem were carried out by Ji Feng at Cornell; we thank him for taking the first steps. We are grateful to Joshua Jortner for providing insightful comments on the manuscript. We would like to thank Neil Ashcroft for stimulating conversations, Matthew Lodge for assistance with some figures, and Neal Skipper for the photos of the lithium–ammonia solutions in Figure 1. The staff of SCM (Scientific Computing and Modelling, http://www.scm.com/) and developers of ADF have provided invaluable technical assistance. In particular we would like to thank: Stan van Gisbergen, Alexei Yakovlev, Jochen Autschbach, Matthias Bickelhaupt, and Tom Ziegler. For funding the research at Cornell we thank the National Science Foundation, Grant CHE-0613306; that at Oxford we thank the Engineering and Physical Sciences Research Council.

Received: January 21, 2009

[1] P. P. Edwards, *Adv. Inorg. Chem. Radiochem.* **1982**, *25*, 135–185.
[2] D. Holton, P. Edwards, *Chem. Br.* **1985**, *21*, 1007–1013.
[3] J. M. Thomas, P. P. Edwards, V. L. Kuznetsov, *ChemPhysChem* **2008**, *9*, 59–66.
[4] S. Naiditch, *Solutions Métal-Ammoniac: Propriétés Physico-Chimiques*, Colloque Weyl I, Lille, France, **1963**; Benjamin, New York, **1964**, p. 113–136.
[5] J. B. Hannay, J. Hogarth, *Proc. R. Soc. London* **1879**, *29*, 324–326.
[6] J. B. Hannay, J. Hogarth, *Proc. R. Soc. London* **1880**, *30*, 178–188.
[7] W. Weyl, *Ann. Phys.* **1864**, *121*, 606–612.
[8] C. A. Seely, *J. Franklin Inst.* **1871**, *61*, 110–114.
[9] W. L. Jolly, *Metal–Ammonia Solutions*, *Benchmark Papers in Inorganic Chemistry*, Dowden, Hutchinson and Ross, Stroudsbury, PA, **1972**. This volume contains key articles (from 1864–1972) which were important in the development of the understanding of metal–ammonia (and related) solutions.
[10] H. P. Cady, *J. Phys. Chem.* **1897**, *1*, 707–713.
[11] For a personal reflection of these ground-breaking studies, see C. A. Kraus, *J. Chem. Educ.* **1953**, *30*, 83–87.
[12] C. A. Kraus, *Solutions Métal-Ammoniac: Propriétés Physico-Chimiques*, Colloque Weyl I, Lille, France, 1963; Benjamin, New York, **1964**, p. 7–10.
[13] C. A. Kraus, *J. Am. Chem. Soc.* **1907**, *29*, 1557–1571.
[14] C. A. Kraus, *J. Am. Chem. Soc.* **1921**, *43*, 749–770.
[15] G. E. Gibson, W. L. Argo, *Phys. Rev.* **1916**, *7*, 33–48.
[16] G. E. Gibson, W. L. Argo, *J. Am. Chem. Soc.* **1918**, *40*, 1327–1361.
[17] MPM = [moles of metal/(moles of metal + moles of solvent)] × 100. For calibration purposes: 1 MPM ~ 2×10^{20} electron cm^{-3}.
[18] N. W. Taylor, G. N. Lewis, *Proc. Natl. Acad. Sci. USA* **1925**, *11*, 456–457.
[19] E. Huster, *Ann. Phys.* **1938**, *33*, 477–482.
[20] S. D. Freed, N. Sugarman, *J. Chem. Phys.* **1943**, *11*, 354–360.
[21] U. Schindewolf, M. Werner, *J. Phys. Chem.* **1980**, *84*, 1123–1129.
[22] The concept of the existence of bipolarons in ionic crystals can be traced to: V. L. Vinetskii, M. Sh. Giterman, *Zh. Eksp. Teor. Fiz.* **1957**, *33*, 730; *Sov. Phys. JETP.* **1958**, *6*, 560–564. Their

existence in metal–ammonia solutions was advanced by: N. F. Mott, *J. Phys. Chem.* **1980**, *84*, 1199 – 1203; Mott recognized these species as two electrons (each in a cavity) associated with a solvated cation.

[23] M. J. Sienko, *Solutions Métal-Ammoniac: Propriétés Physico-Chimiques*, Colloque Weyl I, Lille, France, **1963**; Benjamin, New York, **1964**, p. 23–40.

[24] M. Hirasawa, Y. Nakamura, M. Shimoji, *Ber. Bunsen-Ges.* **1978**, *82*, 815 – 818.

[25] N. F. Mott, *Philos. Mag.* **1961**, *62*, 287 – 309.

[26] *The Metallic and Non-Metallic States of Matter* (Eds.: P. P. Edwards, C. N. R. Rao), Taylor and Francis, London, **1985**.

[27] *Metal–Insulator Transitions Revisited* (Eds.: P. P. Edwards, C. N. R. Rao), Taylor and Francis, London, **1995**.

[28] P. P. Edwards, T. V. Ramakrishnan, C. N. R. Rao, *J. Phys. Chem.* **1995**, *99*, 5228 – 5239.

[29] J. Jortner, M. H. Cohen, *Phys. Rev. B* **1976**, *13*, 1548 – 1568.

[30] N. F. Mott. *Metal–Insulator Transitions*, Taylor and Francis, London, **1990**.

[31] K. F. Herzfeld, *Phys. Rev.* **1927**, *29*, 701 – 705.

[32] P. P. Edwards, *J. Supercond. Novel Magn.* **2000**, *13*, 933 – 946.

[33] J. C. Thompson, *Electrons in Liquid Ammonia*, Oxford University Press, Oxford, **1976**.

[34] J. C. Thompson, *Rev. Mod. Phys.* **1968**, *40*, 704 – 710.

[35] Electrons in Fluids, *Can. J. Chem.* **1977**, *55*, 1081 – 2277.

[36] J. C. Thompson, *The Chemistry of Non-Aqueous Solvents*, Academic Press, New York, **1967**, p. 265 – 317.

[37] M. H. Cohen, J. C. Thompson, *Adv. Phys.* **1968**, *17*, 857 – 907.

[38] *Solutions Métal-Ammoniac: Propriétés Physico-Chimiques* (Eds.: G. Lepoutre, M. J. Sienko), Colloque Weyl I, Lille, France, **1963**; Benjamin, New York, **1964**.

[39] *Metal–Ammonia Solutions* (Eds.: J. J. Lagowski, M. J. Sienko), Colloque Weyl II, Ithaca, New York, **1969**; Butterworths, London, **1970**.

[40] *Electrons in Fluids*, (Eds.: J. Jortner, N. R. Kestner), Colloque Weyl III, Kibbutz Hanita, Israel, **1972**; Springer, Heidelberg, **1973**.

[41] *Electrons in Fluids—The Nature of Metal-Ammonia Solutions*, Colloque Weyl IV; *J. Phys. Chem.* **1975**, 79, 2789 – 3079.

[42] *Excess Electrons and Metal-Ammonia Solutions*, Colloque Weyl V; *J. Phys. Chem.* **1980**, *84*, 1065 – 1298.

[43] *Excess Electrons and Metal-Ammonia Solutions*, Colloque Weyl VI; *J. Phys. Chem.* **1984**, *88*, 3699 – 3914.

[44] *Metals in Solution*, Colloque Weyl VII, Colloque C5, Aussois, France; Supplement au *J. Phys. IV* **1991**, 1(12).

[45] J. L. Dye, *Sci. Am.* **1977**, *237*(1), 92 – 105.

[46] J. L. Dye, *Electrons in Fluids*, Colloque Weyl III, Kibbutz Hanita, Israel, **1972**; Springer, Heidelberg, **1973**, p. 77–95.

[47] P. P. Edwards, *J. Phys. Chem.* **1980**, *84*, 1215 – 1230.

[48] P. P. Edwards, *J. Phys. Chem.* **1984**, *88*, 3772 – 3780.

[49] J. J. Lagowski, *Synth. React. Inorg. Met.-Org. Nano-Met. Chem.* **2007**, *37*, 115 – 153.

[50] H. Thompson, J. C. Wasse, N. T. Skipper, C. A. Howard, D. T. Bowron, A. K. Soper, *J. Phys. Condens. Matter* **2004**, *16*, 5639 – 5652.

[51] H. Thompson, J. C. Wasse, N. T. Skipper, S. Hayama, D. T. Bowron, A. K. Soper, *J. Am. Chem. Soc.* **2003**, *125*, 2572 – 2581.

[52] S. Hayama, N. T. Skipper, J. C. Wasse, H. Thompson, *J. Chem. Phys.* **2002**, *116*, 2991 – 2996.

[53] Z. Deng, G. J. Martyna, M. L. Klein, *Phys. Rev. Lett.* **1992**, *68*, 2496 – 2499.

[54] Z. Deng, G. J. Martyna, M. L. Klein, *Phys. Rev. Lett.* **1993**, *71*, 267 – 270.

[55] A. Chandra, D. Marx, *Angew. Chem.* **2007**, *119*, 3750 – 3753; *Angew. Chem. Int. Ed.* **2007**, *46*, 3676 – 3679.

[56] N. F. Mott, *J. Phys. Chem.* **1980**, *84*, 1199 – 1203.

[57] G. N. Chuev, P. Quémerais, *J. Chem. Phys.* **2008**, *128*, 144503.

[58] G. N. Chuev, P. Quémerais, *J. Chem. Phys.* **2008**, *128*, 027101.

[59] M. H. Miles, W. S. Harris, *J. Electrochem. Soc.* **1974**, *121*, 459 – 463.

[60] R. Catterall, P. P. Edwards, *J. Phys. Chem.* **1980**, *84*, 1196 – 1199.

[61] E. J. Baerends, J. Autschbach, A. Bérces, F. M. Bickelhaupt, C. Bo, P. M. Boerrigter, L. Cavallo, D. P. Chong, L. Deng, R. M. Dickson, D. E. Ellis, M. van Faassen, L. Fan, T. H. Fischer, C. Fonseca Guerra, S. J. A. van Gisbergen, J. A. Groeneveld, O. V. Gritsenko, M. Grüning, F. E. Harris, P. van den Hoek, C. R. Jacob, H. Jacobsen, L. Jensen, G. van Kessel, F. Kootstra, E. van Lenthe, D. A. McCormack, A. Michalak, J. Neugebauer, V. P. Osinga, S. Patchkovskii, P. H. T. Philipsen, D. Post, C. C. Pye, W. Ravenek, P. Ros, P. R. T. Schipper, G. Schreckenbach, J. G. Snijders, M. Solà, M. Swart, D. Swerhone, G. te Velde, P. Vernooijs, L. Versluis, L. Visscher, O. Visser, F. Wang, T. A. Wesolowski, E. van Wezenbeek, G. Wiesenekker. ADF2007.01, SCM, Theoretical Chemistry, Vrije Universiteit, Amsterdam, The Netherlands. URL http://www.scm.com.

[62] G. te Velde, F. M. Bickelhaupt, E. J. Baerends, C. Fonseca Guerra, S. J. A. van Gisbergen, J. G. Snijders, T. Ziegler, *J. Comput. Chem.* **2001**, *22*, 931 – 967.

[63] J. P. Perdew, K. Burke, Y. Wang, *Phys. Rev. B* **1996**, *54*, 16533 – 16539.

[64] Y. Zhang, W. Yang, *Phys. Rev. Lett.* **1998**, *80*, 890.

[65] J. P. Perdew, K. Burke, M. Ernzerhof, *Phys. Rev. Lett.* **1998**, *80*, 891.

[66] B. Hammer, L. B. Hansen, J. K. Norskov, *Phys. Rev. B* **1999**, *59*, 7413 – 7421.

[67] S. H. Vosko, L. Wilk, M. Nusair, *Can. J. Phys.* **1980**, *58*, 1200 – 1211.

[68] E. van Lenthe, E. J. Baerends, J. G. Snijders, *J. Chem. Phys.* **1993**, *99*, 4597 – 4610.

[69] E. van Lenthe, E. J. Baerends, J. G. Snijders, *J. Chem. Phys.* **1994**, *101*, 9783 – 9792.

[70] E. van Lenthe. *The ZORA Equation*. PhD thesis, Vrije Universiteit Amsterdam, Netherlands, **1996**.

[71] A. Klamt, G. Schüürmann, *J. Chem. Soc. Perkin Trans. 2* **1993**, 799 – 805.

[72] A. Klamt, *J. Phys. Chem.* **1995**, *99*, 2224 – 2235.

[73] A. Klamt, V. Jonas, *J. Chem. Phys.* **1996**, *105*, 9972 – 9981.

[74] C. C. Pye, T. Ziegler, *Theor. Chem. Acc.* **1999**, *101*, 396 – 408.

[75] R. Bauernschmitt, R. Ahlrichs, *Chem. Phys. Lett.* **1996**, *256*, 454 – 464.

[76] C. Jamorski, M. E. Casida, D. R. Salahub, *J. Chem. Phys.* **1996**, *104*, 5134 – 5147.

[77] S. J. A. van Gisbergen, J. G. Snijders, E. J. Baerends, *Comput. Phys. Commun.* **1999**, *118*, 119 – 138.

[78] S. J. A. van Gisbergen, F. Kootstra, P. R. T. Schipper, O. V. Gritsenko, J. G. Snijders, E. J. Baerends, *Phys. Rev. A* **1998**, *57*, 2556 – 2571.

[79] T. Ziegler, A. Rauk, E. J. Baerends, *Theor. Chim. Acta* **1977**, *43*, 261 – 271.

[80] K. S. Pitzer, *J. Chem. Phys.* **1958**, *29*, 453 – 454.

[81] D. E. O'Reilly, *J. Chem. Phys.* **1964**, *41*, 3736 – 3742.

[82] R. Rianda, R. P. Frueholz, W. A. Goddard III, *Chem. Phys.* **1977**, *19*, 131 – 136.

[83] S. R. Langford, A. J. Orr-Ewing, R. A. Morgan, C. M. Western, M. N. R. Ashfold, A. Rijkenberg, C. R. Scheper, W. J. Buma, C. A. de Lange, *J. Chem. Phys.* **1998**, *108*, 6667 – 6680.

[84] M. S. Banna, D. A. Shirley, *J. Chem. Phys.* **1975**, *63*, 4759 – 4766.

[85] G. Burton, W. F. Chan, G. Cooper, C. E. Brion, *Chem. Phys.* **1993**, *177*, 217 – 231.

[86] P. Stampfli, K. H. Bennemann, *Phys. Rev. Lett.* **1987**, *58*, 2635 – 2638.

[87] G. H. Lee, S. T. Arnold, J. G. Eaton, H. W. Sarkas, K. H. Bowen, C. Ludewigt, H. Haberland, *Z. Phys. D* **1991**, *20*, 9 – 12.

[88] I. R. Lee, W. Lee, A. H. Zewail, *ChemPhysChem* **2008**, *9*, 83 – 88.
[89] J. Jortner, *Z. Phys. D* **1992**, *24*, 247 – 275.
[90] D. K. Coles, W. E. Good, J. K. Bragg, A. H. Sharbaugh, *Phys. Rev.* **1951**, *82*, 877 – 878.
[91] I. S. Lim, P. Botschwina, R. Oswald, V. Barone, H. Stoll, P. Schwerdtfeger, *J. Chem. Phys.* **2007**, *127*, 104313.
[92] A. D. Boese, A. Chandra, J. M. L. Martin, D. Marx, *J. Chem. Phys.* **2003**, *119*, 5965 – 5980.
[93] E. H. T. Olthof, A. van der Avoird, P. E. S. Wormer, *J. Chem. Phys.* **1994**, *101*, 8430 – 8442.
[94] P. E. Janeiro-Barral, M. Mella, *J. Phys. Chem. A* **2006**, *110*, 11244 – 11251.
[95] L. Rao, H. Ke, G. Fu, X. Xu, Y. Yan, *J. Chem. Theory Comput.* **2009**, *5*, 86 – 96.
[96] J. Ireta, J. Neugebauer, M. Scheffler, *J. Phys. Chem. A* **2004**, *108*, 5692 – 5698.
[97] C. A. Burns, G. Vanko, H. Sinn, A. Alatas, E. E. Alp, A. Said, *J. Chem. Phys.* **2006**, *124*, 024720.
[98] U. Pinsook, R. H. Scheicher, R. Ahuja, S. Hannongbua, *J. Phys. Chem. A* **2008**, *112*, 5323 – 5326.
[99] K. Mierzwicki, Z. Latajka, *Chem. Phys.* **2001**, *265*, 301 – 311.
[100] G. J. Martyna, M. L. Klein, *J. Phys. Chem.* **1991**, *95*, 515 – 518.
[101] K. Hashimoto, K. Morokuma, *J. Am. Chem. Soc.* **1995**, *117*, 4151 – 4159.
[102] T. R. Hughes, *J. Chem. Phys.* **1963**, *38*, 202 – 209.
[103] R. Catterall, *Metal-Ammonia Solutions*, Colloque Weyl II, Ithaca, New York, **1969**; Butterworths, London, **1970**, p. 105 – 131.
[104] D. E. O'Reilly, *J. Chem. Phys.* **1964**, *41*, 3729 – 3735.
[105] A. J. Lough, S. Park, R. Ramachandran, R. H. Morris, *J. Am. Chem. Soc.* **1994**, *116*, 8356 – 8357.
[106] E. Peris, J. C. Lee, R. H. Crabtree, *J. Chem. Soc. Chem. Commun.* **1994**, 2573.
[107] J. Kohanoff, F. Buda, M. Parrinello, M. L. Klein, *Phys. Rev. Lett.* **1994**, *73*, 3133 – 3136.
[108] T. A. Kaplan, J. F. Harrison, J. L. Dye, R. Rencsok, *Phys. Rev. Lett.* **1995**, *75*, 978.
[109] T. Sommerfeld, *J. Phys. Chem. A* **2008**, *112*, 11817 – 11823.
[110] I. A. Shkrob, *J. Phys. Chem. A* **2006**, *110*, 3967 – 3976.
[111] T. Clark, G. Illing, *J. Am. Chem. Soc.* **1987**, *109*, 1013 – 1020.
[112] M. D. Newton, *J. Phys. Chem.* **1975**, *79*, 2795 – 2808.
[113] R. Catterall, N. F. Mott, *Adv. Phys.* **1969**, *18*, 665 – 680.
[114] J. Jortner, *J. Chem. Phys.* **1959**, *30*, 839 – 846.
[115] R. A. Ogg, *J. Am. Chem. Soc.* **1946**, *68*, 155.
[116] R. A. Ogg, *J. Chem. Phys.* **1946**, *14*, 114 – 115.
[117] R. A. Ogg, *Phys. Rev.* **1946**, *69*, 243 – 244.
[118] K. K. Irikura, *J. Phys. Chem. A* **2008**, *112*, 983 – 988.
[119] M. Marchi, M. Sprik, M. L. Klein, *Faraday Discuss. Chem. Soc.* **1988**, *85*, 373 – 389.
[120] Z. Xu, K. Vanka, T. K. Firman, A. Michalak, E. Zurek, C. Zhu, T. Ziegler, *Organometallics* **2002**, *21*, 2444 – 2453.
[121] G. N. Chuev, P. Quémerais, J. Crain, *J. Chem. Phys.* **2007**, *127*, 244501.
[122] T. Kuhn, *The Structure of Scientific Revolutions*, University of Chicago Press, Chicago, **1962**.
[123] A. Depriester, J. Fackeure, J. P. Lelleur, *J. Phys. Chem.* **1981**, *85*, 272 – 275.
[124] S. Neukermans, E. Janssens, Z. F. Chen, R. E. Silverans, P. von R. Schleyer, P. Lievens, *Phys. Rev. Lett.* **2004**, *92*, 163401.
[125] D. E. O'Reilly, *J. Chem. Phys.* **1971**, *55*, 474 – 475.
[126] N. R. Kestner, *Electrons in Fluids*, Colloque Weyl III, Kibbutz Hanita, Israel, **1972**; Springer, Heidelberg, **1973**, p. 1 – 28.
[127] N. R. Kestner, B. K. Rao, C. W. Finley, *J. Phys. Chem.* **1983**, *87*, 1464 – 1466.
[128] J. Kaplan, C. Kittel, *J. Chem. Phys.* **1953**, *21*, 1429 – 1433.
[129] R. Catterall, M. C. R. Symons, *J. Chem. Soc. A* **1966**, 13 – 16.
[130] R. L. Harris, J. J. Lagowski, *J. Phys. Chem.* **1980**, *84*, 1091 – 1096.
[131] J. L. Dye, *Metal-Ammonia Solutions*, Colloque Weyl II, Ithaca, New York, **1969;** Butterworths, London, **1970**, p. 1 – 17.
[132] E. Duval, P. Rigny, G. Lepoutre, *Chem. Phys. Lett.* **1968**, *2*, 237 – 240.
[133] J. L. Dye, M. G. DeBacker, L. M. Dorfman, *J. Chem. Phys.* **1970**, *52*, 6251 – 6258.
[134] R. C. Douthit, J. L. Dye, *J. Am. Chem. Soc.* **1960**, *82*, 4472 – 4478.
[135] H. Blades, J. W. Hodgins, *Can. J. Chem.* **1955**, *33*, 411 – 425.
[136] J. Lindner, A. N. Unterreiner, P. Vöhringer, *ChemPhysChem* **2006**, *7*, 363 – 369.
[137] D. F. Burow, J. J. Lagowski, *Adv. Chem. Ser.* **1965**, *50*, 125.
[138] C. M. Stupak, T. R. Tuttle, S. Golden, *J. Phys. Chem.* **1984**, *88*, 3804 – 3810.
[139] F.-Y. Jou, G. R. Freeman, *J. Phys. Chem.* **1981**, *85*, 629 – 635.
[140] D. A. Copeland, N. R. Kestner, J. Jortner, *J. Chem. Phys.* **1970**, *53*, 1189 – 1216.
[141] A. Dreuw, J. L. Weisman, M. Head-Gordon, *J. Chem. Phys.* **2003**, *119*, 2943 – 2946.
[142] T. Ziegler, *J. Chem. Soc. Dalton Trans.* **2002**, 642 – 652.
[143] P. R. T. Schipper, O. V. Gritsenko, S. J. A. van Gisbergen, E. J. Baerends, *J. Chem. Phys.* **2000**, *112*, 1344 – 1352.
[144] P. F. Rusch, W. H. Koehler, J. J. Lagowski, *Metal–Ammonia Solutions*, Colloque Weyl II, Ithaca, New York, **1969**; Butterworths, London, **1970**, p. 41.
[145] L. Variali, N. M. Tonge, N. Bhalla, A. M. Ellis, private communication.
[146] D. M. Compton, J. A. Brant, R. A. Cesna, B. L. Gehman, *Pulse Radiolysis*, Academic Press, New York, **1965**, p. 43.
[147] J. C. Wasse, S. Hayama, S. Masmanidis, S. L. Stebbings, N. T. Skipper, *J. Chem. Phys.* **2003**, *118*, 7486 – 7494.
[148] J. C. Wasse, S. Hayama, N. T. Skipper, C. J. Benmore, A. K. Soper, *J. Chem. Phys.* **2000**, *112*, 7147 – 7151.
[149] I. V. Hertel, C. Hüglin, C. Nitsch, C. P. Schulz, *Phys. Rev. Lett.* **1991**, *67*, 1767 – 1770.
[150] T. E. Salter, A. M. Ellis, *J. Phys. Chem. A* **2007**, *111*, 4922 – 4926.
[151] T. E. Salter, V. A. Mikhailov, C. J. Evans, A. M. Ellis, *J. Chem. Phys.* **2006**, *125*, 034302.
[152] T. E. Salter, V. Mikhailov, A. M. Ellis, *J. Phys. Chem. A* **2007**, *111*, 8344 – 8351.
[153] W. S. Glaunsinger, T. R. White, R. B. Von Dreele, D. A. Gordon, R. F. Marzke, A. L. Bowman, J. L. Yarnell, *Nature* **1978**, *271*, 414 – 417.
[154] W. S. Glaunsinger, R. B. Von Dreele, R. F. Marzke, R. C. Hanson, P. Chieux, P. Damay, R. Catterall, *J. Phys. Chem.* **1984**, *88*, 3860 – 3877.
[155] W. Press, P. Damay, F. Leclercq, P. Chieux, *J. Chem. Phys.* **1989**, *91*, 1167 – 1172.
[156] J. C. Wasse, C. A. Howard, H. Thompson, N. T. Skipper, *J. Chem. Phys.* **2004**, *121*, 996 – 1004.
[157] A. L. Sobolewski, W. Domcke, *Phys. Chem. Chem. Phys.* **2002**, *4*, 4 – 10.
[158] J. L. Dye, *Science* **2003**, *301*, 607 – 608.
[159] J. L. Dye, *Inorg. Chem.* **1997**, *36*, 3816 – 3826.
[160] J. L. Dye, *J. Phys. IV* **1991**, *1*, 259 – 282.
[161] D. M. Holton, P. P. Edwards, W. McFarlane, B. Wood, *J. Am. Chem. Soc.* **1983**, *105*, 2104 – 2108.
[162] S. Matsuishi, Y. Toda, M. Miyakawa, K. Hayashi, T. Kamiya, M. Hirano, I. Tanaka, H. Hosono, *Science* **2003**, *301*, 626 – 629.

